



저작자표시-비영리-변경금지 2.0 대한민국

이용자는 아래의 조건을 따르는 경우에 한하여 자유롭게

- 이 저작물을 복제, 배포, 전송, 전시, 공연 및 방송할 수 있습니다.

다음과 같은 조건을 따라야 합니다:



저작자표시. 귀하는 원저작자를 표시하여야 합니다.



비영리. 귀하는 이 저작물을 영리 목적으로 이용할 수 없습니다.



변경금지. 귀하는 이 저작물을 개작, 변형 또는 가공할 수 없습니다.

- 귀하는, 이 저작물의 재이용이나 배포의 경우, 이 저작물에 적용된 이용허락조건을 명확하게 나타내어야 합니다.
- 저작권자로부터 별도의 허가를 받으면 이러한 조건들은 적용되지 않습니다.

저작권법에 따른 이용자의 권리는 위의 내용에 의하여 영향을 받지 않습니다.

이것은 [이용허락규약\(Legal Code\)](#)을 이해하기 쉽게 요약한 것입니다.

[Disclaimer](#)

Doctor of Philosophy

A study on the spark discharge effect on ignition and emission characteristics of LPG engine using RCEM

The Graduate School

of the University of Ulsan

Department of Mechanical Engineering

Cahyani Windarto

A study on the spark discharge effect on ignition and emission characteristics of LPG engine using RCEM

Supervisor: Prof. Lim, Ocktaeck

A Dissertation

Submitted to

the Graduate School of the University of Ulsan

In partial Fulfillment of the Requirements

for the Degree of

Doctor of Philosophy

by

Cahyani Windarto

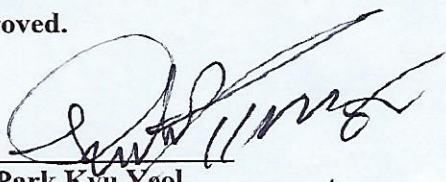
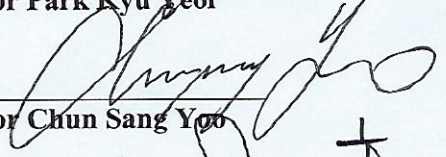
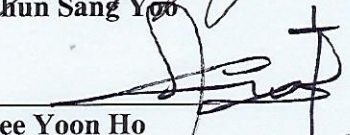
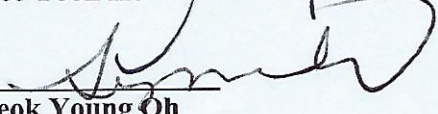
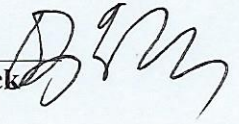
Department of Mechanical Engineering

University of Ulsan, Republic of Korea

December 2023

A study on the spark discharge effect on ignition and emission characteristics of LPG engine using RCEM

This certifies that the dissertation of Cahyani Windarto is approved.

Committee Chair	 Professor Park Kyu Yeol
Committee Member	 Professor Chun Sang Yoo
Committee Member	 Professor Lee Yoon Ho
Committee Member	 Professor Seok Young Oh
Committee Member	 Professor Lim Ock Taeck

Department of Mechanical Engineering

University of Ulsan, Republic of Korea

December 2023

ABSTRACT

A study on the spark discharge effect on ignition and emission characteristics of LPG engine using RCEM

**Department of Mechanical Engineering
Cahyani Windarto**

A spark ignition strategy in compression ignition has been considered to achieve high performance and reduce pollutant emissions of direct injection engines. It is challenging to optimize the operating parameters of spark discharge duration effect of the internal combustion engine. The potential improvement in in-cylinder performance and emission characteristics of CI engines fueled with gasoline, diesel and propane mode was investigated in an experimental and simulation series in this study. Analyzing the novel technique of liquid fuel injection is worthwhile given the potential for high-efficiency compression ignition engines to achieve marine diesel-like, high-efficiency combustion in a RCEM research engine. The spark ignition energy depends on the discharge current and the spark discharge duration. Since propane has a low cetane number, spark plug operating is provided to achieve reliable ignition. However, the respective roles of both on the rapid compression and expansion machine (RCEM) running with spark ignition and gasoline direct injection in-cylinder pressure have not been fully investigated. The effects of spark release duration on propane direct injection were studied using experiments and simulation on a modification head of large-bore RCEM using three spark ignition strategies. The validated model CFD was applied to study the combustion and emission of propane as well as the spatial distribution of propane in the research engine. The main objective was to determine how high-pressure direct injection of propane can increase the efficiency of CI engines and reduce particulate and standard emissions. Three spark ignition strategy ranging from 50 mA up to 200 mA is applied to enhance the ignition discharge energy according to six selected cases of ignition timing duration (0.7 ms, 1.0 ms, 2.0 ms, 3.0 ms, 4.0 ms, and 5.0 ms). The emissions reduction was realized with DI-propane combustion compared to diesel combustion. Propane produces fewer particulates than diesel. THC and NO_x emissions from diesel vehicles were 1.8% lower and 32.3% higher, respectively, than propane combustion. It is feasible to decrease NO_x, particulate, and unburned fuel pollutants while maintaining CO₂ emissions at levels comparable to a diesel engine. Both the onset of propane injection and the length of ignition timing have been shown to be optimum factors in emissions and performance. Finally, the establishment of a compression ignition engine combined with spark energy discharge might contribute to faster plasma formation, as well as expose the kernel development to a wider range of spark duration.

Keywords: RCEM; spark discharge energy; computational fluid dynamics; in-cylinder performance; direct injection; propane; emission.

ACKNOWLEDGEMENT

I am sincerely grateful to my advisor, Professor Lim Ocktaeck for giving me the opportunity to study in the Smart Powertrain Laboratory and for his continuous guidance on my research. And also, for his patience, motivations and insightful feedback to help me sharpen my thinking and take my work to the next level. Without his support and encouragement, I would not have been able to complete this dissertation. I would like to express my gratitude to the Graduate School of Mechanical and Automotive Engineering, University of Ulsan and Ministry of Manpower of the Republic of Indonesia for providing me the opportunity, approval, and support to pursue my Ph.D. program.

I feel very fortunate to be a member of the Smart Powertrain Laboratory at University of Ulsan. I would like to thank all my current and former colleagues – Dr. Bambang Wahono, Dr. Yanuandri Putrasari, Ardhika Setiawan, and all laboratory members for the many fond memories we have spent together and their valuable support during my research. This work could only be realized thanks to their unconditional help and honest feedback.

I would like to thank the sponsors of the research: National Research Foundation of Korea, Regional Innovation Strategy (RIS), Hyundai Heavy Industries Co., Ltd., and the University of Ulsan.

My special thanks go to my lovely mother, my wife Nurul Hidayah and my children, Ridwan, Shofi and Zubair. Without their unwavering support, I would not have been able to complete this important journey in my life. This dissertation is dedicated to them.

Finally, I would like to thank the members of my dissertation committee for their time and valuable comments to improve the quality of this work.

This dissertation contains all of the research conducted during the doctoral studies. The entire content of this thesis was written to partially fulfil the requirements of the PhD of Science in Mechanical and Automotive Engineering at the University of Ulsan.

Cahyani Windarto

TABLE OF CONTENTS

ABSTRACT.....	iv
ACKNOWLEDGEMENT	v
TABLE OF CONTENTS.....	vi
LIST OF FIGURES	x
LIST OF TABLES.....	xvi
NOMENCLATURES	xvii
1. INTRODUCTION	1
1.1 Background.....	1
1.2 Strategies for compression ignition engines improvement.....	3
1.3 Challenges for ignition systems and the discharge duration.....	5
1.4 Objectives of the study.....	7
1.5 Scope of the study.....	8
1.6 Thesis outline	9
2. LITERATURE REVIEW	11
2.1 Low-carbon combustion of direct-injection propane strategy	11
2.2 Ignition strategy with high-inductive discharge duration	12
2.3 Review of previous studies on in-cylinder performance, emission characteristics and combustion operating parameter optimization.....	15
2.3.1 In-cylinder performance previous studies review	16
2.3.2 Emission characteristics previous studies review	17
2.3.3 Combustion operating parameter optimization previous studies review	19
2.4 Summary	23
3. RESEARCH METHODOLOGY	25
3.1 Experiment set up	25

3.1.1	RCEM with a high spark inductive ignition platform.....	25
3.1.2	Spark plasma visualization in CVCC.....	30
3.1.3	Fuel injection test rate strategy	31
3.1.4	Propane as a low-carbon fuel for CI engine.....	33
3.1.5	Test procedure and ignition strategy	39
3.1.6	Accuracy of measurements and uncertainty	42
3.2	Simulation Model.....	42
3.2.1	Governing formulas for the in-cylinder performance	42
3.2.2	CFD modelling and simulation	44
3.2.3	Model validation	46
3.3	Summary	48
4.	EFFECT OF SPARK DISCHARGE DURATION ON IN-CYLINDER PERFORMANCES OF COMPRESSION IGNITION DIRECT INJECTION ENGINE	50
4.1	Spark discharge duration effect on the discharge energy release rate	50
4.2	Velocity distribution flow trend with varying discharge energy	52
4.3	Flow characteristics inside a cylinder	54
4.3.1	Variations in the tumble ratio for the discharge energy	55
4.3.2	Energy fluctuation in a turbulent kinetic energy (TKE) pattern	56
4.4	Impact of the spark released energy on combustion performance.....	59
4.4.1	Combustion efficiency	59
4.4.2	Cycle performance analysis	61
4.4.3	Combustion phasing period and ignition delay.....	66
4.4.4	Spark discharge source flow	69
4.5	Summary	71
5.	EFFECT OF SPARK DISCHARGE DURATION ON LOW CARBON COMBUSTION AND EMISSION	73
5.1	Effects of spark discharge duration on the combustion of CI engines	73
5.1.1	In-cylinder pressure for various spark duration timing.....	73

5.1.2	Heat release rate for various spark duration timing	75
5.1.3	In-cylinder temperature for various spark duration timing	77
5.2	Effects of spark discharge duration on performance of CI engine	79
5.3	Effects of spark discharge duration on the emissions of an CI engine	82
5.3.1	Hydrocarbon emissions (HC).....	83
5.3.2	Carbon monoxide emissions (CO).....	84
5.3.3	Carbon dioxide emissions (CO ₂).....	85
5.3.4	Nitrogen oxides emissions (NO _x).....	86
5.4	Summary	87
6.	OPTIMIZATION OPERATING PARAMETER OF SPARK DISCHARGE DURATION ON THE PERFORMANCE AND EMISSION CHARACTERISTICS	89
6.1	Modelling of artificial neural network	89
6.1.1	Data pre-processing.....	89
6.1.2	Architecture of the ANN model.....	90
6.1.3	Assessment of ANN prediction.....	92
6.2	Effects of spark discharge duration on performance of CI engine	93
6.3	Data generation for artificial neural networks optimization	95
6.3.1	Regression modelling.....	95
6.3.2	Validation of experimental data by simulation results.....	97
6.4	Optimization of in-cylinder combustion, performance and emission using genetic algorithm	100
6.4.1	Optimization of spark duration effect on the in-cylinder combustion	101
6.4.2	Optimization of spark duration effect on the in-cylinder performance.....	102
6.4.3	Optimization of spark duration effect on the emission	103
6.5	GA optimization of operating parameters optimization of spark duration effect.....	104
6.6	Validation of the optimized results	110
6.7	Summary	116
7.	SUMMARY AND CONCLUSION	118

REFERENCES	122
APPENDICES	138

LIST OF FIGURES

Figure 1.1	Pollutant reduction effects after converting vessels from HFO oil to LPG fuel use	2
Figure 1.2	Typical combustion pressure and pressure rise rate	4
Figure 1.3	Flowcharts of the strategies to obtain effects of spark discharge duration on compression ignition engine through experimental and simulation approach	8
Figure 1.4	Thesis outline	10
Figure 2.1	Connection between the coil and spark plug of the multi-coil system	13
Figure 2.2	An example of re-strike phenomena on one shot and non-averaged discharge waveforms	14
Figure 2.3	Flow speed and spark stretch relationship for the calculation of stretch distance and flow speed determination	15
Figure 2.4	Comparison of in-cylinder pressure at the injection pattern for operating	17
Figure 2.5	Regulated emissions data from all fuels	18
Figure 2.6	The ANN method's schematic process flow	21
Figure 3.1	Diagram of an improved ignition system with 10 ignition coils and measurement point	26
Figure 3.2	Three modes of ignition control strategy (a) individual mode 1 coil, (b) pair mode 2 coils, and (c) simultaneous mode 10 coils	27
Figure 3.3	RCEM with spark plug schematic diagram	28
Figure 3.4	Experimental setup of the spark plasma visualization	30
Figure 3.5	Schema of the injection fuel rate measurement	32
Figure 3.6	Comparison of emitted carbon intensity (g CO ₂ e/MJ) emissions from LPG analyzed using CA_GREET3.0.	34
Figure 3.7	Propane (LPG) product pricing in the EU28 weighted average prices versus G20 (trade) weighted average prices	37

Figure 3.8	Propane pressure-enthalpy diagram and thermodynamic paths for different thermal conditions	38
Figure 3.9	Research flow diagram organization of spark discharge study on gasoline RCEM with spark application	41
Figure 3.10	RCEM with spark model	46
Figure 3.11	Validation of in-cylinder pressure in RCEMs using different ignition strategies and propane direct injection. (a) Motoring pressure; (b) In-cylinder pressure and spark times ranging from 0.7 to 5.0 milliseconds.	48
Figure 4.1	Calculating the released current, discharge voltage, and energy	51
Figure 4.2	Spark plasma propagation in the CVCC chamber using different ignition strategy (individual 1 coil, pair 2 coils, and simultaneous 10 coils)	52
Figure 4.3	Flow velocity motif of spark release duration study on RCEM fueled with diesel and propane DI through ignition strategies (individual, pair, and simultaneous) and spark period acquired at a crank angle of $\sim 11^{\circ}$ CA BTDC with SOI propane 20° CA BTDC, spark at 15° CA BTDC, speed of 240 RPM, slice z position of -0.004 m, and slice y position of 0.01 m, in comparison to diesel RCEM auto ignition	54
Figure 4.4	The in-cylinder bore tumble ratio of spark discharge duration study on RCEM fueled with diesel and propane direct injection through ignition strategies (individual, pair and simultaneous) and spark durations ranging from 0.7 ms till 5.0 ms in comparison to diesel RCEM auto ignition	55
Figure 4.5	TKE of spark release duration on RCEM fueled with diesel and propane direct injection with ignition strategies (individual, pair and simultaneous) and spark durations ranging from 0.7 ms till 5.0 ms in comparison to diesel RCEM auto ignition	57
Figure 4.6	Streamlines the TKE flow pattern's flow visualization of spark release duration on RCEM fueled with propane direct injection with different ignition strategies (individual, pair and simultaneous) and spark durations acquired at crank angle $\sim 11.97^{\circ}$ CA BTDC with	59

	SOI 20 oCA BTDC, spark at 15 oCA BTDC, speed of 240 RPM slice z position of -0.004 m, slice y position of 0.01 m	
Figure 4.7	Combustion efficiency of spark release duration study on RCEM fueled with diesel and propane direct injection with ignition strategies (individual, pair and simultaneous) and spark durations ranging from 0.7 ms till 5.0 ms in comparison to diesel RCEM auto ignition	61
Figure 4.8	Pressure, temperature, and IHR inside the bore of spark discharge duration study on RCEM fueled with diesel and propane direct injection with ignition strategy (individual, pair and simultaneous) for various spark durations from 0.7 till 5.0 ms in comparison to diesel RCEM auto ignition	63
Figure 4.9	PRR of spark release duration on RCEM fueled with diesel and propane direct injection with different ignition strategies (individual, pair, and simultaneous) and spark durations ranging from 0.7 till 5.0 ms in comparison to diesel RCEM auto ignition	64
Figure 4.10	Torque (Nm), indicated power (kW), and power (kW) of spark discharge duration study on RCEM fueled with diesel and propane direct injection with different ignition strategies (individual, pair, and simultaneous) and spark durations ranging from 0.7 till 5.0 ms in comparison to diesel RCEM auto ignition	66
Figure 4.11	(a) Combustion phasing, (b) Combustion duration, and (c) Ignition delay, of spark discharge duration study on RCEM fueled with diesel and propane direct injection with different ignition strategies (individual, pair, and simultaneous) and spark durations ranging from 0.7 till 5.0 ms in comparison to diesel RCEM auto ignition	67
Figure 4.12	Velocity magnitude flow area around the spark plug spark release duration on RCEM fueled with diesel and propane direct injection with different ignition strategies (individual, pair, and simultaneous) and various spark durations ranging from 0.7 till 5.0 ms captured at a crank angle of ~3.98oCA BTDC with a SOI of 10oCA BTDC, spark of 5oCA BTDC, speed of 240 RPM, and slice z position of -0.004 m, in comparison to diesel RCEM auto ignition	71

Figure 5.1	In-cylinder pressure for varied spark durations between 0.7 and 5.0 ms in a propane-fueled RCEM with direct injection.	74
Figure 5.2	Heat release rate and in-cylinder temperature distribution of the RCEM combustion chamber fueled with propane-DI with spark ignition strategy for spark durations from 0.7-5.0 ms, speed 240 RPM, slice z position – 0.004 m	76
Figure 5.3	In-cylinder temperature for varied spark length between 0.7 and 5.0 ms on a propane-fueled RCEM with direct injection	78
Figure 5.4	The impact of spark lengths from 0.7 to 5.0 ms on the IMEP and indicated thermal efficiency for RCEMs powered by propane direct injection.	79
Figure 5.5	The impact of spark lengths from 0.7 to 5.0 ms on the peak of pressure rise rate and BSFC for RCEMs powered by propane direct injection	81
Figure 5.6	The impact of spark lengths from 0.7 to 5.0 ms on the peak of pressure rise rate and CA 50 for RCEMs powered by propane direct injection	82
Figure 5.7	Validation of in-cylinder pressure in RCEMs between simulation and experiment	83
Figure 5.8	(a) THC comparison on different spark ignition strategy on RCEM fueled with propane and (b) THC and BSFC comparison on different spark duration on RCEM fueled with propane.	84
Figure 5.9	(a) CO comparison on different spark ignition strategy on RCEM fueled with propane and (b) CO and indicated thermal efficiency comparison on different spark duration on RCEM fueled with propane.	85
Figure 5.10	(a) CO ₂ comparison on different spark ignition strategy on RCEM fueled with propane and (b) CO ₂ and indicated thermal efficiency comparison on different spark duration on RCEM fueled with propane.	86
Figure 5.11	(a) NO _x comparison on different spark ignition strategy on RCEM fueled with propane and (b) NO _x and indicated thermal efficiency	87

	comparison on different spark duration on RCEM fueled with propane.	
Figure 6.1	A schematic diagram of main elements used to construct ANN models	91
Figure 6.2	ANN architecture with 5 inputs, 2 hidden layers, and 6 output in this study	92
Figure 6.3	Framework of research methodology in ANN genetic algorithm system	94
Figure 6.4	RCEM with the spark model	98
Figure 6.5	Validation of in-cylinder pressure in RCEMs using different ignition strategies and propane direct injection. (a) Motoring pressure; (b) In-cylinder pressure and spark times ranging from 0.7 to 5.0 milliseconds.	100
Figure 6.6	Pareto front for optimization considering in-cylinder combustion	102
Figure 6.7	Pareto front for optimization considering in-cylinder performance	103
Figure 6.8	Pareto front for optimization considering emission	104
Figure 6.9	Variation of MSE and R2 in regard to the number of hidden neurons. (a) Mean squared error (MSE); (b) Correlation coefficient (R2)	105
Figure 6.10	Comparing in-cylinder performance estimated by ANN and actual results from experimental and simulation results for the training and validation dataset: (a) TKE, (b) HRR, (c) IMEP, (d) Indicated thermal efficiency, (d) CO, and (e) NO _x .	110
Figure 6.11	Comparison of ANN optimised results with experimental results of turbulent kinetic energy on RCEM fueled with propane direct injection at spark duration 3 ms.	111
Figure 6.12	Comparison of experimental findings from HRR of spark duration effect on RCEM powered by propane direct injection and ANN-optimized results.	112
Figure 6.13	Comparison of IMEP experimental data with ANN-optimized results for the spark discharge effect on RCEMs using propane direct injection and varied spark durations from 0.7 to 5.0 ms.	113

Figure 6.14	Comparison of experimental and ANN-optimized results of the spark duration effect on a propane-fueled, direct-injection RCEM for varied spark durations ranging from 0.7 to 5.0 milliseconds.	114
Figure 6.15	CO comparison of experimental and ANN-optimized data on a propane-fueled, direct-injection RCEM for varied spark durations ranging from 0.7 to 5.0 ms	115
Figure 6.16	Comparison of ANN optimised results with experimental results of NOx of spark duration effect on RCEM fueled with propane direct injection with ignition strategy	116

LIST OF TABLES

Table 2.1	Various ANN method for CI engine responses prediction	22
Table 3.1	RCEM specification	29
Table 3.2	RCEM operating conditions and ignition strategy	29
Table 3.3	Physical properties of fuel	31
Table 3.4	Spark discharge operating injection strategies	33
Table 3.5	The physiochemical properties of propane and diesel	35
Table 3.6	Ship bunker fuel cost estimation (Unit: US \$/MMBTU)	36
Table 3.7	Specification for propane	39
Table 3.8	Uncertainty of measured parameters	42
Table 3.9	CONVERGE key research processes	45
Table 3.10	Simulation initial and boundary conditions	45
Table 6.1	Selected ANN network parameters generated on the MATLAB framework	95
Table 6.2	Symbol used in modelling for the variables in the regression formulas	96
Table 6.3	Regression model and corresponding R2 values.	97
Table 6.4	CONVERGE key research processes	98
Table 6.5	Properties of GA algorithm in MATLAB	101
Table 6.6	Optimum combination of selected operating parameter	105
Table 6.7	The R2 coefficient and MSE calculated for the training and validation dataset based on the spark ignition strategy of the RCEM fueled with propane.	107
Table 6.8	Comparison between ANN optimized results with experimental and simulation results.	116

NOMENCLATURES

AFR	: air-fuel ratio
ANN	: artificial neural network
ATDC	: after top dead center
BMEP	: brake mean effective pressure, (Bar)
BSFC	: brake specific fuel consumption, (g/KWh)
BTDC	: before top dead center
BTE	: brake thermal efficiency
CA	: crank angle, deg
CAD	: computer aided design
CFD	: computational fluid dynamics
CH ₄	: methane
CI engine	: combustion ignition engine
CO	: carbon monoxide
CO ₂	: carbon dioxide
CoV	: coefficient of variation

CR	: compression ratio
CVCC	: constant volume combustion chamber
DPDFLTC	: dual-fuel low-temperature combustion
FIP	: fuel injection pump
GA	: genetic algorithm
GHG	: greenhouse gas
HC	: hydrocarbon
HFO	: heavy fuel oil
ICD	: ignition coil driver
ICE	: internal combustion engine
IMEP	: indicated mean effective pressure
kPa	: kilopascal
LDV	: light-duty vehicles
LHV	: lower heating value
LPG	: liquefied petroleum gas
MON	: motor octane number
MRR	: maximum pressure rise rate
NO _x	: nitrogen oxides
OEM	: original equipment manufacturer
PM	: particulate matter

RCEM : rapid compression expansion machine

RON : research octane number

SI engine : spark ignition engine

SOI : start of injection

SO_x : sulphur oxides

TDC : top dead center

THC : total hydrocarbon emissions

η_t : indicated thermal efficiency, %

P_i : indicated work/power, J/cycle

Q_{in} : input energy, J/cycle

x_n : the normalized value of variable x

x_{max} : the maximum of x

x_{min} : the minimum of x

y_{max} : the maximum of the normalized targets

y_{min} : the minimum of the normalized targets

w_i : the connected weights

x_i : the input i

p : the total quantity of inputs

b : the bias value for the neuron

η_{ith} : indicated thermal efficiency

- n_1 : the quantity of hidden layers
- n_2 : the quantity of input variables
- a : a constant that fluctuates between 1 and 10
- x_{mean} : the average value of the measured data
- x_{exp} : measured values
- x_{pre} : predicted values by ANN

1. INTRODUCTION

Internal combustion engines with compression ignition serve as power devices that are widely applied in the fields of transport, engineering machinery, stationary power generation, light duty, and other heavy-duty engines. The efficiency and lower environmental impacts of such engines have been the focus of improvement research for decades. In this chapter, the research backgrounds are introduced for the work undertaken. An overview is produced on the trends and challenges of spark ignition research on compression ignition, by correlating the relevant literature and the recent progress of the author's laboratory. The research objectives and scope are presented at the end of this chapter, followed by the outlines of the thesis.

1.1 Background

Nowadays urgent subjects include energy efficiency, reducing emissions, and supplying energy in a sustainable and environmentally responsible manner. Because liquid hydrocarbon fuels are plentiful, affordable, and practical, internal combustion (IC) engines will likely be the primary users of them in the near future [2], [3]. The continued use of energy globally is expected to drive up demand for these fuels [1]. It's critical to support and develop innovative machine technologies in order to produce extremely efficient and clean internal combustion engines [4]. Transportation, which uses 20% of the world's energy, makes up a substantial percentage of the global economy [3]. Moreover, transport is responsible for 14% of global greenhouse gas emissions [5]. Despite the fact that global maritime emissions increased from 2.76% in 2012 to 2.89% in 2018 [6]. Many nations have enacted stringent fuel consumption laws in response to growing environmental concerns, with the goal of enhancing the performance and fuel efficiency of internal combustion engines. Moreover, a target has been set to reduce greenhouse gas (GHG) emissions in the worldwide maritime industry by a minimum of fifty percent between 2008 and 2050. Reliance on hydrocarbon fuels as the main marine fuel should be gradually decreased in order to meet the low-carbon maritime transportation goal by 2050 [7]. Propane is gaining traction as a feasible 'green' transportation fuel in response to the challenge of reducing greenhouse gas emissions and transitioning to a greater use of renewable energy sources, especially for maritime applications [8] rather than using ammonia, which has also

been explored as a marine engine fuel to lower carbon emissions [9]. Natural gas is a plentiful global resource; propane is produced from the liquid components that are recovered during the processing of natural gas. Propane gas may easily be converted to liquefied petroleum gas (LPG) at the proper temperature and pressure, making it a viable substitute for liquid petroleum-based fuels [10]. Economically, shipping companies seeking to lower carbon emissions in marine operations discovered that LPG was at least as attractive as LNG as a fuel source to power their vessels. This was because LPG has lower investment costs, shorter payback periods, and less sensitivity to changes in fuel prices. Moreover, LPG provides emission benefits comparable to LNG and does not require a certain ship size, in contrast to modern marine fuels like heavy fuel oil (HFO), which leak and release marine contaminants. Fig. 1.1 illustrates the impact of switching to LPG fuel on air pollutant emissions based on the kind of oil used in the target ship. The air pollution emissions from current and LPG fuels are shown by black and red bars, respectively. It has been demonstrated that ships employing HFO (0.5% S), such as LPG carriers, had the biggest impact on reducing pollution. Specifically, it would be possible to completely remove most emissions of SO_x, PM₁₀, and PM_{2.5} and cut NO_x by about 46%.

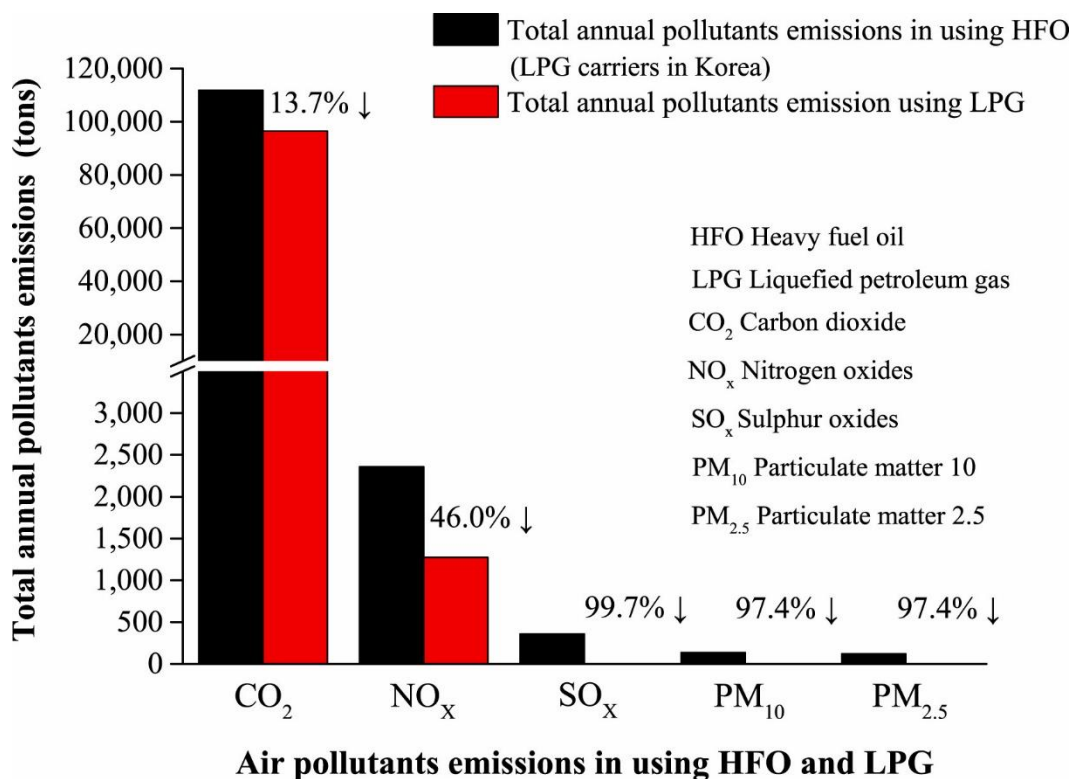


Fig. 1.1 Pollutant reduction effects after converting vessels from HFO oil to LPG fuel use (Adapted from [7]).

Research on ship-related industries is progressively favouring LPG fuel over propane and diesel for small boats due to the environmental consequences. This is because small boats, such as fishing boats, speed boats, and narrow boats, typically go through interior waterways such as lakes and rivers, where marine pollutants can have detrimental effects on fish, wildlife, and the surrounding ecology [7]. At room temperature and pressure between 760 and 1030 kPa, propane can be liquefied and combined in any volume with diesel. Consequently, compared to other gaseous fuels, LPG storage and transportation are easier. Lower heating value (LHV), octane number, cetane number, and relatively high resistance to knock are all higher in LPG compared to diesel (RON112, MON97) [11]. Given its high octane value (which translates to a low cetane number), the gasoline is potentially appropriate for use in high compression ratio CI engines [12]. It is especially appropriate for compression ignition (CI) engines, which have the ability to boost efficiency and solve the high NO_x-soot emission issue at the same time [13], this represents one of the main drawbacks of diesel engines. In terms of pollution emissions, LPG use is also advantageous for the environment. It can be used to comply with local and international laws pertaining to low sulphur levels and effectively removes sulphur emissions. The engine technology used determines how much NO_x emissions can be reduced. NO_x emissions from a two-stroke diesel engine are expected to be decreased by 10–20% when compared to the usage of HFO; on the other hand, the reduction for a four-stroke Otto cycle engine is larger and might even be below Tier III NO_x regulations. Particulate matter and black carbon emissions will be greatly decreased by using LPG as a low-carbon fuel [14]. Fuel-lean equivalency ratios indicate that compression-ignition (CI) engines use pressurized air to start combustion in place of an electrical spark, leading to comparatively reduced THC and CO emissions [15].

1.2 Strategies for compression ignition engines improvement

CI machinery are more efficient than SI engines for a variety of reasons. Because the compression stroke in a CI machine solely compresses air rather than a fuel-air blend, the machine can operate at aspect load, for example, and obtain a cycle efficiency that is rather close to optimal [16]. Moreover, CI machines are able to achieve higher compression ratios than SI machines since they do not knock under heavy loads. In theory, propane's higher octane value—which translates to a lower cetane number—makes it appropriate for use in higher compression ratio CI machines [11]. Because compression-ignition (CI) engines initiate

combustion with compressed air rather than an electrical spark, they have fuel-lean equivalency ratios and comparatively low CO and THC emissions [15]. Various novel compression ignition combustion strategies have been explored to minimize NO_x and soot emissions in-cylinder while preserving high thermal efficiency. These strategies include spark-assisted HCCI, partial fuel stratification (PFS), reactivity-controlled compression ignition (RCCI), partially premixed compression ignition, and all types of low temperature combustion (LTC). Because propane has a bigger lower heating value than diesel, it produces higher output torque and improved thermal efficiency in diesel engines [17]. By reducing the charge temperature, which lessens NO_x formation, it also helps to reduce NO_x pollutants [18]. Propane has a poor knock resistance despite having a desirable calorific value. Although propane's higher reactivity results in faster burn rates and maybe higher brake thermal efficiencies, early propane autoignition or later part knock may limit the machine's operating range (workable loads and speeds) [8]. The use of spark ignition is necessary for reliable ignition of propane due to its extremely low cetane number [10]. These considerations mean that in order to achieve high efficiency similar to a diesel engine and low emissions akin to a propane engine, a unique combustion method must be developed. To examine the impact of the spark released energy of CI engines fed with propane, the combustion and performance of a diesel machine operating only on diesel fuel—known as the diesel baseline—and running on propane are compared. Simultaneous computational and experimental fluid dynamics modelling is used for this comparison. Fig. 1.2 shows a typical pressure time curve that was obtained from the engine. The slope of the pressure time curve or the rate of pressure rise at each data point are determined using the pressure time data.

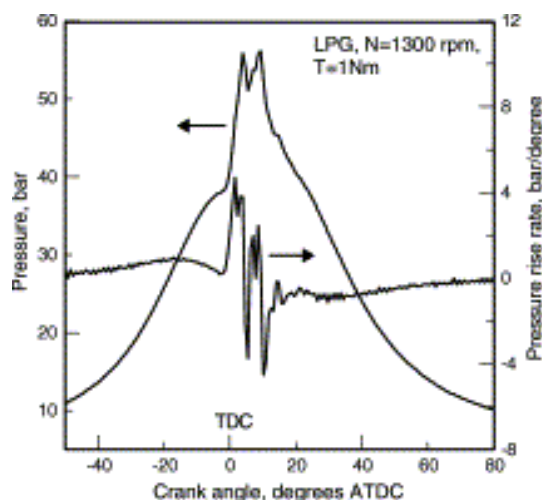


Fig. 1.2 Typical combustion pressure and pressure rise rate (Adapted from [19])

There are two gaseous fuelling strategies used in compression ignition engines. The most popular is dual fuel, which is gaseous fuel injected through the intake port [20] and diesel fuel injected directly as igniter [21]. A liquid mixture of gaseous and diesel fuel is created, known as mixed or blended fuel injection, and is used to inject the fuel directly into the cylinder. Numerous writers examined the behaviour of dual fuel combustion in different CI engines utilizing diesel and propane [12], [21], [22]. The usage of propane direct injection techniques is driven by the system's adaptation and the possible advantages of integrating it with spark application in terms of engine performance. These factors need the development of a novel combustion method to achieve low emissions similar to a propane engine and high efficiency comparable to a diesel machine. In a spark ignition system, the amount of discharge energy that reaches the spark plug depends on both spark timing and discharge current. Prior studies have demonstrated that creating flames requires more spark energy, and that flow vortices near the spark plug contribute to this as well. Both discharge current and voltage have an impact on the amount of energy transmitted to the spark electrode since spark energy is the result of their integration. The effect of discharge energy and duration on the in-cylinder pressure of the propane-powered RCEM has not yet been properly studied. Investigating the effects of released energy and the spark phase at the start of the combustion cycle is the aim of this study. Experimental and computational fluid dynamics simulation are used to compare the combustion efficiency of an RCEM modified with spark and direct injection of propane. The effects of the spark released energy on the ignition schema and the interactional correlation between the spark released energy and streamflow characteristics are also discussed. We used experimental and CFD simulation to determine the best interactions among ignition strategies. We also looked into how the multi-coil spark impacts the in-cylinder work on RCEM with a spark and fueled with liquid direct fuel injection of propane method. But the main subject of the investigation is the standard coil ignition system.

1.3 Challenges for ignition systems and the discharge duration

The ignition system of a combustion engine is an essential part that has significant implications for the environment [23]. Its goal is to generate enough energy to ignite an electrical spark in the engine bore, burning a mixture of fuel and air [24]. Examining the ignition system in particular is necessary since it initiates the machine's combustion mechanism, which modifies torque, capacity, fuel consumption, and the exhaust gas's toxicity [25]. There have been many advancements in internal combustion engine (ICE) performance [26]. One of the main

problems with combustion devices is the ignition process. In typical combustion systems, the ignition of the combustion process requires the transfer of external energy [27]. Although there are other techniques to increase the energy in the combustion chamber, the reliable, portable, and easy-to-use spark discharge method is a popular option. The energy from a spark release is classified as either capacitive [28] or inductive [29], depending on whether a coil is employed to increase the electric potential difference or if a capacitor is present in the electrical system. The amount of spark energy carried in the flow and the flow's initial composition both affect how effectively an ignition incident develops, spark gap [30], pressure, temperature [31], and turbulence rank [32]. The performance of the combustion mechanism in an ICE is dependent on the in-cylinder flow area of the machine bore. The compression and intake strokes are two combustion processes that affect the type of airflow model introduced to the engine bore during the intake phase [33]. Given their complexity and reliance on cylinder flow and ignition, these systems must be made as efficient as feasible. This requires a thorough understanding of the link between discharge energy, air flow, and plasma. It's critical to have the flexibility to adjust to the ideal efficiency zone [34]. Swirl flow and tumble flow are the two primary forms of flow in the cylinder. While the swirl flow enters the bore simultaneously with the bore turning point, the tumble flow departs the bore with a cross-wise rotation [35]. While 2-valve and 4-valve diesel machines commonly employ swirl flow analysis, 4-valve propane machines typically use traditional tumble motion [36].

Spark ignitions are commonly used to ignite an air-fuel mixture in an internal combustion engine (ICE). Most spark research in the realm of ICE has been done with the same goal in mind: to speed up the flame kernel's expansion. According to Pavel, a spark might be produced by a laser or an electrical power source [37]. The applied electrical field accelerates electrons in the air, and when a spark is lit, these accelerated electrons crash with neutral atoms and molecules. A detailed description of the spark ignition mechanism, which begins with the formation of a kernel and ends with the spread of a spark upon the application of electrical power via the reactants, may be found in [38]. The discharge zone has a very high starting pressure (200 bar) due to the quick production of spark energy [39]. Furthermore, in the flow stream near the electrode, vortices form. The construction and evolution of the kernel are complicated by the intricate flow pattern surrounding the electrodes. The flow pattern was observed using both computational and experimental methods to improve understanding. The kernel expands during this stage as internal reactions brought on by the disruption energy and spark period take place.

1.4 Objectives of the study

This study focuses on the combination experimental and simulation methods to investigate the spark discharge duration effect to improve compression ignition engine performance and emission characteristics on propane fuel combustion.

The objectives of this study are given below:

- (i) Setup an experimental system to provide the basic information to validate the simulation model. The basic data are spark discharge duration, peak pressure, peak temperature, injection rate.
- (ii) Setup a simulation model base on Converge software to estimate the engine performance and engine emission characteristic with the various spark discharge duration.
- (iii) to study the fundamental roles that the discharge current and spark duration play in the early combustion process.
- (iv) to develop a better understanding of the multi-coil spark discharge strategies.
- (v) To control and investigate the effects of spark discharge duration on in-cylinder characteristics of spark ignition direct injection engines.
- (vi) To investigate the effects of spark discharge duration on in-cylinder characteristics of compression ignition engines.
- (vii) To optimize the operating parameter of spark discharge duration on the performance and emission characteristics.

To obtain above targets, the brief explanation in the effect flowchart as seen in the Fig 1.3.

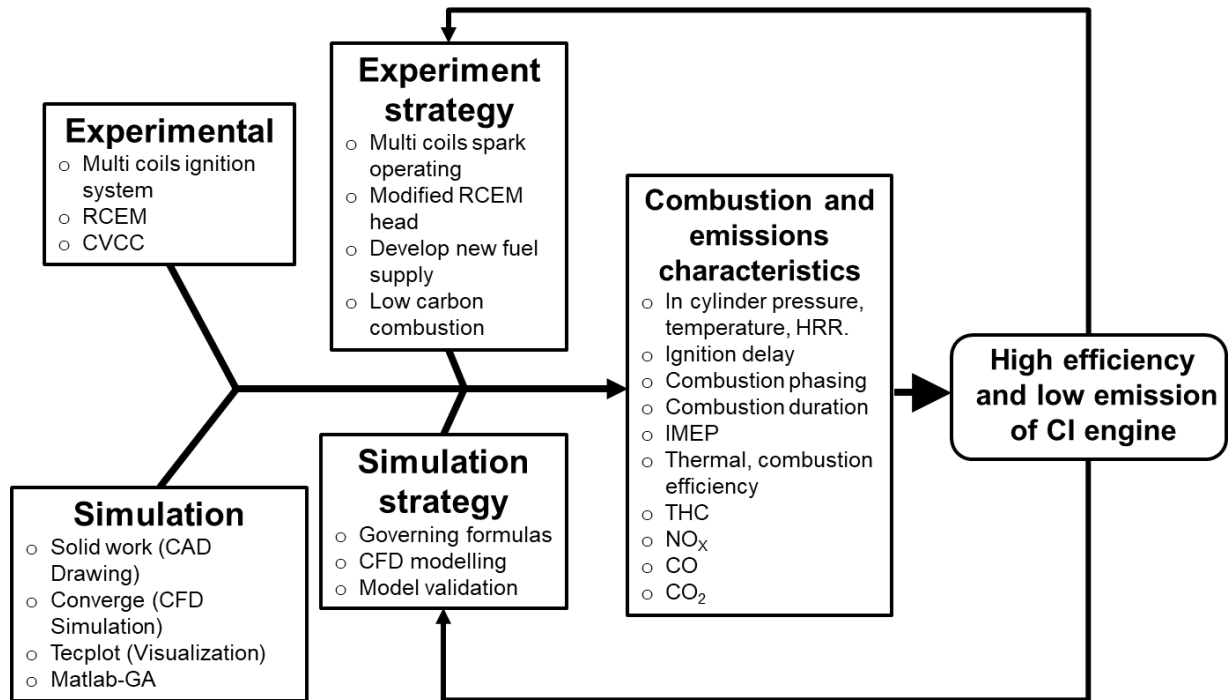


Fig. 1.3 Flowcharts of the strategies to obtain effects of spark discharge duration on compression ignition engine through experimental and simulation approach

1.5 Scope of the study

In the efforts of provides a good accuracy method to control combustion duration, prediction of exhaust residual gas and to determine optimal parameters to improve engine efficiency and engine emission. This method also helps to eliminate the drawback of the experimental method in the scope of research on engine hardware and software optimization.

The scopes of the study include:

- a. Modify cylinder head of rapid compression and expansion machine by adding spark plug.
- b. Develop a high spark inductive ignition platform using one spark plug, two spark coils, 10 simultaneous spark coils, and an ignition driver controller.
- c. Injection quantity test comparison between diesel and propane by using different injection timing, duration, and pressure.
- d. RCEM research engine experimental under the different operating condition such us spark discharge duration, start of injection, coil numbers, fueled with diesel and propane fuel.

- e. Combustion analysis for experimental works is based on cylinder pressure trace and its derivative parameters, while thermal efficiency was calculated based on fuel consumed during the combustion process.
- f. The simulation validation is taken from the experiments results from rapid compression and expansion machine research engine.
- g. The multi-functions of the simulation model are using CFD Converge version 3.0.
- h. Analysis of regular exhaust emissions such as CO, HC, NO_x, and CO₂.
- i. The NO_x, CO, CO₂ and HC emission is used to estimate the engine emission characteristics.
- j. The obtained results may only be valid for the engine used in this study.

1.6 Thesis outline

The thesis consists of seven chapters, which are organized into five main sections, as illustrated in Fig. 1.4. The first section consists of chapter 1 and chapter 2. Chapter 1 gives a briefly introduction of thesis general topic area of the spark discharge duration effect to improve compression ignition engine performance and emission characteristics, explanation how important if spark duration effect on in-cylinder performance and emission, brief introduction the effective solution which research specific aims and scope of the research. Meanwhile, chapter 2 gives a briefly literature review of the research object most closely related to the work such as: low-carbon combustion of direct-injection propane, spark ignition strategy, in-cylinder performance and emission. A briefly review of familiar previous research that has been done in this area. Highlight the gap of the research on engine optimization that has not been well researched or solved. This gap will be filling up by this thesis work.

The second section is chapter 3, in which detailed descriptions of the research methodology, engine specification, experimental system and simulation model.

The third section consists of chapter 4 and chapter 5. Chapter 4 presents the experiment and simulation results and discussion in detail of engine performance and emission of compression ignition direct injection engines. The spark discharge duration effect, velocity distribution flow trend, combustion performance will be completely studied. In chapter 5, the experiment and simulation results and discussion of spark discharge duration effect on low-carbon combustion

are explored and explained based on the effect of spark discharge duration on combustion performance and emissions of CI engines.

The fourth section is chapter 6, which presents the optimization operating parameter of spark discharge duration effect on the in-cylinder performance and emission.

The final section of this thesis is chapter 7, which comprises the summary of this research, and recommendations to the future work research outcomes, along with the additional information in the references and appendices.

Research objectives and literature review	Chapter 1. INTRODUCTION Key point: background, challenges, objectives, scope Chapter 2. LITERATURE REVIEW Key point: Low carbon, ignition strategy, review on previous study
Research platform	Chapter 3. RESEARCH METHODOLOGY Key point: experiment set up, simulation model
Research on ignition and emission characteristics	Chapter 4. EFFECT OF SPARK DISCHARGE DURATION ON IN-CYLINDER PERFORMANCES OF COMPRESSION IGNITION DIRECT INJECTION ENGINE Key point: spark duration effect, flow characteristics, impact on combustion performance Chapter 5. EFFECT OF SPARK DISCHARGE DURATION ON LOW CARBON COMBUSTION AND EMISSION Key point: spark duration effect, effect on emission
Research on optimization operating parameters	Chapter 6. OPTIMIZATION OPERATING PARAMETER OF SPARK DISCHARGE DURATION ON THE PERFORMANCE AND EMISSION CHARACTERISTICS Key point: ANN modelling, optimization, validation
Research outcomes	Chapter 7. SUMMARY AND CONCLUSION Key point: summary, future work

Fig. 1.4 Thesis outline

2. LITERATURE REVIEW

This chapter provides a summary of prior and current research on spark ignition techniques and low carbon combustion. The ignition schemes based on the traditional coil ignition system are the primary focus of the review.

2.1 Low-carbon combustion of direct-injection propane strategy

Research into alternative fuels has been done in response to the need for internal combustion engines to operate efficiently [40] and decrease of net CO₂ emissions [41] has grown during the last ten years. Compression ignition (CI) engines have been used in a number of projects to evaluate alternative fuels, including biodiesel [42], liquefied petroleum gas (LPG) [43], ammonia [44], and methanol [45]. Because propane and liquefied petroleum gas (LPG) have a lower carbon content than traditional diesel fuels, they present an appealing alternative fuel option for carbon emission reduction for CI machines, particularly in heavy-duty vehicle applications. Because of its high octane number, propane is a beneficial and eco-friendly energy source [46], sensitivity [47], high compression ratio and boost operation [48], liquid state at low pressure [49], lower fuel cost [50], permitted to utilize the present fuel transport and production systems [51], lower carbon content [52], and higher H/C ratio than conventional fuels [53]. The majority of the ingredients in LPG fuel include propane, ethane, n-butane, propene, isobutane, butene, and a trace quantity of methane [54]. Natural gas streams from oil and gas sources or as a byproduct of refining crude oil are the usual sources of LPG. The species composition of LPG fuels is significantly influenced by the extraction site, season, and processing technique. Liquid petroleum gas (LPG) is a widely used substitute fuel for internal combustion engines in a number of nations, including South Korea, the United States, Europe, Australia, and Indonesia. Its composition varies significantly between countries when used as car fuel, with propane concentrations ranging from more than 100% to as low as 50% [50].

Propane as a fuel reduces emissions significantly in a number of experimental experiments [55], [56], [57], and [58], while maintaining engine performance close to diesel. The authors' previous study [59] demonstrated the potential use of propane in high-performance compression ignition devices. Hodges et al., [12] examined the effects of propane energy

substitution % on diesel-ignited propane dual-fuel low-temperature combustion (DPDFLTC) using a single-cylinder research engine. They discovered that excessive cyclic combustion variability (COVIMEP11%) limited the maximum propane energy fraction to 90%, and the onset of engine knock (MPRR10.5 bar/deg) limited the minimum propane energy fraction to 53%. Elnajjar et al. [60], state that engine performance is significantly influenced by the following engine parameters: indicated mean effective pressure, maximum in-cylinder pressure, thermal efficiency, and maximum rate of pressure rise. Different LPG fuel compositions, however, had little to no effect on the engine's efficiency and a direct impact on the noise the engine made during combustion. Chakraborty et al. [61] demonstrated how various parametric combinations of input elements greatly influence the combustion parameter (ignition delay), power output, and emissions when using liquefied petroleum gas in diesel operation. The impact of LPG direct injection on engine emissions and performance characteristics nearing the end of the air intake phase was noted by Aydin et al. [17]. LPG fuel can be used in gaseous or liquid form in diesel engines. During the gas phase, it is created in the intake manifold and atomized in the intake air. Liquid LPG is pressurized by the high-pressure pump prior to being sent to the injection nozzle. When compared to diesel, propane fuel has been demonstrated to extend combustion at low temperatures, lessen cyclic variations, and emit fewer greenhouse gases (HC and CO). Thus, it is imperative to examine the effects of propane usage on combustion, in-cylinder performance, and emissions in high-pressure direct-injection engines.

2.2 Ignition strategy with high-inductive discharge duration

An essential part of the combustion engine is the ignition system, which also has a big environmental effect. Its goal is to produce enough energy for an electrical spark to ignite the mixture of gasoline and air in the engine cylinder [24], [62]. Because the ignition system affects the engine's combustion process, which in turn affects torque, power, fuel consumption, and the toxicity of the exhaust gas, an examination of the engine's operation is necessary [25]. Many improvement efforts have been made to enhance the efficiency of the internal combustion engine (ICE) [26]. The ignition process is a major concern for combustion devices. In typical combustion systems, ignition requires the transfer of external energy to the combustion process [27]. While there are several ways to introduce energy into the combustion chamber, a spark discharge is a common choice since it is small, easy to use, and dependable. Spark discharge

energy is categorized as either capacitive [28] or inductive [29], based on whether the spark increases the electric voltage by an electrical frequency circuit with a capacitor or a coil. It is possible to charge and discharge the coils simultaneously or alternately. The output terminals of the ignition coil are linked in series with a high voltage diode and a common spark plug, as seen in Figure 2.1. The primary purpose of the inline high voltage diodes is to allow each coil to discharge independently, particularly in situations where two coils are not charged and discharged at the same time.

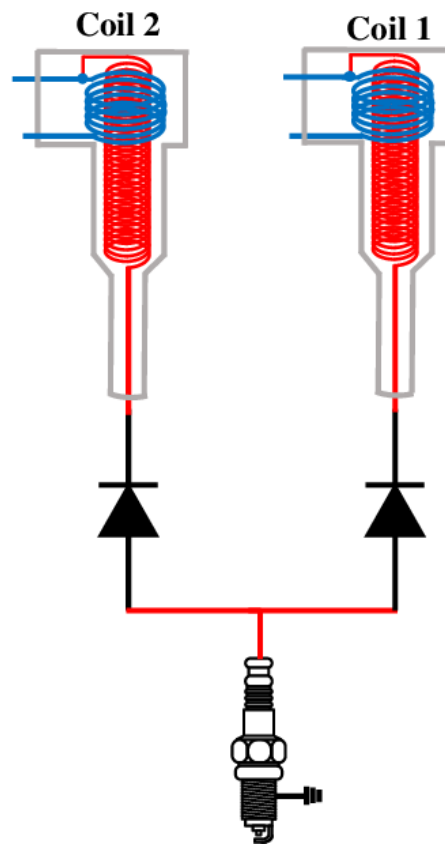


Fig. 2.1 Connection between the coil and spark plug of the multi-coil system (Adapted from [63]).

The initial makeup of the flow and the quantity of spark energy placed in it, spark gap [30], temperature, pressure[31], and turbulence level [32], all have an effect on how a successful ignition event forms [64]. During a single firing cycle ($\lambda=2.0$, discharge interval 0.4 ms), Tsuboi recorded the discharge waveforms. [29]. As demonstrated in Fig. 2.2, the discharge current abruptly increased to zero throughout the discharge period (discharge interruption) and then immediately returned to its original high current value (re-breakdown).

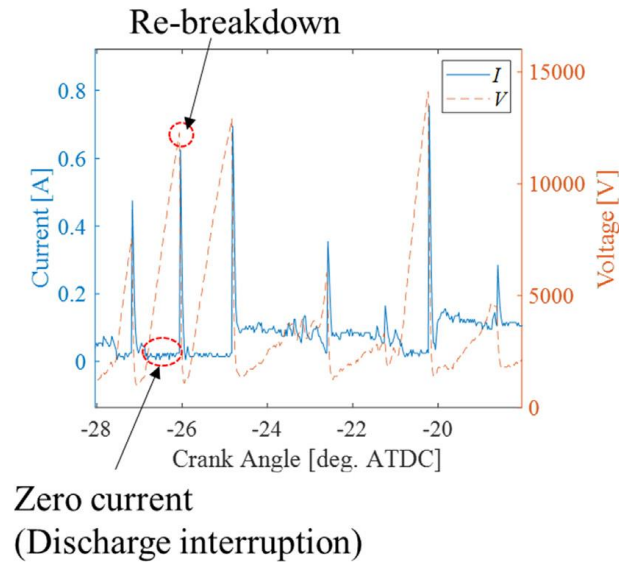


Fig. 2.2 An example of re-strike phenomena on one shot and non-averaged discharge waveforms (Adapted from [29])

The in-flow field of the engine cylinder determines how well the combustion process operates in an internal combustion engine (ICE) [65]. The character of the airflow pattern that enters the engine cylinder along with the intake stroke is influenced by two combustion processes: the intake and compression cycles [33]. To optimise these systems, one must have a solid understanding of the relationship between air flow, discharge energy, and flame because this is a very complicated system that depends on the cylinder's flow and ignition. The ability to adapt to the maximum degree of efficiency is crucial. There are essentially two forms of flow in the cylinder: swirl flow and tumble flow. The swirl flow enters the cylinder and rotates parallel to the cylinder turning point, while the tumble flow exits the cylinder and rotates transverse to the cylinder turning point [35]. Over time, several cylinder head inlet port designs in the automobile industry have been compared and the mass movement of swirl flow or tumble flow over the intake stroke has been evaluated using steady-state flow benches using dimensionless parameters like swirl and tumbling ratios. Four-valve petrol engines employ conventional tumble motion, or a tumble, whereas two-valve petrol engines and two-valve and four-valve diesel engines mostly use swirl flow analysis [36]. As seen in Fig. 2.3, Nishiyama et al. [66] investigated the movement of the spark behavior with the in-cylinder flow over the spark plug for all cycles. Thus, this data suggests a tendency towards increased flow rate, greater spark length, and shorter ignition delay. Additionally, it seems that the power of the flow and the stretch's length are slightly correlated.

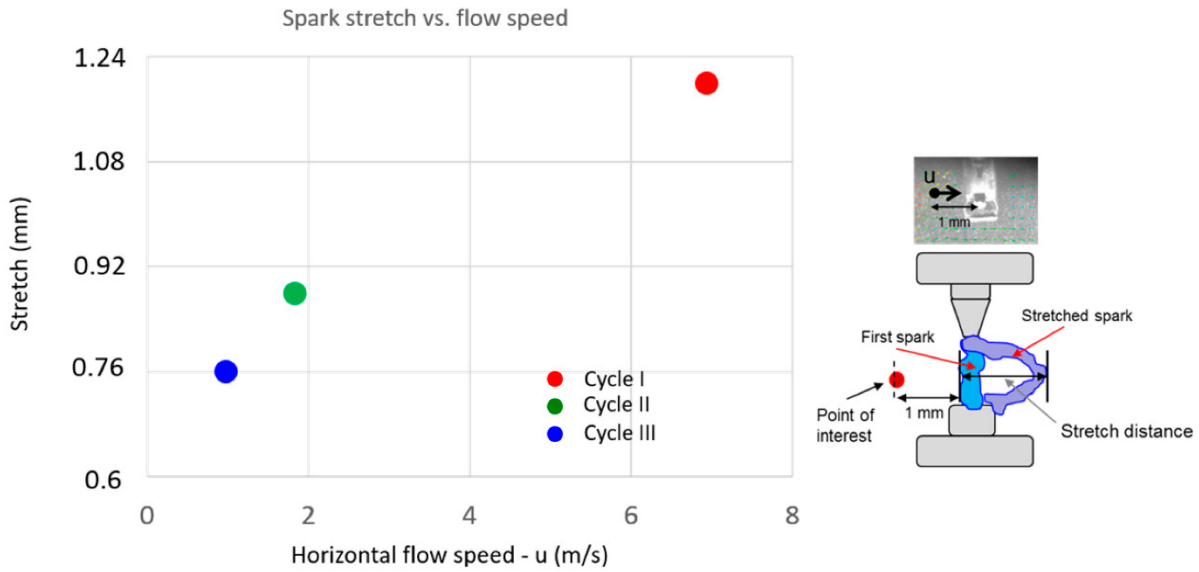


Fig. 2.3 Flow speed and spark stretch relationship for the calculation of stretch distance and flow speed determination (Adapted from [66])

One method that is commonly used to engage the burning of an air-fuel mixture on an internal combustion engine is spark ignition. The primary objective of most spark research conducted in the internal combustion engine industry has been to accelerate the growth rate of flame kernels. A laser or an electrical power source can produce a spark, claims Pavel [37]. When the spark ignites, the applied electrical field accelerates airborne electrons, causing them to collide with neutral atoms and molecules. The spark ignition process starts with the creation of a kernel and concludes with the spread of a flame through the reactants when electrical energy is introduced into the reactants. The rapid deposition of spark energy causes the initial pressure in the discharge zone to be exceptionally high (200 bar) [39]. Furthermore, the flow stream creates vortices close to the electrode [67]. Because of the complex flow pattern surrounding the electrodes, kernel formation and structure are complex processes. To gain a deeper understanding of the flow pattern, it was observed using a range of computational and experimental techniques. As a result of internal reactions resulting from the timing of the spark and the breakdown energy, the kernel grows during this time.

2.3 Review of previous studies on in-cylinder performance, emission characteristics and combustion operating parameter optimization

This section provides an overview of well-known earlier studies that have been conducted in this field. The earlier findings of research on the impact of engine performance and emission characteristics on residual gas, exhaust valve closing timing, bore-stroke ratio, port diameter-bore ratio, and combustion duration will be displayed. The shortcomings of such studies are also identified and will be addressed.

2.3.1 In-cylinder performance previous studies review

CI machinery are more efficient than SI engines for a variety of reasons. For example, a CI machine can operate at aspect load by reducing the amount of fuel injected; furthermore, because the CI machine's compression stroke compresses air exclusively, not a fuel-air mixture, the result is relatively near to the optimal cycle efficiency [16]. Moreover, CI machines are able to achieve higher compression ratios than SI machines since they do not knock under heavy loads. In theory, propane's higher octane value—which translates to a lower cetane number—makes it appropriate for use in higher compression ratio CI machines [11]. Engines using compression-ignition (CI) result in comparatively minimal emissions of THC and CO [68] and fuel-lean equivalence ratios since they initiate combustion with compressed air rather than an electrical spark [15], [69]. Because propane has a bigger lower heating value than diesel, it produces higher output torque and improved thermal efficiency in diesel engines [17]. Because propane has a bigger lower heating value than diesel, it produces higher output torque and improved thermal efficiency in diesel engines [17]. Additionally, by lowering the charge temperature, which lessens NO_x formation, it helps to reduce NO_x pollution [18]. In order to reach a consistent NO_x target, Ianniello et al. [70] investigated a single-cylinder engine using two fuels: diesel and LPG, in volume ratios of 20/80 and 35/65, running at 1200 rpm per 2 pressure and 1500 rpm per 5 bar, respectively. As illustrated in Fig. 2.4, they found that an increase in engine load led to a longer peak combustion duration because of the cooling effect on the in-cylinder charge, which enhances premixed combustion prior to the main combustion phase (mixing controlled combustion).

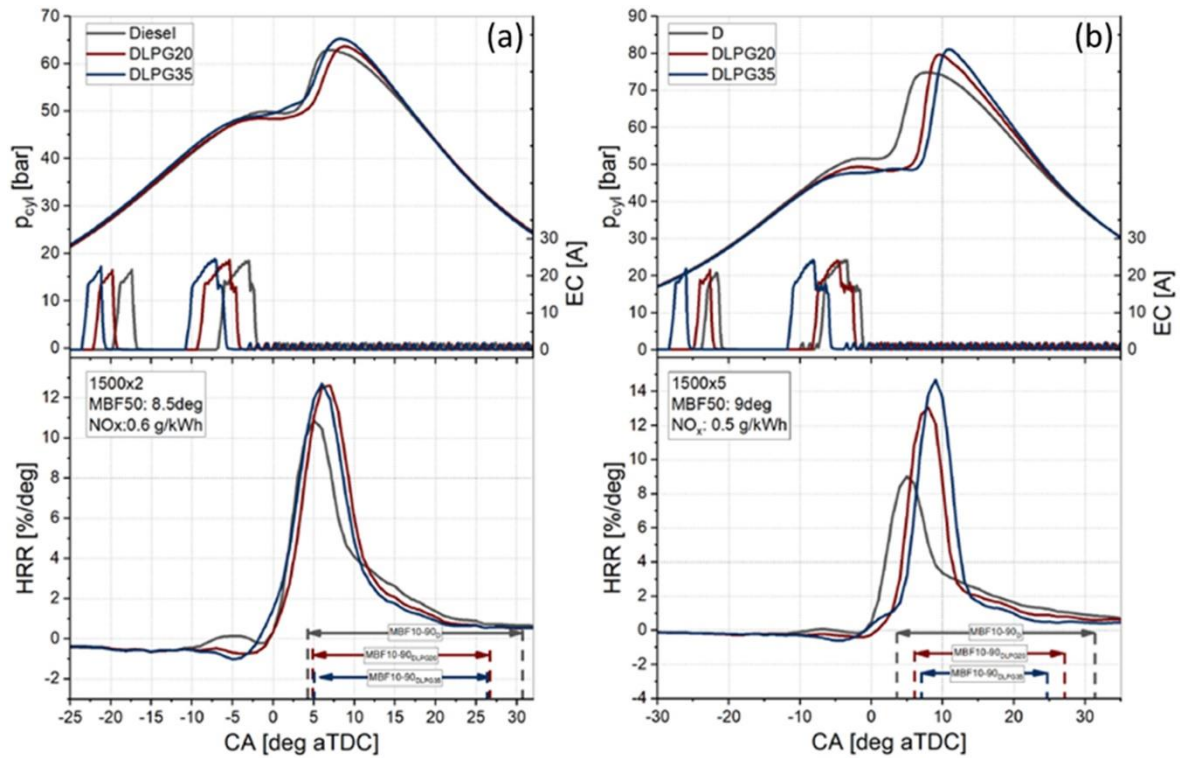


Fig. 2.4 Comparison of in-cylinder pressure at the injection pattern for operating (Adapted from [70])

Propane has a poor knock resistance despite having a desirable calorific value. Although propane's higher reactivity results in faster burn rates and maybe higher brake thermal efficiencies, early propane autoignition or later part knock may limit the machine's operating range (workable loads and speeds) [8]. The use of spark ignition is necessary for reliable ignition of propane due to its extremely low cetane number [10]. These data indicate that in order to achieve high efficiency similar to a diesel engine and low emissions similar to a propane engine, a unique combustion method must be developed. To examine the impact of the spark released energy of CI engines fed with propane, the combustion and performance of a diesel machine operating only on diesel fuel—known as the diesel baseline—and running on propane are compared. Simultaneous computational and experimental fluid dynamics modelling is used for this comparison.

2.3.2 Emission characteristics previous studies review

Various combustion processes have been developed to satisfy fuel economy and emission standards. One such method that has garnered a lot of interest is direct injection, which involves injecting fuel directly into the cylinder using a high-pressure fuel delivery system [71]. Evaporating the fuel that is directly pumped into the combustion chamber is an easy way to

reduce its temperature [72]. A higher charge density results in improved volumetric efficiency [73]. Propane is thought to be a practical solution for lowering particle emissions, which will eventually lower NOX emissions [74] when used with diesel engines [55]. For a particular car or engine, Ryskamp gave a graphic illustration of the high standard deviation and coefficient of variation for LPG. The 75th and 25th quartiles of the data are represented by the upper and lower ranges of the box in Fig. 2.5, while the maximum and minimum values of the data are indicated by the upper and lower edges of the whiskers. The data average is represented by the asterisk, the median is shown by the line across the box, and statistical outliers from the data set are shown by the independent crosses. When there is a negative percentage difference, the vehicle powered by LPG produced fewer emissions than the comparator, and vice versa.

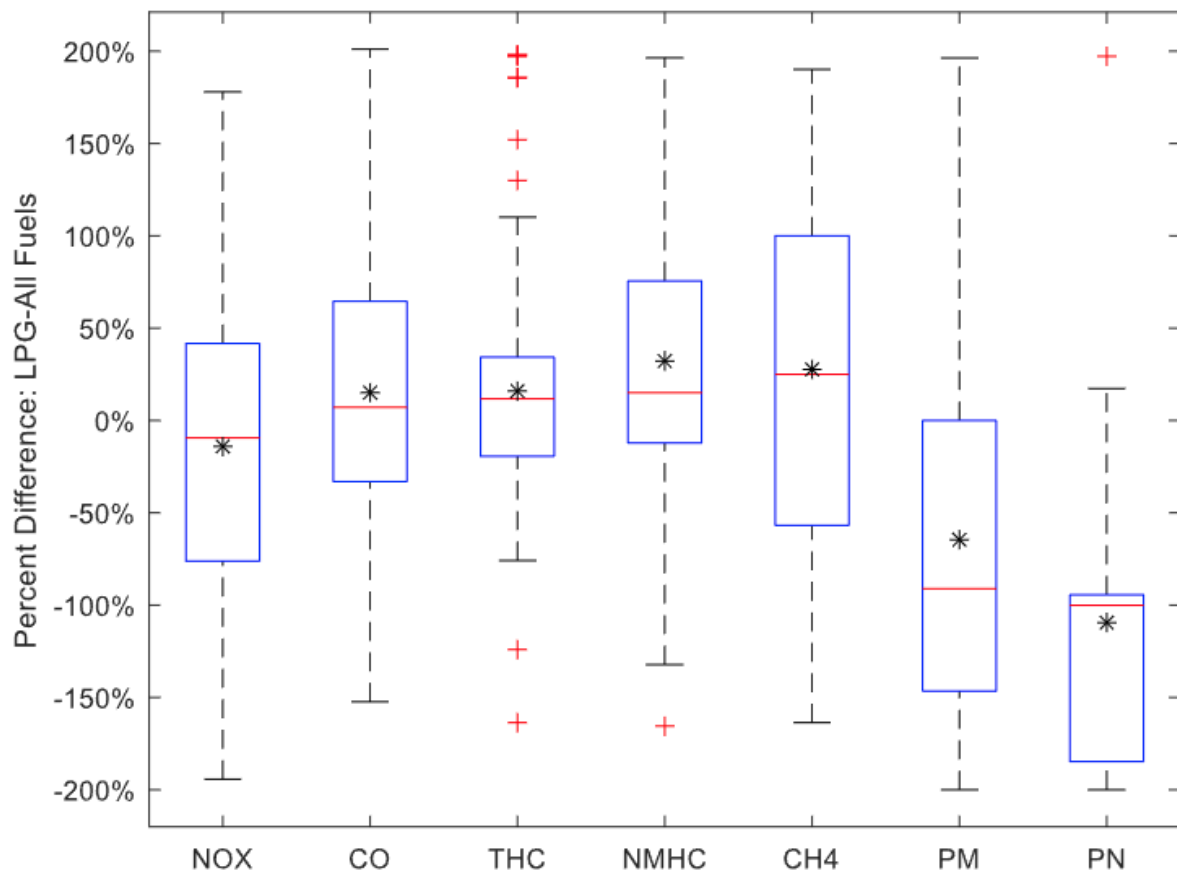


Fig. 2.5 Regulated emissions data from all fuels (Adapted from [75])

Nevertheless, its primary drawbacks are that it is difficult to employ in compression-ignition engines due to its low cetane number [10] and poor auto-ignition behavior [76] This poses a challenge for engines that use compression ignition. Therefore, in order to attain high efficiency comparable to that of a diesel engine while producing the fewest emissions possible, a novel

combustion technique needs to be created. Previous research has shown that flame formation benefits from higher spark energy [24], [29], [30]. Nevertheless, not much research has been done on how long of a discharge affects emissions, in-cylinder performance, and combustion in low-temperature direct-injection propane combustion. Characterizing the combustion behavior of propane-fueled CI is necessary to verify that the engines can operate as needed with the anticipated discharge time alterations. An analysis of the efficiency and emissions of direct-injection propane combustion at low temperatures is also necessary, given the kinetic interaction that propane has with the thermodynamic states inside the cylinder. Using high-pressure direct injection of propane and spark modification, this study begins with an experimental investigation in an RCEM to ascertain the effects of discharge time on emissions, in-cylinder performance, and combustion while burning propane with low-temperature direct injection.

2.3.3 Combustion operating parameter optimization previous studies review

Diverse combustion techniques have been created to meet fuel economy and environmental requirements. Direct injection is one of these that has garnered a lot of attention [71]. It includes using a high-pressure fuel delivery system to feed petrol straight into the cylinder. One easy technique to lower the temperature in the combustion chamber is to allow the fuel that was directly injected to evaporate [72]. This increases the charge density and enhances volumetric efficiency [73]. Propane is considered a viable option for reducing particle emissions and eventually NO_x emissions when used with diesel engines [55]. Despite the low cetane number of propane making it challenging to use in compression-ignition engines [10] and poor auto-ignition behavior [76], these factors are its principal drawbacks. To achieve high efficiency—on par with a diesel engine—while producing minimal pollution, a unique combustion method needs to be developed. Previous research have found that increased spark energy is beneficial for flame production [24], [29], [30], and [77]. Nevertheless, the effects of spark discharge duration on low-temperature direct-injection propane combustion emissions, in-cylinder performance, and combustion have not been thoroughly studied. Reducing exhaust pollution and increasing engine efficiency are mutually exclusive. Because multiple operational parameters control engine performance and emissions, there is no short cut to determining the ideal operational parameter values. Extensive experimental experiments can be used to achieve this, but they cost money and time [78]. Consequently, in order to achieve objectives,

optimisation is surely necessary to find the optimal combinations of operational parameters, such as compression ratio, commencement of injection, load, and equivalency ratio in propane.

Input parameters for the artificial neural network model included the mix %, engine workload, compression ratio, and equivalency ratio. Engine output parameters, such as BTE, BSFC, CO, unburned HC, and NO_x, were computed. A genetic algorithm was used by Liu et al. [79] to simultaneously optimize the fuel consumption, NO_x emissions, and CH₄ emissions of a dual fuel engine powered by natural gas and diesel. Li et al. [80] found a more effective technique to lessen nitrogen oxide (NO_x) emissions and improve fuel economy by combining an artificial neural network (ANN) and genetic algorithm (GA) with less computation time. In order to optimize the six reaction rate parameters within specified uncertainty limits, DeVescovo et al. [54] employed a genetic algorithm technique to execute RCM simulations and compare the results to two separate sets of known literature ignition delay lengths for propane. ANN output values have been predicted and compared to experimental values in a number of studies, demonstrating the degree to which the projected values agree with the values discovered via experimentation. The neural network toolbox of MATLAB R2017b served as the primary inspiration for the creation of the ANN model, whose learning rate and training epochs were set at 0.001 and 1000, respectively. The process flow of the ANN approach for training and predicting the effects of spark discharge energy on the in-cylinder performance of a large bore compression ignition engine is schematically represented in Fig. 2.6.

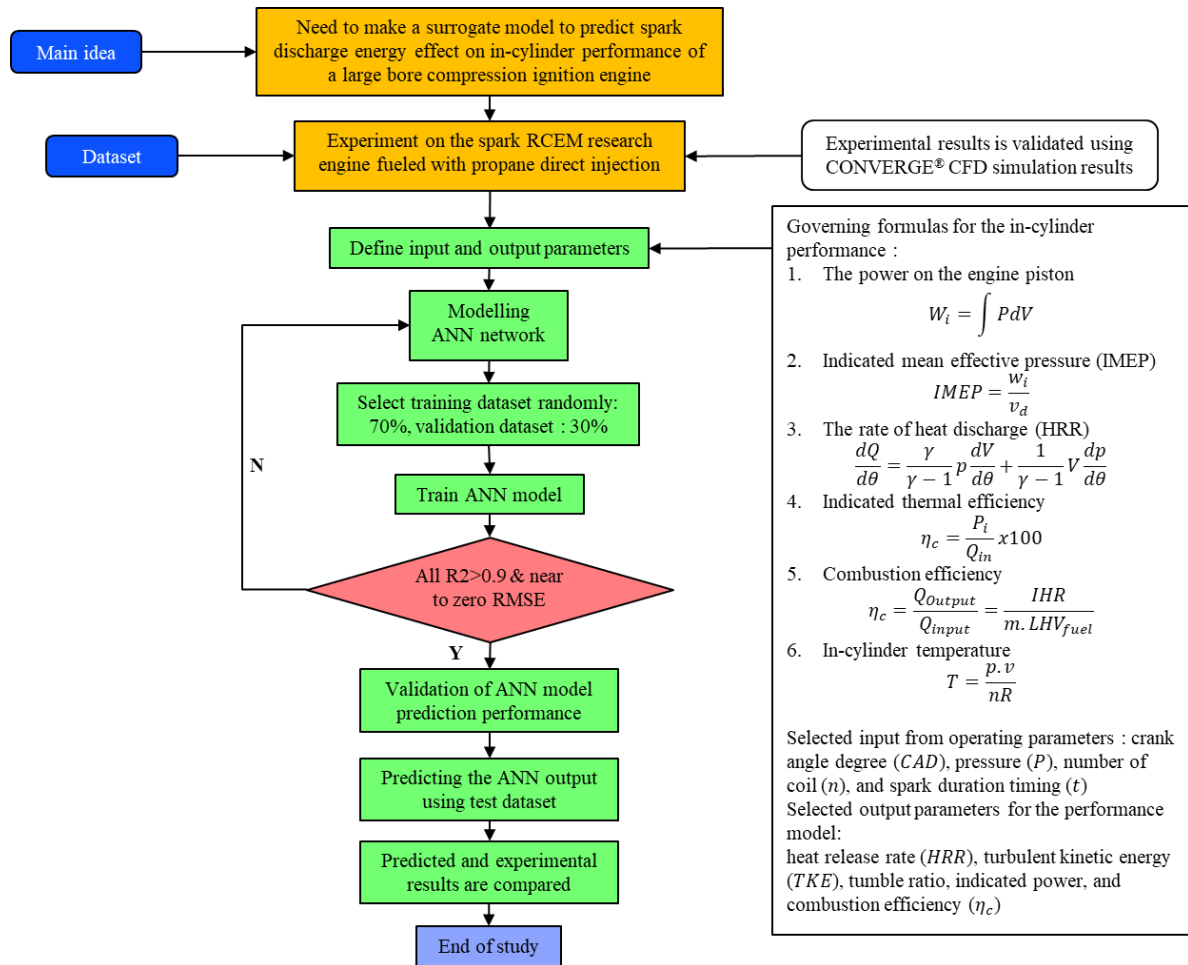


Fig. 2.6 The ANN method's schematic process flow

Selected research on artificial neural networks for predicting the required compression ignition engine characteristics is shown in Table 2.1. Effective predictions are produced with input parameters that span the whole issue domain under investigation. There are chosen numbers of neurons in the first and second hidden layers, respectively, to ensure that every input contributes evenly to the ANN. The activation function of the network was linear in the output layer and tan sigmoid in the hidden layer. The back-propagation technique is a widely used method for training networks. Because it can train small and medium-sized networks and handle non-linear difficulties, the feedforward network training methodology known as the Levenberg-Marquardt method is employed.

Table 2.1. Various ANN method for CI engine responses prediction.

Author	ANN Method (algorithm)	Input parameters	Output parameters	Main finding
Mebin et al. [81]	Feed-Forward Backpropagation	Load, DTBP, RH, Water	BSFC, BTE, CO, HC, NO _x , and Smoke	The use of ANN to predict multi-component fuel mixtures improves in reducing the quantity of experimental work required to determine engine output characteristics.
Channapattana et al. [82]	Levenberg-Marquardt back propagation	CR, SIT, FIP, Load, Blend	BTE, BSEC, EGT, CO, CO ₂ , NO _x , HC, Smoke	The ANN model can forecast engine combustion and emission behaviour under various operating situations.
Babu et al. [83]	Back-propagation multilayer perceptron feed-forward neural network (BPNN) - Levenberg-Marquardt	PrIT, MIT, PIT, Test fuels	BSEC, BTE, ID, CD, CPP, CO, CO ₂ , UBHC, NO, Smoke	To forecast the output more accurately, an artificial neural network is recommended above other theoretical and empirical models.
Seo et al. [84]	Multi-layer, feedforward neural network	vehicle specific power, velocity, engine speed, engine coolant temperature and engine torque	CO ₂ , NO _x , HC total, and CO emissions	During the cold start period, the suggested ANN models correctly anticipated fast increases in carbon monoxide, hydrocarbons, and nitrogen oxides.
Hoang et al. [85]	ANN	Load, Fuel blend, Injection	BTE, EGT	The ANN model may be capable of accurately predicting engine behaviour to a level over 95%.
Foroutani et al. [86]	Standard back-propagation learning algorithm	Injection timing, fuel type, fuel consumption	Indicated power, thermal efficiency, No _x , PM, CO, CO ₂	The findings for the best ANN model demonstrated that the built model accurately predicted the operation and pollutants of the CI diesel engine.
Farzad et al. [87]	The back propagation learning algorithm	Percentage of biodiesel, engine speed, engine load	$T_{exhaust}$, SFC, Power, Torque, CO, CO ₂ , HC, NO _x	With determination coefficient (R^2) values quite closer to 1, the ANN estimated data closely matched the experimental results overall, demonstrating great accuracy.
Fang et al. [88]	Levenberg-Marquardt algorithm	Speed/load condition, exhaust back-pressure, boost pressure, inlet Temperature, and , rail pressure	IMEP, NO _x , volumetric efficiency, brake power	The ability of ANN to forecast pollutants outside of its training variety with a high degree of precision makes it a valuable tool for directing future experimental and numerical research on NO _x emissions.
El-Shafay et al. [89]	Feed-forward back propagation	Engine speed, load, fuel-blend ratio	BSFC, BTE, T_{exh} , AF equivalence ratio, HC, CO, NO _x , smoke, ID	When contrasted with diesel powered by Palm biodiesel mixes, ANN is an efficient modelling technique with great accuracy in engine performance, combustion, and emission cuts.
Niu et al. [90]	Support Vector Machine (SVM)	Pressure, injection timing, temperature	Engine response	The comparative study of ANN and SVM shows that ANN may converge to local minima and encounter an overfitting issue, but SVM can discover the best global solution with less experimental data and has strong generalisation and prediction accuracy capabilities.
Taghavifar et al. [91]	Levenburg-Marquardt	Crank angle, heat release rate, SMD, NO _x , pressure	Chemical availability, thermos-mechanical, irreversibility rate	Neural network-based data analytics can offer a suitable method in diesel engines for increasing energy efficiency and lowering pollutants.

2.4 Summary

This chapter gives an introduction of research engine and a literature review about the effect the spark discharge effect on ignition and emission characteristics of LPG engine using RCEM. All previous studies have focused on the behavior of dual fuel combustion using propane and diesel in various CI engines.

The usage of propane direct injection techniques is driven by the system's adaptation and the possible advantages of integrating it with spark application in terms of engine performance. Given these factors, a combustion strategy must be developed to provide low emissions similar to a propane engine and high efficiency akin to a diesel machine. In a spark ignition system, the amount of discharge energy that reaches the spark plug depends on both spark timing and discharge current. Previous studies have demonstrated that creating flames requires more spark energy, and that flow that generates vortices around the spark plug also contributes to this. Both discharge current and voltage have an impact on the amount of energy transmitted to the spark electrode since spark energy is the result of their integration. The effect of discharge energy and duration on the in-cylinder pressure of the propane-powered RCEM has not yet been properly studied. This study aims to investigate the effects of released energy and the spark phase at the start of the combustion cycle. In addition to comparing the effects of the spark released energy on the ignition schema and the interactional correlation between the spark released energy and streamflow features, the combustion efficiency of an RCEM modified with spark and direct injection of propane is also contrasted, using both experimental and computational fluid dynamics simulation. In order to determine the best interactions among ignition strategies, we used experimental and CFD simulation to examine how the multi-coil spark affects the in-cylinder work on RCEM with a spark and fueled with liquid direct fuel injection of propane method. We also looked into how far the in-cylinder stream field impacts to the spark flame.

Therefore, a three-dimensional (3D) computational fluid dynamics (CFD) model of the test engine was numerically represented in order to comprehend the principles of the emission processes at various spark discharge durations. Models of computational and experimental fluid dynamics were employed for study. The development of an internal RCEM prototype that has been modified with spark discharge and outfitted with a high-pressure direct propane

injection system using a common rail injection control mechanism is what makes this study novel. With these characteristics, the current study stands out from previous research on the behaviour of propane in compression ignition engines and compares the effects of spark duration on in-cylinder combustion, performance, and emissions in RCEM research engines.

3. RESEARCH METHODOLOGY

This chapter details the research platforms of experiment and simulation used for the empirical study. Three types of experiment platforms are employed: (1) a set high spark inductive ignition platform; (2) a set of constant volume combustion chambers, with optical access for high-speed imaging; and (3) a rapid compression and expansion research engine modified with spark plug. Meanwhile, simulation platform is employed using CFD Converge.

3.1 Experiment set up

3.1.1 RCEM with a high spark inductive ignition platform

The experimental system and research engine are introduced in this section. Rapid compression and expansion characterise the research engine. The experimental setup's sole goal is to provide credible simulation model support for fundamental engine behaviour data, including ignition characteristics, in-cylinder pressure, cylinder pressure, cylinder temperature, and engine torque. Below is an introduction to the experimental system and research engine in detail. An ignition driver controller, two spark coils, ten simultaneous spark coils, one spark plug, and two spark plugs were used to create a high spark inductive ignition platform for this study. As shown in Fig. 3.1, two sets of ignition coils were connected and paralleled with a single spark plug. Each ICD-212 ignition driver was connected to a discharge coil. MOBIQ used an ICD-212 ignition coil driver, which provides three different modes of ignition control: simultaneous mode (parallel simultaneous output for all coil channels), individual mode (series of individual outputs for each coil channel), and pair mode (series of pairing two coil channels). It is possible to change the ignition signal timing between channels from 0.7 to 65.4 ms. The second ignition signal was sent in the time domain that matched the timing of the first ignition signal after it had been transmitted. The ICD-212's block scheme schematic and discharge voltage waveforms are shown in Fig. 3.2.

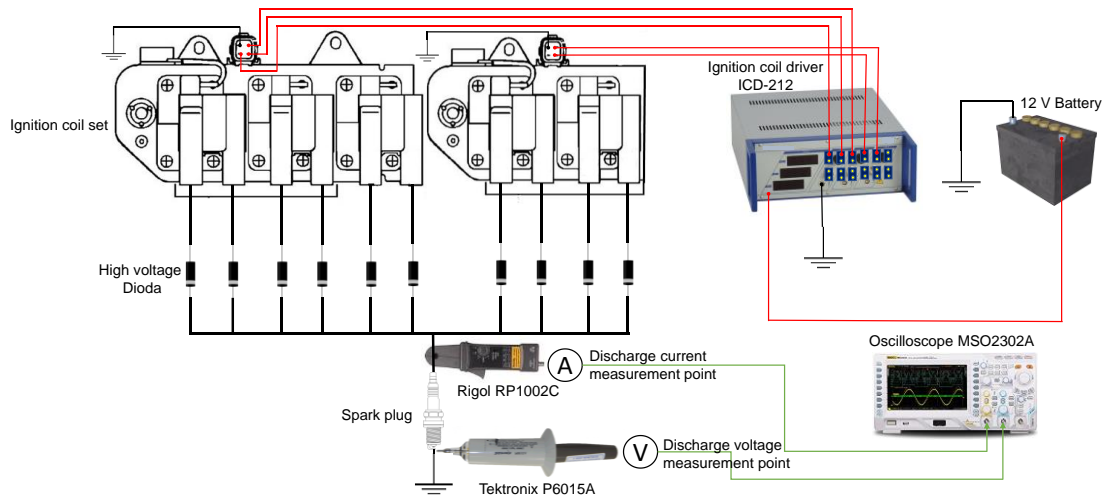


Fig. 3.1. Diagram of an improved ignition system with 10 ignition coils and measurement point

The primary current between the battery and the ignition coil was measured using a Rigol RP1002C ammeter, which has an accuracy of $\pm 3\%$ or $\pm 20\text{mA}$. To measure the discharge voltage and current, the high-voltage probes—Tektronix P6015A, which has an accuracy of $\pm 1.5\%$, and Rigol RP1002C—were assembled. Measurements of discharge voltage and current were obtained with an MSO2302A oscilloscope. The electrode spark plug for the HR7PSP11 was attached to the high-voltage line. The electrodes of the HR7PSP11 electrode spark plug were made of fine-tipped iridium wire. A high-voltage diode, HVRL300, was positioned between the spark plug and the ignition coil. This stops the stream from flowing in the other direction while allowing it to flow freely in the desired direction. The spark plug gap is 0.9 mm, and the diameters of the center electrode's and ground electrode's wire tips are 0.7 mm. The formation and propagation of flame kernels are influenced by the flow direction, the flow structure's size, and its energy content. In order to allow for the greatest amount of spark-channel stretch feasible, the spark plug was positioned so that the ground electrode was perpendicular to the direction of in-cylinder flow.

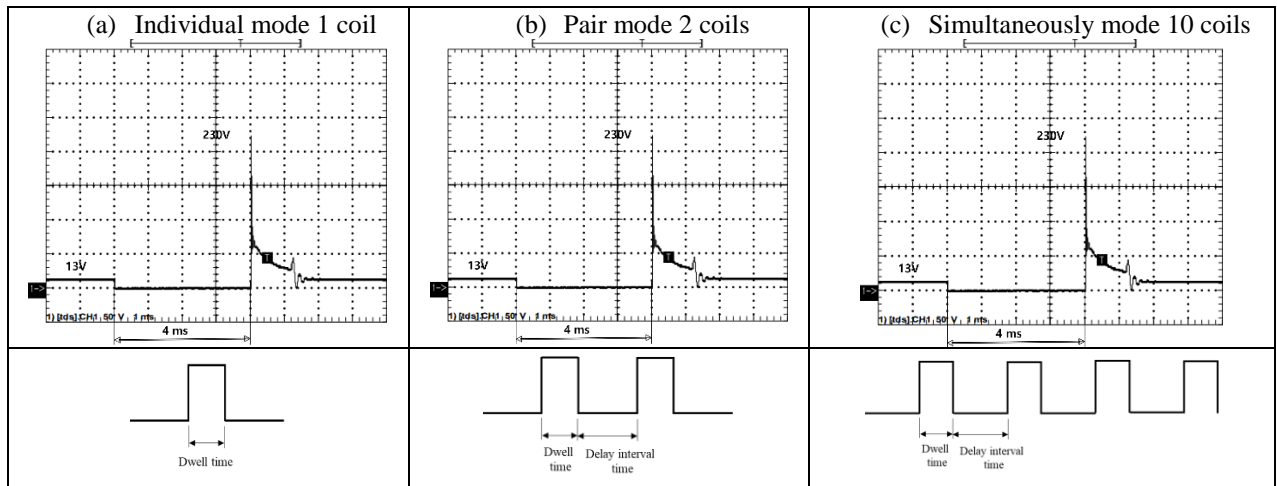
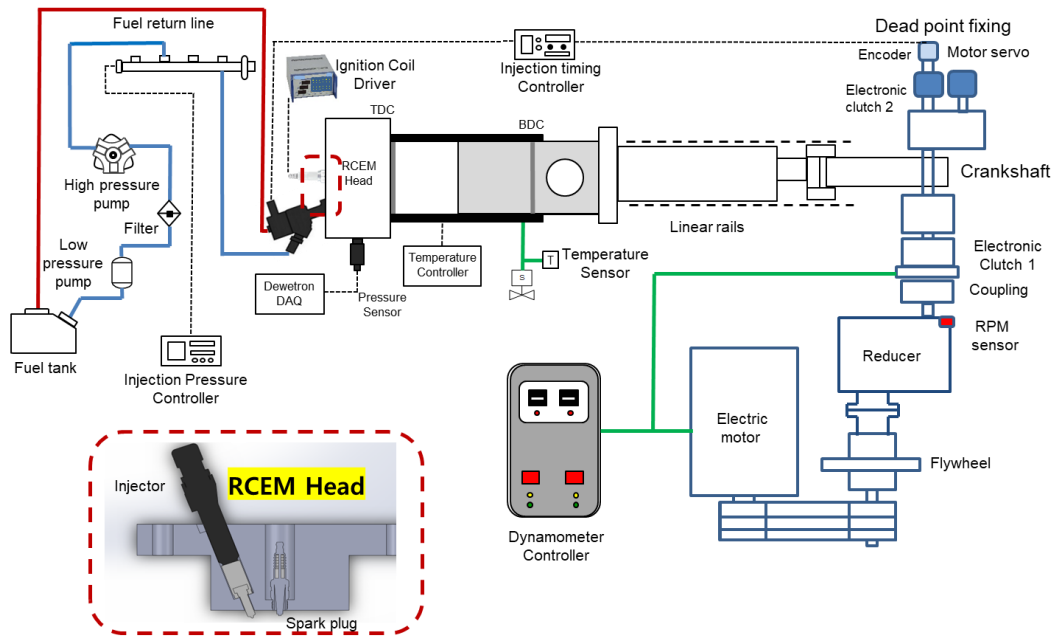
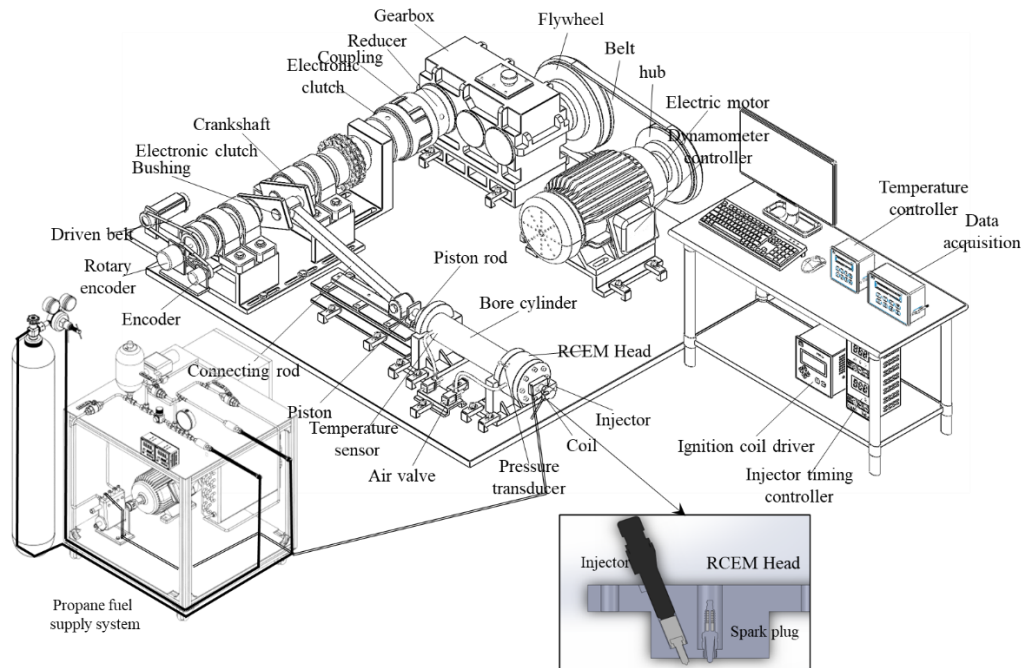


Fig. 3.2. Three modes of ignition control strategy (a) individual mode 1 coil, (b) pair mode 2 coils, and (c) simultaneous mode 10 coils

The RCEM was used to reproduce the features of a CI system during the single cycle of the experiment. RCEM can be used to study a single rapid compression cycle of a tested fuel in a precisely defined and regulated environment, without the complicated fluid dynamics features of a traditional ICE engine. A spark plug-equipped RCEM schematic diagram is displayed in Fig. 3.3. Powered by a 22-kW electric motor, it features a 100-mm bore and 450-mm stroke. Table 3.1 provides an overview of the research engine's features. The compression ratio of the flat-top piston in the RCEM research engine can be adjusted from 10 to 23 by adjusting the screw located at the piston shaft's base. In order to track the correctness of the starting temperature—which has the potential to reach 393 K—temperature sensors were installed in the RCEM cylinder body, TDC, and BTDC. To track the pressure inside the cylinder, a Kistler 5018 amplifier and a piezoelectric pressure transducer with an accuracy of ± 0.005 readings are used. With a resolution of 0.1 degrees of crank angle, an Autonics rotary encoder type E40S8-1800-3-T-24 was used to measure the crank angle position. The sensors were fastened to a Dewetron type DEWE-800-CA acquisition device in order to capture the information. To control the timing and duration of the injection, the fuel injector was fitted with a Zenobalti type ZB-5100 common rail solenoid injector peak & hold driver and a Zenobalti type ZB-8035 multi-stage injection mechanism.



(a) Schematic diagram



(b) RCEM Setup

Fig. 3.3. RCEM with spark plug schematic diagram

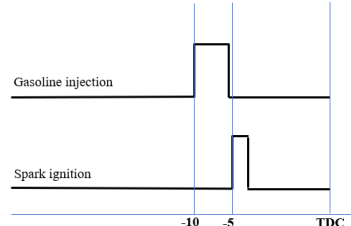
It is more difficult to ignite gasoline at light to medium loads when compression ignition is used [92]. The effect of input temperature on petrol compression engines has been the subject of numerous investigations. In order to maintain normal combustion, the intake temperature was maintained at 80 degrees Celsius during this experiment. This should have very minor

effects on the indicated mean effective pressure, the greatest pressure increase rate, and the combustion phasing. Utilizing an experimental setup based on established parameters, the RCEM fueled propane with spark model is used to adjust the amount of energy discharged in the ignition strategy by varying the amount of energy based on the coil configuration calculation. Next, a compression ratio of 17 was applied to it in order to obtain the same compressed-gas pressure for the adiabatic condition and experiment. In fact, it presents a challenge for future research to evaluate the in-cylinder characteristics of the spark ignition engine (CR 10) near compression ratio and to use diesel as the pilot for dual fuel injection propane and diesel. Table 3.2 displays the engine operating conditions and injection techniques.

Table 3.1. RCEM specification

Engine Parameters	Value
Displacement	3535.71 cm ³
Stroke	450 mm
Bore	101 mm
Compression Ratio	17
Crank Radius	225 mm
Con. Rod Length	900 mm
Piston type	Flat top

Table 3.2. RCEM operating conditions and ignition strategy

Parameters	Unit	Value
Speed	RPM	240
Inj. Pressure	MPa	50
Injection timing	CA	10 BTDC
Injection quantity	mg	127.5782
Injection mode		
Spark timing	CA	5 BTDC
T intake (°C)	°C	30
T heater (°C)	°C	80

3.1.2 Spark plasma visualization in CVCC

Experiments on spark plasma flame visualisation in ambient air were conducted using a constant volume combustion chamber (CVCC). The CVCC system consists of the glass chamber, computer system, driver controller, ignition system, intake system, and National Instrument DAQ. In order to test the interior of the chamber with a mirror lens and cameras set up, two quartz facings will be placed. An engine controller from Zenobalti multistage injection type ZB-8035 controls the number of spark cycles, while a Zenobalti hold driver type ZB-5100 device synchronises the ignition timing with the controller and high-speed camera. The optical setup used in this experiment was constructed using the Schlieren imaging method. Halogen lamps, high-speed cameras, and spherical concave mirrors with 150 mm diameters and 2000 mm focal lengths are used to take the spark plasma images from the chamber. An experimental arrangement of the optical structure is shown in Fig. 3.4. Images were captured with a Photron high-speed camera type SA3, equipped with an objective optical lens of 60 mm, namely the AF Micro-Nikkon, with an aperture of f/2.8 in collinear mode at 10,000 frames per second and 512x256 pixel resolution.

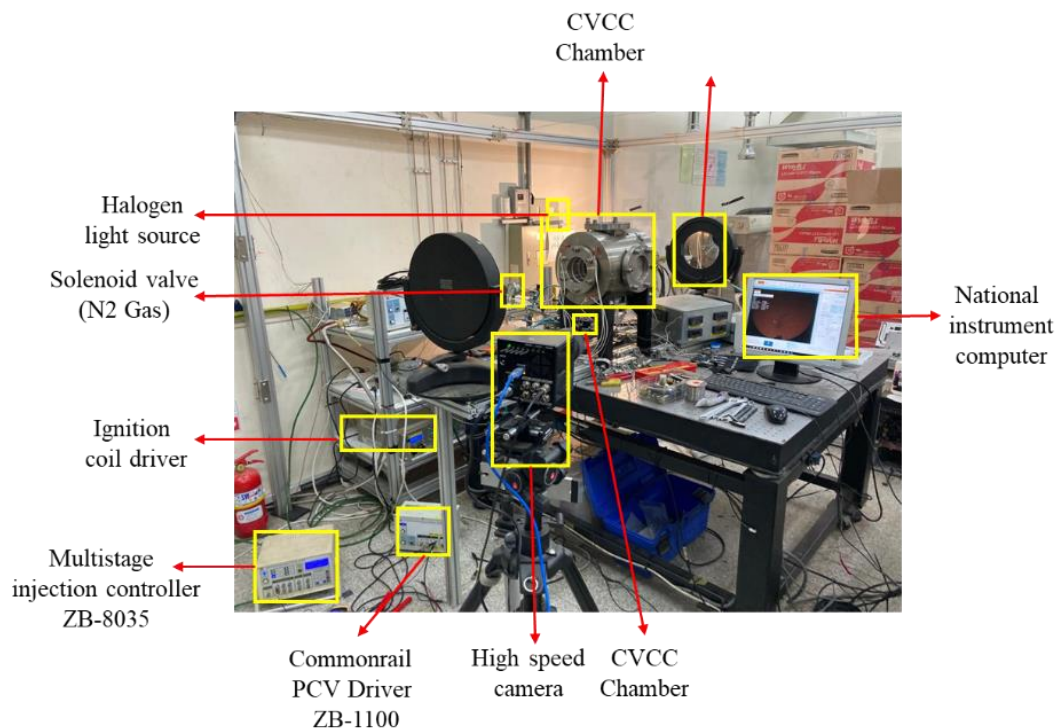


Fig. 3.4. Experimental setup of the spark plasma visualization

3.1.3 Fuel injection test rate strategy

The characteristics of petrol and diesel laboratory testing, as per an international standard, are displayed in Table 3.3. A Bosch 7-hole injector, model 0445110 327, coupled to an injection rate monitoring device allowed for the determination of the injection flow rate. An engine controller of Zenobalti multistage injection type ZB-8035 in conjunction with a peak and hold driver common rail solenoid injector type ZB-5100 was used internally to activate the injector solenoid and regulate the timing of the SOI. A common rail PCV driver ZB-1100 and a three-phase electric motor controller kept an eye on the injection pressures, which were kept at 50 MPa by a high-pressure injection pump and a common rail controller, respectively. 500 cycles before achieving the same energy content from each fuel with a 0.5 equivalency ratio, the injection amount test was carried out. A schematic of the injection fuel rate measurement system is presented in Figure 3.5.

Table 3.3. Physical properties of fuel

Properties	Unit	Test Method	Gasoline	Diesel
Chemical formula			C_8H_{18}	$C_{12}H_{23}$
Heating Value	MJ/kg	ASTM D240:2009	45.86	45.93
Lubricity	mm	ISO 12156- 1:2012	548	238
Kinematic Viscosity (40 °C)	mm ² /s	ISO 3104:2008	0.735	2.798
Pour Point	°C	ASTM D6749:2002	-57	-9
Cloud Point	°C	ISO 3015:2008	-57	-5
Density (15 °C)	kg/m ³	ISO 12185:2003	712.7	826.3
Octane Number			91 - 84	

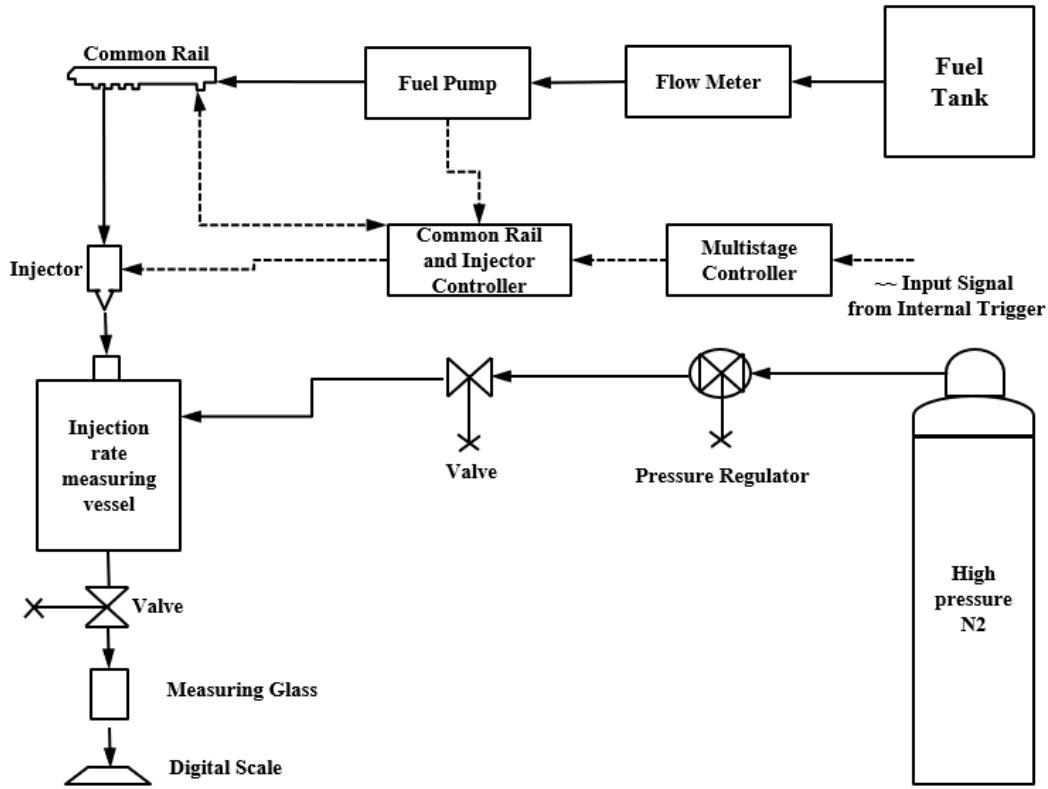
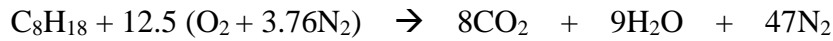


Fig. 3.5. Schema of the injection fuel rate measurement

The following is the stoichiometric combustion of gasoline with air, which contains 21% oxygen and 79% nitrogen:



The fuel or oxidizer ratio in practice is compared to the fuel or oxidizer ratio in the stoichiometric formula to determine the equivalence ratio (ϕ) as shown in equation (14).

$$\phi = \frac{(A/F)_{stoic}}{A/F} = \frac{X_{C_8H_{18}}/X_{O_2}}{(X_{C_8H_8}/X_{O_2})_{stoich}} = 12.5(X_{C_8H_{18}}/X_{O_2}) \quad (14)$$

Propane burns stoichiometrically with air, which has a 21% oxygen content and a 79% nitrogen content, in the reaction that follows.



To calculate the equivalence ratio (ϕ) as displayed in formula (14), the oxidizer ratio of fuel in use is contrasted with the oxidizer ratio of fuel in the stoichiometric equation.

$$\phi = \frac{(A/F)_{stoic}}{A/F} = \frac{X_{C_8H_{18}}/X_{O_2}}{(X_{C_8H_8}/X_{O_2})_{stoich}} = 5(X_{C_8H_8}/X_{O_2}) \quad (14)$$

Table 3.4 shows the engine operating parameters and injection strategy for FCEM with spark plug application.

Table 3.4. Spark discharge operating injection strategies

Ignition mode	Timing	Injected fuel	Driver type	Injector Type
Diesel Self Ignition	- 10~0 °CA BTDC	2900 μ s (130.24 mg)	ZB-5100	Bosch 0445110 327
Propane Self Ignition	- 20~0 °CA BTDC	6250 μ s (122.13 mg)	ZB-5014	Denso 33800 52800
Spark discharge operating	- Propane 20~0 °CA BTDC - Spark +0~5 after SOI Propane	6250 μ s (122.13 mg)	ZB-5014	Denso 33800 52800

3.1.4 Propane as a low-carbon fuel for CI engine

The hydrocarbons make up the majority of the light hydrocarbon mixture found in LPG are propane (C_3H_8) and butane (C_4H_{10}). The demand for propane as a fuel for internal combustion engines developed quickly as a result of the oil crises of the 1970s and the rising price of oil [75], [93]. The majority of these cars were first constructed with gasoline engines but were switched to propane engines [94]. Direct injection technology is the next possible approach for propane converters and original equipment manufacturers (OEMs). It offers the chance to produce more power with less pollution than diesel. Fig. 3.6 compares the greenhouse gas emissions from LPG using CA_GREET3.0. In California, ethanol is mixed with reformulated petrol to create a mixture known as CARBOB. During the course of their lifetime, vehicles powered by LPG emit 20% less greenhouse gases than vehicles powered by conventional petrol. In comparison to co-produced renewable diesel, conventional fuels have a carbon intensity of almost 70% higher than emissions from tallow-derived bio-propane [95]. Propane can also be produced during the processing of biofuels [96], [97] and other industrial processes, despite the fact that it is largely produced as a by-product of the refining of petroleum (45%) and wet natural gas cleaning (55%) [98]. The physiochemical characteristics of diesel and propane are contrasted in Table 3.5.

The use of propane as an engine fuel has a long history. Propane is the most widely used alternative vehicle fuel in the world. Outside the United States, propane is sometimes referred to as “autogas” [99]. About 1910, research on propane started, and by the 1920s, fleets in

California were utilising it to power their cars [100]. In the US, there are already over 140,000 cars that run on propane. The number has decreased in recent years and has stayed relatively consistent about 140,000 after reaching a record of almost 200,000 in 2003. North Carolina, Texas, California, Georgia, and Florida had the most propane-powered automobiles in 2011 [101]. Over 25 million LPG vehicles were in use globally in 2014; the majority of these were light-duty vehicles (LDVs), with the remaining vehicles being heavy-duty vehicles. Several countries, including Australia, Turkey, India, South Korea, Russia, Poland, Australia, and Thailand, have successfully pushed LPG as an alternative fuel for automobiles. With more automobiles on the road, more people using them, and more refueling stations, Thailand is aggressively pushing LPG as an alternative fuel throughout Southeast Asia [102].

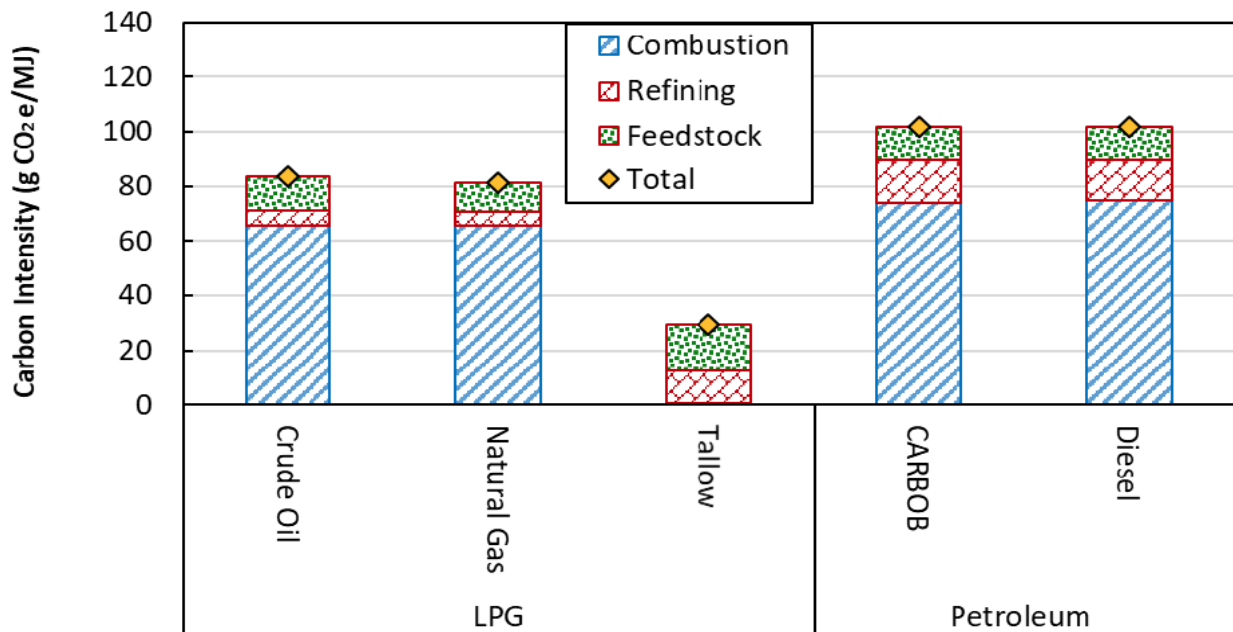


Fig. 3.6. Comparison of emitted carbon intensity (g CO₂ e/MJ) emissions from LPG analyzed using CA_GREET3.0. Adapted from ref. [95]

Table 3.5. The physiochemical properties of propane and diesel. Adapted from ref. [103], [104], [105], [106], [107][108]

Properties	Propane	Diesel
Chemical symbol	C ₃ H ₈	C _n H _{1.8n}
Physical state	Liquid/Gas	Liquid
Mol. wt. g/mol	44.09	170
Density/kg/m ³ @15.5°C	505	827-840
Cetane number	5	52
Stoichiometric A/F ratio	15.7	14.5
Composition:		
Carbon mass (%)	82	86
Hydrogen mass (%)	18	14
Liquid density (kg/m ³)	500.3	831
Liq. viscosity(kg/ms@25°C)	0.2	2-4
Boiling point (°C)	-42	180/370
Energy density (MJ/l)	23.5	35.08
Low heating value, MJ/kg	46.35	42.7
Combustion range, λ	0.42/2.0	0.48
Combustion range, Gas in Air (%)	2.0/9.5	0.6/6.5
Vapor pressure (atm@25°C)	9.3	0.035max @21°C
Latent heat of evaporation, kJ/kg	372	250
Liquid specific heat, kJ/kg·K	2.5	2.2
Gas specific heat, kJ/kg·K	1.67	1.7
Auto-ignition temperature (°C)	465	257
Flammability limit, rich (vol%)	29.5	5
Flammability limit, rich (vol%)	2.4	1

3.1.4.1 Propane economics

Due to the US shale oil boom and the growth of the Middle Eastern LPG export market, marine LPG exports increased by 78.9% from 60 million tonnes in 2014 to about 110 million tonnes in 2018. Furthermore, there was a global increase in maritime LPG imports of 18% between 2016 and 2018 [109]. Europe saw the strongest growth in propane imports, rising 17% from 2017 to 2018, despite Asia being the world's largest propane importer. There are no unexplored propane markets in the world after the US began selling propane to India in 2019. At the moment, the US is the world's biggest supplier of propane and a significant participant in the propane export industry [101]. It is anticipated that propane will become more accessible during the coming years. According to the US Energy Information Administration (EIA) [110], by 2040, the average yearly output of propane is anticipated to reach between 2.25 and 3 million barrels per day.

While LNG is expected to cost less than LPG overall (Table 3.6), LPG can be handled at the current facilities, which will require less building money than LNG. LPG is therefore a practical option for fuel for coastal transit. Such price differences were discovered in feedstock distribution system characteristics in the Republic of Korea [7]. Throughout its life cycle, the manufacturing of LPG generates less pollutants than that of natural gas or fuels derived from petroleum. Furthermore, a recent investigation looked at the feasibility of LPG; it was determined that it was efficient and competitive as a possible fuel source for Korean ships by looking at the economic relationships between the pricing of LNG, LPG, HFO, and MGO and the price of crude oil globally.

Table 3.6. Ship bunker fuel cost estimation (Unit: US \$/MMBTU). Adapted from ref. [7]

	Base case			High oil price case			Low oil price case		
	2020	2030	2040	2020	2030	2040	2020	2030	2040
Brent	12.5	16.35	18.24	21.17	32.1	36.49	5.34	6.54	7.75
LPG	18.41	24.98	27.88	32.35	48.91	55.75	8.15	9.99	11.83
LNG	10.88	10.88	10.88	10.88	11.94	11.94	9.82	10.88	10.88
MGO	18.06	24.52	27.36	31.74	48.00	54.71	8.00	9.81	11.61
HFO 380	37.89	51.42	57.37	66.58	100.68	114.75	16.78	20.57	24.36
Brent (US\$ /BBL)	70	95	106	123	186	212	31	38	45

A price analysis of propane (LPG) products in the EU28 and G20 trading partners is shown in Fig. 3.7. In the EU28 and G20, propane prices are said to be among the lowest, especially when compared to those of petrol and diesel. Cars fueled by propane have a comparable driving range to those powered by conventional fuels, and propane engine fuel is generally less expensive per gallon than diesel. Using propane as an engine fuel reduces air pollution and the environmental effects of vehicles while also improving energy economy and enabling cost-effective on-site refueling.

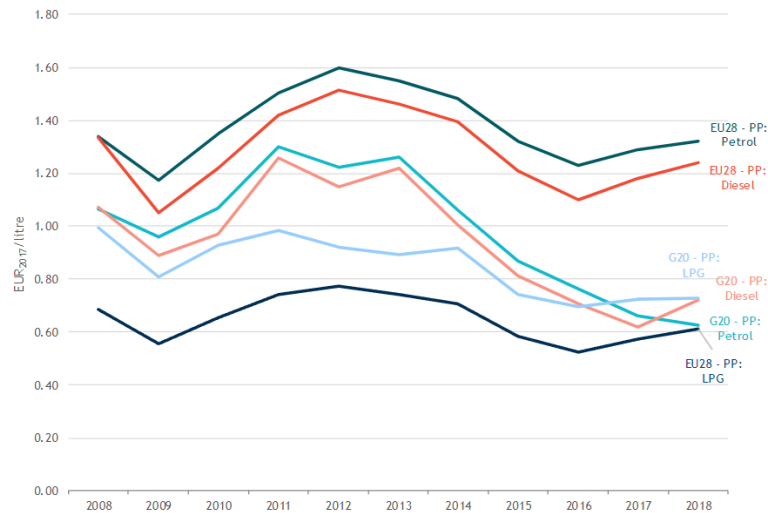


Fig. 3.7. Propane (LPG) product pricing in the EU28 weighted average prices versus G20 (trade) weighted average prices. Adapted from ref. [111]

3.1.4.2 Propane gas characteristics

Propane (C_3H_8) is an alkane gas consisting of three carbons that is normally present at atmospheric pressure but has the ability to liquefy at low pressures. Liquid propane is more feasible and less expensive to store and transport than gaseous propane since it has 270 times the energy density [100]. The ability of LPG to liquefy easily and be transported at room temperature and pressures between 10 and 20 bar gives it a significant advantage over other fuels. It can also withstand being liquid for an extended period of time. Because it is not kept frozen, LPG experiences less temperature issues than LNG. LNG necessitates the use of electrical equipment with a lowering surface temperature, whereas LPG has a lower auto-ignition temperature [14]. LPG has certain drawbacks, though, including a lesser igniting range, a lower explosive limit (around 2%), and a larger density than gas. Propane has a lower boiling point than oxygen, hence when using LPG as fuel in colder climates, it should include more propane than oxygen. As seen in Fig. 3.8, Zhang et al. investigated the thermodynamic states at nozzle exit under three choking situations; these states are indicated by blue squares. Shock structures are created because the flow is choked, the exit speed is sonic, and the pressure at the nozzle exit is greater than the surrounding pressure.

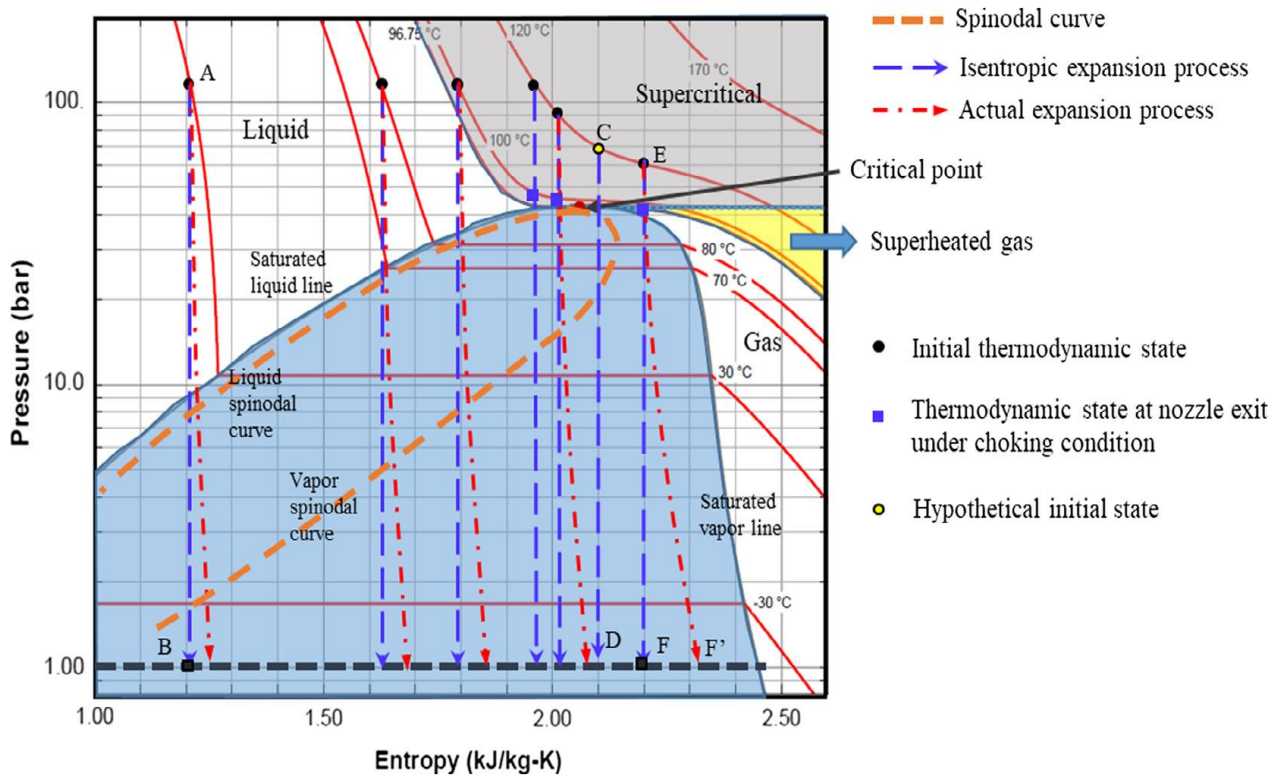


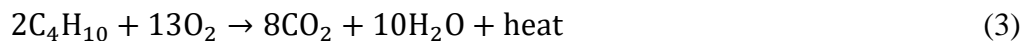
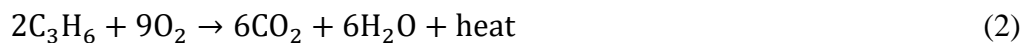
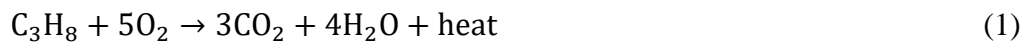
Fig. 3.8. Propane pressure-enthalpy diagram and thermodynamic paths for different thermal conditions (Adapted from [112]).

Commercial propane, commercial B-P mixes, commercial butane, and propane HD-5 are four mixtures that are utilised for a range of commercial, governmental, and household applications. The Gas Processors Association offers specifications for each batch [95]. The main differences in the requirements are the maximum allowable propylene, butane, and sulfur contents, as shown in Table 3.7.

Table 3.7. Specification for propane. Adapted from ref. [113]

	Product type				ASTM Test Methods
	Commercial Propane	Commercial Butane	Commercial PB Mixtures	Special-Duty Propane	
Vapor pressure at 37.8 °C (100 °F), kPa (psig) max	1435 (208)	483 (70)		1435 (208)	D1267 or D2598 or D6897
Heavier hydrocarbon contaminants:					
Butane and heavier, % by volume, max	2.5	2.5	D2163
Pentane and heavier, % by volume, max	...	2.0	2.0	...	D2163
Propylene content, % by volume, max	5.0	D2163
Residual matter:					
One of the following requirements shall be:					
(1) Residue on evaporation of 100 mL, mL, max, and	0.05	0.05	0.05	0.05	D2158
Oil stain observation	pass	pass	pass	pass	D2158
or					
(2) Residue by gas chromatography, mg/kg, max	350	350	350	350	D7756
Density at 15 °C or relative density at 15.6°C/15.6°C (60°F/60°F)				...	D1657 or D2598
Corrosion, copper, strip	No. 1	No. 1	No. 1	No. 1	D1838
Sulfur, mg/kg (ppm by mass), max	185				D6667
Hydrogen sulfide	pass	pass	pass	pass	D2420
Moisture content	pass	pass	D2713
Free water content	...	none	none

When a fuel burns completely, carbon dioxide, water vapour, and heat are released. Equations (1), (2), and (3) represent the fundamental processes that arise from the perfect combustion of propane, propylene, and butane.



The hydrogen and carbon in the hydrocarbon fuel would, in the perfect circumstances, be completely converted to water and carbon dioxide by the oxygen in the air. The air's nitrogen content remains unchanged. However, due to less-than-ideal combustion conditions, species of unburned hydrocarbon (HC), carbon monoxide (CO), and nitrous oxide (NO_x) are produced.

3.1.5 Test procedure and ignition strategy

The CVCC optical chamber, the RCEM research engine, and CONVERGE CFD simulations were used in an experiment. A 500-bar injection pressure was used to deploy gasoline fuel in experiments on a rapid compression and expansion machine (RCEM), which is similar to a gasoline compression ignition (GCI) engine in certain ways. Starting of injection (SOI) was set at 17 degrees, with top dead center (BTDC) being 10 degrees ahead of the compression ratio. The spark timing was adjusted to be five degrees after the injection started. Spark plasma flame visualization tests were conducted using a constant volume combustion chamber (CVCC). To accurately replicate surrounding air, the gas is diluted with 20% O₂ and 80% N₂ inside a CVCC. A mass flow valve limits the gas pressure to 1 bar at 295 K in order to prevent internal gas expansion.

Nowadays, industry and academia employ computational fluid dynamics (CFD) as a popular technique to predict the performance of internal combustion engines (ICEs) and provide data that may be used to improve the design of future combustion systems. In accordance with user-specified grid control parameters, CONVERGE will produce a fully orthogonal and ordered grid at runtime. A steady-state flow bench engine and CONVERGE CFD simulations were used for the experiment. CAD software can be used to prepare the stereolithography (STL) input file required by the CONVERGE programme. Using the graphical user interface pre-processor, the stereolithography (STL) geometry is arranged and transmitted to the CONVERGE solver. The surface specification file identifies surface geometry, and the CONVERGE solver automatically generates mesh volumes. For this inquiry, steady-state conditions were chosen as the boundary conditions. Based on the experimental conditions, the temperature and airflow pressure are set at 300 K and 1 bar, respectively. According to mass and the ideal gas law, 21% of the airflow is oxygen and 77% is nitrogen. The renormalized group (RNG) k-turbulence sub RCEM with spark application model was used to simulate the flow and solid surface in CONVERGE in order to compute the wall law. [114]. The cylinder temperature is maintained at 300 K while the steady-state model is examined at different mass flow rates. The mass equation, momentum equation, and energy conversion equation are the most often used formulas for designing cylinder airflow patterns. Using a Cartesian grid and an implicit discretization technique, the Navier-Stokes equation is found. The velocity-pressure coupling problem is handled by the Rhie-Chow approach, and the division of operators (PISO)

technique is used to solve the pressure implicit. This CFD model was used to simulate the effects of various spark discharge energy on the flow at the cylinder.

Furthermore, the experimental setup is ready to investigate the electrical properties of spark discharge. The spark plug emitted energy in this study is measured using two parameters: the voltage and the discharge current. The time during which the rate of discharge energy release is positive is known as the duration of spark discharge [115]. Voltage and current accumulation during the discharge period was used to calculate the overall discharge energy [116]. A method for methodically examining the effect of spark discharge energy on the in-cylinder characteristics performance of RCEM with direct injection strategy for spark ignition and the subsequent combustion performance of the spark ignition engine is depicted in Fig. 3.9. In this study, a single spark plug, two spark coils, and ten spark coils were used to build an inductive ignition system. To ensure the accuracy of the data, the testing room's temperature and humidity levels were kept constant over the whole experiment. In order to guarantee the dependability of measurement instruments, each piece of apparatus has undergone a specified period of calibration. To prevent the uncertainty reading, the repeated measurement is done three times for each test condition.

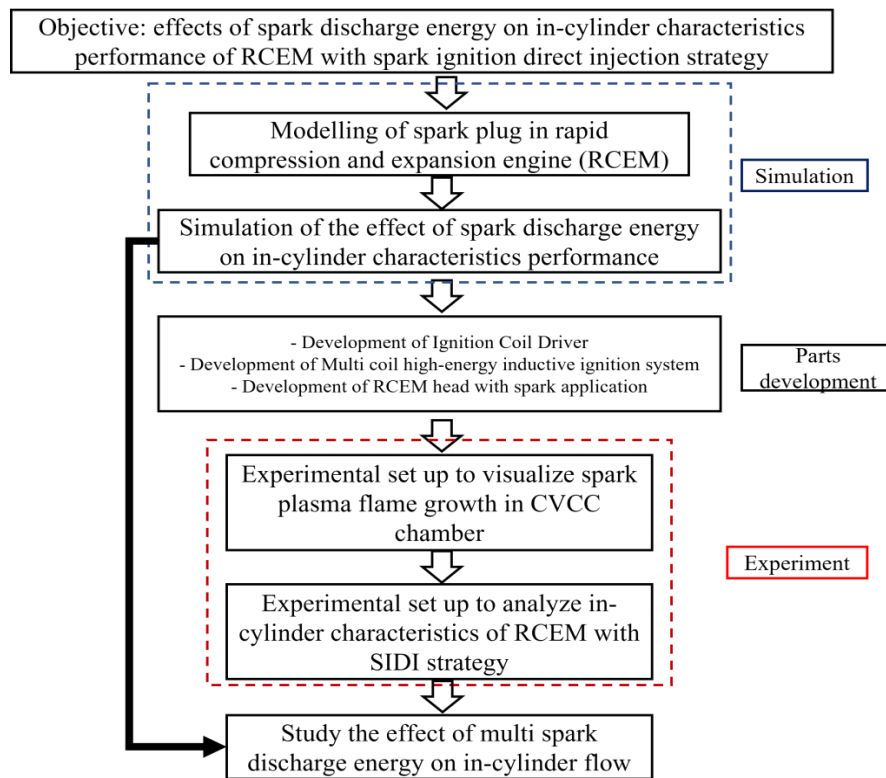


Fig. 3.9. Research flow diagram organization of spark discharge study on gasoline RCEM with spark application

3.1.6 Accuracy of measurements and uncertainty

To ensure the reliability of measurement instruments, each piece of equipment was calibrated within a set amount of time. After every measurement, all electric equipment is cleaned and calibrated before the next measurement cycle. Three repeated measurements of each set of test conditions were made in order to remove reading uncertainty. To estimate the limiting inaccuracy associated with each calculated parameter, a comprehensive uncertainty analysis is performed based on the confidence of the instrument utilized and the measured rate [117]. The uncertainty range of the measured parameters is summarized in Table 3.8 [118].

Table 3.8. Uncertainty of measured parameters

Measured parameter	Uncertainty (%)
Pressure	<2
Temperature	<2
Fuel rate	<1
Research engine crank angle	<1
Research engine speed	<1

3.2 Simulation Model

3.2.1 Governing formulas for the in-cylinder performance

Measurements were made of the ignition system resistance in order to determine the precise quantity of electric released energy used in the bore. The corresponding schematic utilised throughout the inquiry is shown in Fig. 2. Equation (1) states the total resistance of the ignition system. The sum of discharge power P_{TOTAL} was obtained applying Equation (2). The discharged power of in-cylinder P_{IN} was specified using Eq. (3). P_{IN} represents the power applied to the spark plug gap, and P_{TOTAL} is presented to the inductive strength of coil in the similar schema. Eq. (4) [29] displays the ratio of energy discharge transmit to inductive energy from the ignition coil.

$$R_{TOTAL} = R_{GAP} + R_{PC} + R_{IP} \quad (1)$$

$$P_{TOTAL} = R_{TOTAL} I^2 \quad (2)$$

$$P_{IN} = R_{GAP} I^2 \quad (3)$$

$$\eta = \frac{P_{IN}}{P_{TOTAL}} = \frac{R_{GAP}}{R_{TOTAL}} = \frac{R_{GAP}}{R_{GAP} + R_{PC} + R_{IP}} \quad (4)$$

R_{GAP} , R_{IP} , and R_{PC} , respectively, stand for the impedances of the gap of spark electrode gap, ignition spark plug, and plug cord. Eq was used to determine the resistance of the spark

channel, R_{GAP} . By utilizing the time-resolved discharge waveform, Eq. (6) was applied to calculate the in cylinder released energy, E_{IN} .

$$R_{GAP} = \frac{V}{I} - R_{PC} - R_{IP} \quad (5)$$

$$E_{IN} = \int R_{GAP} I^2 dt \quad (6)$$

Using Equations (7) and Eq. (8), it was possible to determine the electrical discharge patterns of numerous spark discharges for the time interval between spark energy released (Δt_i). The multiple spark discharge method can change depending on the time interval, as demonstrated here.

$$\frac{dE_d}{dt(t)} = V_d(t) \times I_d(t) \quad (7)$$

$$E_d(t) = \int \frac{dE_d}{dt(t)} dt \quad (8)$$

The power on the engine piston could be calculated using the in-cylinder pressure. Following the display of the pressure vs. cylinder volume on a P-V chart, the following is a formula for calculating the work [26].

$$W_i = \int P dV \quad (9)$$

The pressure inside the cylinder varies throughout the combustion cycle. Because the mean effective pressure varies with engine size and speed, it is an excellent tool for comparing engine output or design. To compare machines, torque will make a larger bore engine seem better. Deliberate rotation must be considered in power comparisons. The specified work generates the IMEP, as indicated below.

$$IMEP = \frac{W_i}{V_d} \quad (10)$$

By dividing the provided work/power by the input energy for each cycle, the indicated thermal efficiency is determined. The η_t formula is represented by the following equation.

$$\eta_t = \frac{P_i}{Q_{in}} \times 100 \quad (11)$$

Here,

η_t = indicated thermal efficiency, %

P_i = indicated work/power, *J/cycle*

Q_{in} = input energy, *J/cycle*

The pressure inside the cylinder reveals the thermodynamic state. The first law of thermodynamics can be used to calculate the percentage of combustion with a few basic assumptions. Use the formula below to find the rate of heat discharge.,

$$\frac{dQ}{d\theta} = \frac{\gamma}{\gamma-1} p \frac{dV}{d\theta} + \frac{1}{\gamma-1} V \frac{dp}{d\theta} \quad (12)$$

in which γ is the ratio of specific heat, p is the in-cylinder pressure, and V is the volume of the combustion area. For a CI engine, the ideal value of γ is 1.3 [26], [119]. The following equation can be used to calculate the in-cylinder temperature based on information from the in-cylinder volume and pressure investigation and the law of ideal gas, in which p denotes the pressure, V denotes the volume, n denotes the quantity of matter, and R denotes the gas constant.

$$T = \frac{p.V}{n.R} \quad (13)$$

where p is the pressure, V is the volume, n is quantity of substance, and R is gas constant, respectively.

3.2.2 CFD modelling and simulation

CONVERGE 3.0 was used to generate the simulation. The grid autonomy of the turbulent flow and engine models was investigated using the renormalized group (RNG) model. A roundabout discretization method based on a volume element was used to overcome the challenge of applying the discretized Navier-Stokes formula on a Cartesian grid. To shorten the computing time, the processes of combustion, expansion, and compression were all modelled. Utilising information from experimental observations, the main fuel variables, air conditions, and ambient temperature were determined. Up to the experimented pressure is convinced, the origin temperature, flow velocities, and pressure are increased. Hockett et al. [120] developed a set of redesigned kinetic processes to minimize computing overhead. Table 3.9 provides an overview of the models employed in this investigation. A Windows PC with an Intel® Core i7™ 7700 60 GHz processor and 32 GB of RAM was used for this experiment. Additionally, this section describes the basic calculation process and covers the surface treatment, beginning and boundary requirements, computer network computation, and post-treatment of the graphics preprocessor. A Tecplot is also used to display the results.

Table 3.9. CONVERGE key research processes

Physical Model	Physical process	Model
Turbulence Modeling	Renormalization group (RNG) k-ε	Reynolds-averaged Navier-Stokes (RANS)
	Wall heat transfer	O'Rourke and Amsden
Ignition Spark Modeling	Source	Energy
	Shape	Sphere type
	Motion	Move with flow
Combustion Modeling	Chemistry solver	SAGE
	Emissions	Extended Zeldovich
	SOOT	Hiroyasu SOOT
Spray Modeling	Spray break up	Kelvin-Helmholtz (KH) – Rayleigh-Taylor (RT)
	Drop drag	Dynamic drop drag
	Collision	NTC
	Turbulent dispersion	O'Rourke model
	Spray wall interaction	Wall film

Every sequence was repeated at 720 degrees for the whole time allotted. The pressure and temperature at the input and output were 1 Bar (0.1 MPa) and 300 K, respectively. Except for the valves and piston, which were also identified as movable limitations in this study, all of the barriers were assumed to be stationary. Temperatures and pressures were set at 383 K and 1 Bar (0.1 MPa) for both the input and outflow. Table 3.10 displays the modelling limit scenarios. 24,363,436 points are used to create the RCEM model with a spark plug application. Using the spark model and the predetermined parameters, the case setup was carried out on the RCEM. For instance, altering the energy amount in accordance with the coil configuration's counting produced different results for the ignition method's spark release temperature.

Table 3.10. Simulation initial and boundary conditions

Boundary & initial conditions	Value
TKE of cylinder region	62.03 m ² /s ²
Pressure of intake	101 kPa
Piston Temperature	553 K
Cylinder wall initial temperature	353.15 K
Initial pressure of cylinder	101 kPa
Initial temperature of cylinder	298 K
Grid size	0.004 m

The surface geometry was modelled using Solidworks, one of the CAD programmes. For flow analysis, the surface geometry was entered into the engine model of CONVERGE. Once modelled geometries with initial boundary regions on the surface have been identified, the CONVERGE solver automatically generates the volume mesh during runtime. A new boundary technique is used by the CONVERGE programme to circumvent the need for

computational grids to fit interesting geometries. To ensure simulation realism, the grid size was reduced to 4 mm, and the automatic mesh refinement (AMR) tool was used to revise the main area valves. This improves the grid's resolution when the velocity gradient is greater than 1 m/s. The RCEM model employing a spark plug is displayed in Fig. 3.9. Twenty-six thousand seven hundred and sixty-seven thousand points make up this mesh model. As an example, to adjust the spark discharge energy in the ignition strategy, one adjusts the amount of energy based on the coil configuration calculation. A case setup is performed on the RCEM with spark model in accordance with the parameters that have been established.

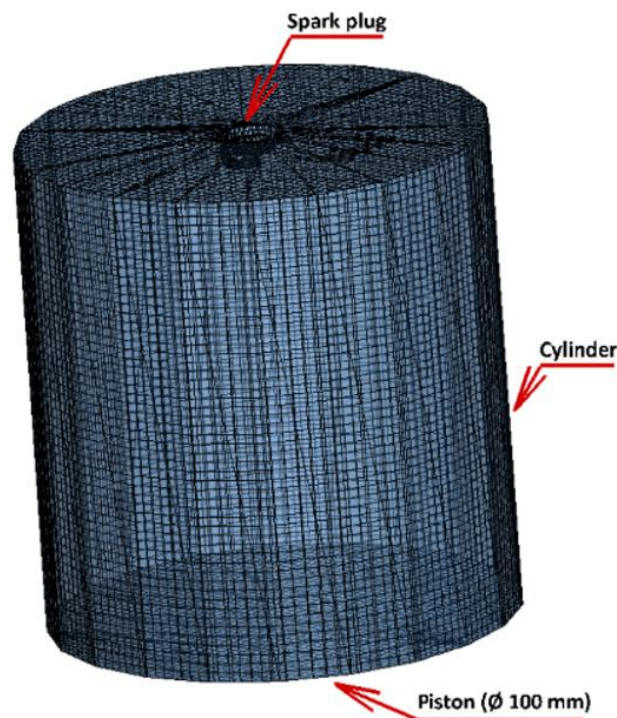


Fig. 3.10. RCEM with spark model

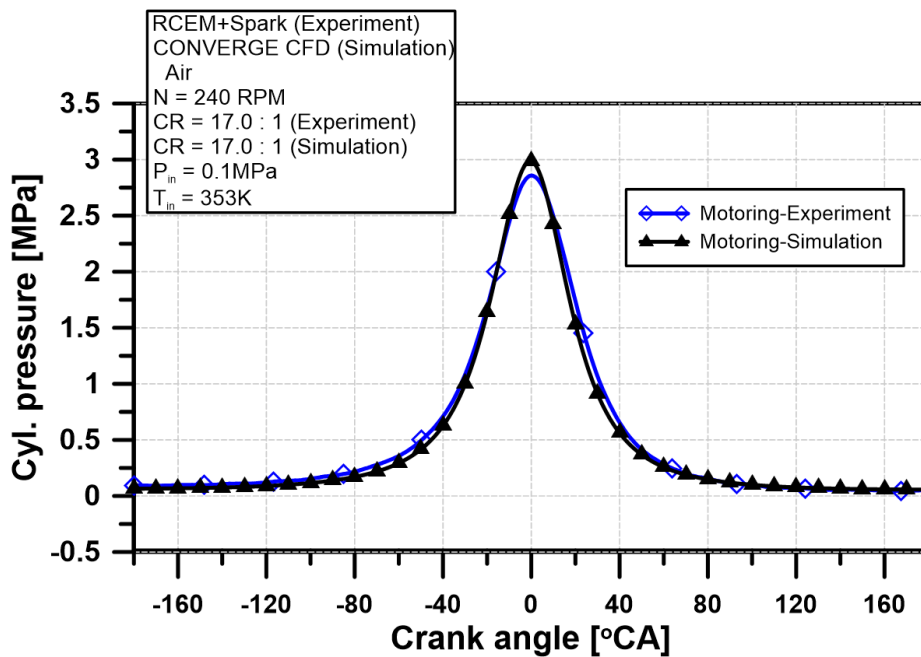
In order to evaluate heat exchange between the gas blend inside the in-cylinder bore and wall, the heat exchange connection was put into place. Next, after comparing the motoring in-cylinder pressure of the experiment with the worry of heat transfer correlations raised by RCEM modelling, more calculations were performed.

3.2.3 Model validation

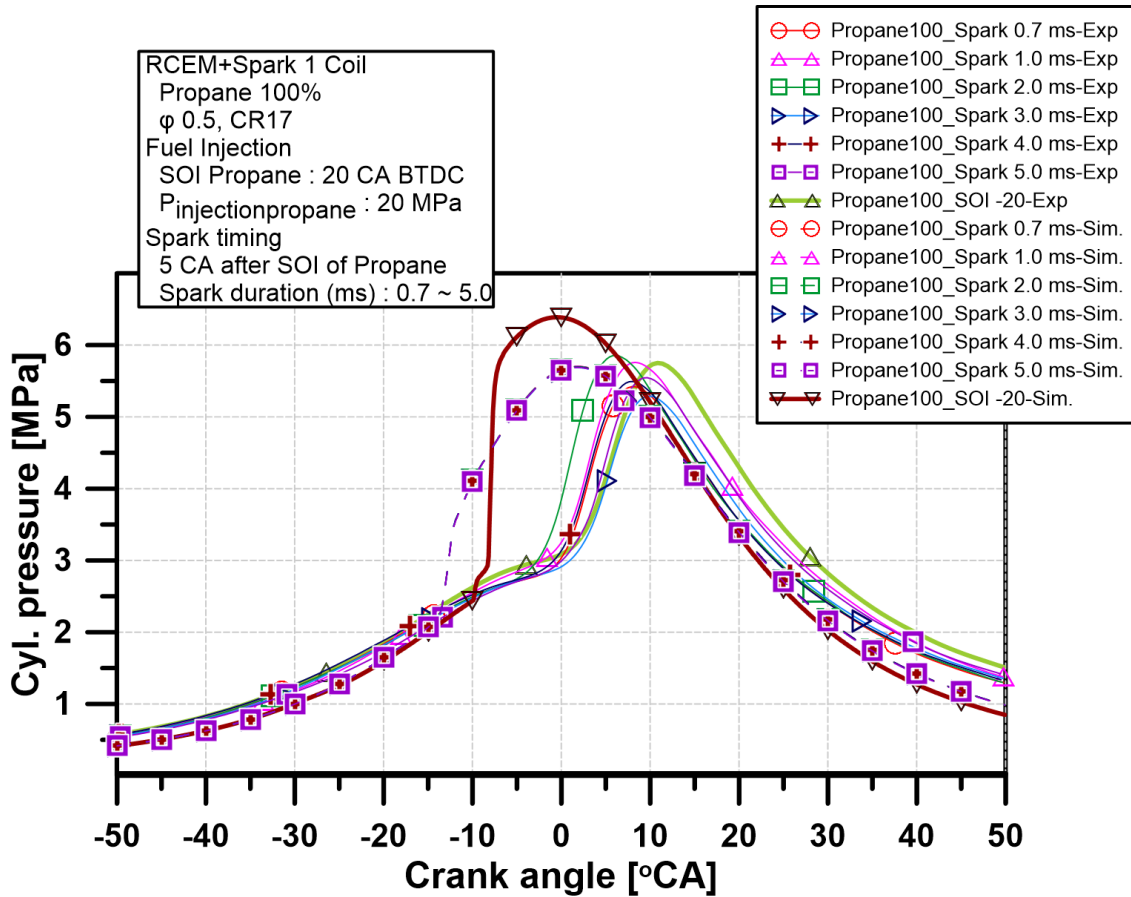
The physical representation is verified using different experimental data in terms of the pressure between the experimental data and simulation results. Table 3.9 provides a quick description of the models applied in this investigation. On a Windows computer with a 60 GHz

Intel® Core i7™ 77003 processor and 32 GB of RAM, this simulation was conducted. At the input and outflow, 383 K and 1 bar of pressure, respectively, were set as the temperatures. The case set up was carried out on the RCEM with the spark model according to the parameters that were determined.

Fig. 3.11 displays the validation of the simulated and experimental findings for driving pressure and crank angle. The comparison between the findings of the simulation and the experiment is shown in Fig. 3.12(a). In contrast, Fig. 3.12(b) shows the impact of the three-spark approach over the course of the whole spark duration interval (0.7–5 ms) on maximum temperature, HRR, and internal pressure. To ensure that the readings for each test circumstance were accurate, three pressure measurements were taken. Propane's high-octane rating caused the in-cylinder pressure of the RCEM to rise to its ideal level, which was reached around the top dead center. The pressure dropped 0.183 MPa from the diesel engine. At a crank angle of 10.83 degrees, the highest pressure was recorded (-9.08 degrees).



(a)



(b)

Fig. 3.11. Validation of in-cylinder pressure in RCEMs using different ignition strategies and propane direct injection. (a) Motoring pressure; (b) In-cylinder pressure and spark times ranging from 0.7 to 5.0 milliseconds.

3.3 Summary

This chapter has detail explained about the research platforms of experiment and simulation. Based on this experimental system, the combustion characteristics and emission characteristics will be obtained using diesel and propane fuels. This output experimental data will be used to validate the engine simulation model.

This chapter has explained the simulation modeling setup base on the Converge software with version 3.0. The simulation is validated based on the comparison between simulation results and experimental results in cylinder pressure. The investigation the effect of spark discharge

duration on engine performance and emission characteristics could be carried out via simulated approach. A detail of optimization operating parameter of spark discharge duration on the performance and emission characteristics will be investigated in chapter 4, 5, and 6.

4. EFFECT OF SPARK DISCHARGE DURATION ON IN-CYLINDER PERFORMANCES OF COMPRESSION IGNITION DIRECT INJECTION ENGINE

In the continual effort to investigate the effect of spark discharge duration on in-cylinder performances of CI engines, this part presents the effects of spark discharge duration on discharge energy release rate, flow characteristics, and combustion performances of a CI engine. An experimental system was established and studied spark model via a simulation.

4.1 Spark discharge duration effect on the discharge energy release rate

By measuring the discharge energy, it is possible to determine the duration (Δt_i) of 5 ms between spark discharges, which is an electrical characteristic of the power generation from numerous ignition discharges when utilizing an adjusted time interval. The voltage and current that were identified throughout this investigation are shown in Fig. 4.1. The proportion of release energy was calculated by multiplying the discharge current and voltage. The discharge energy rates of one coil, two coils, and ten coils were compared in order to ultimately estimate the energy released from the spark plugs in relation to the in-cylinder flow behavior. Average discharge currents for three ignition mode techniques ranged from about 50 mA to about 200 mA, and average released voltages were between about 1 kV and about 14 kV. The two coil and one coil ignition schemes and simultaneous ignition approach came next, with the simultaneous ignition method having the largest total released energy (about 190 mJ/s).

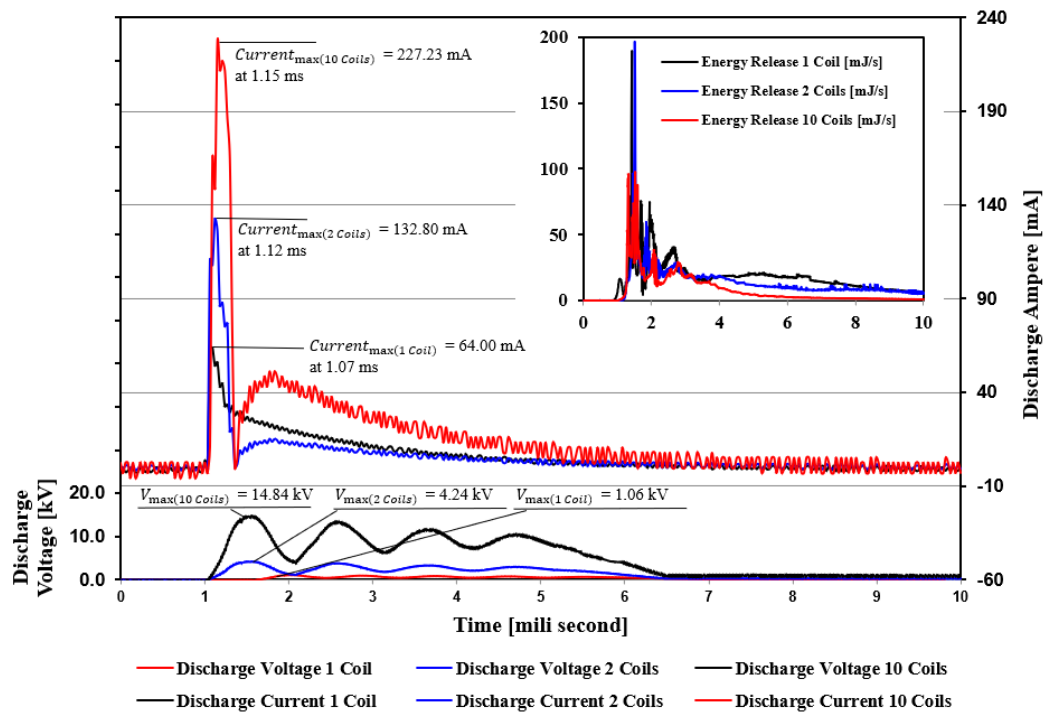


Fig. 4.1. Calculating the released current, discharge voltage, and energy

The oscilloscope shows the increment time of the break-down output power, which is also referred to as the spark plug discharge energy waveform. The electrical current around the spark working electrode is started by this waveform. The waveform has an enhanced period of approximately 1 s and a frequency of 250 kHz. The flame is started by the electric arc at the wave's terminus. The spark duration is the amount of time needed for the flame to ignite and start. The duration of the spark depends on its magnitude. This conclusion is consistent with the discharge characteristics, including the energy transmitted as a result of the in-cylinder remitted energy increasing with higher discharge timing, as per previous research [29], [121] and [122].

To examine how spark timing affected the ignition phase, the release current was changed from 50 mA to 200 mA using the MOBIQ ICD-12. Figure 4.2 depicts images of spark plasma propagation for six different ignition period differences (0.7, 1.0, 2.0, 3.0, 4.0, and 5.0 ms). The combustion chamber's temperature is fixed at 298 K, and the initial pressure is constant at 4 bar to guarantee that the initial conditions are the same before each test. Steady flow velocities are approximately 8 m/s in an anticlockwise direction. Inside the combustion chamber, smooth plasma propagation occurred during the individual coil. For simultaneous ignition coils, however, spark plasma propagation was either rarely produced or markedly slowed down. There was minimal variation in the flame plasma length among the three ignition procedures.

Even after selecting the simultaneous 10 coil spark and increasing the released current to 200 mA, the plasma growth stayed mostly unaltered. Therefore, there was little effect of accelerating the discharge spark timing period on the flame plasma formation stage.

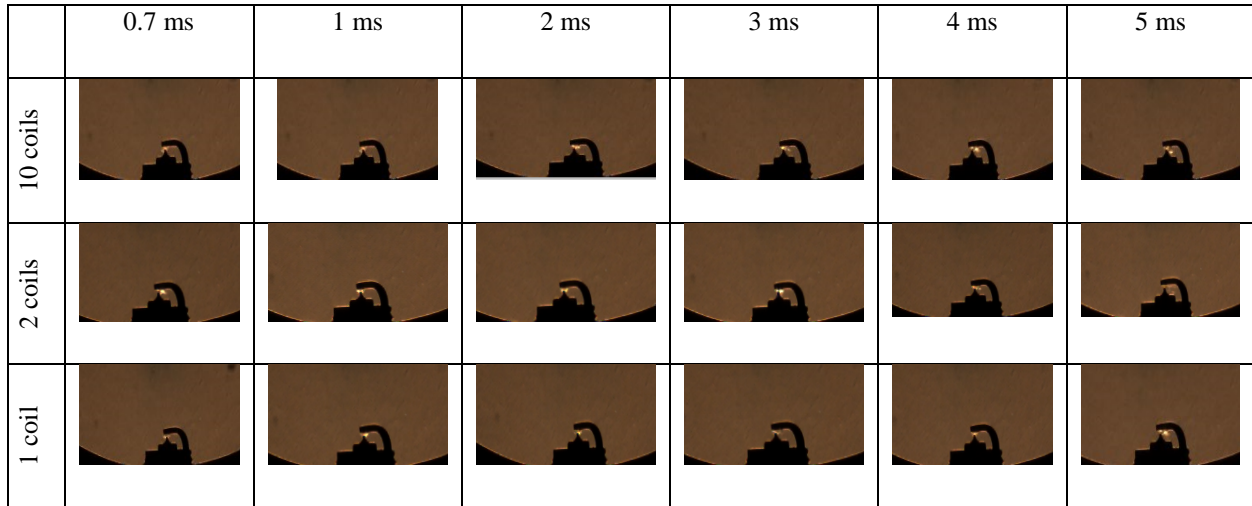


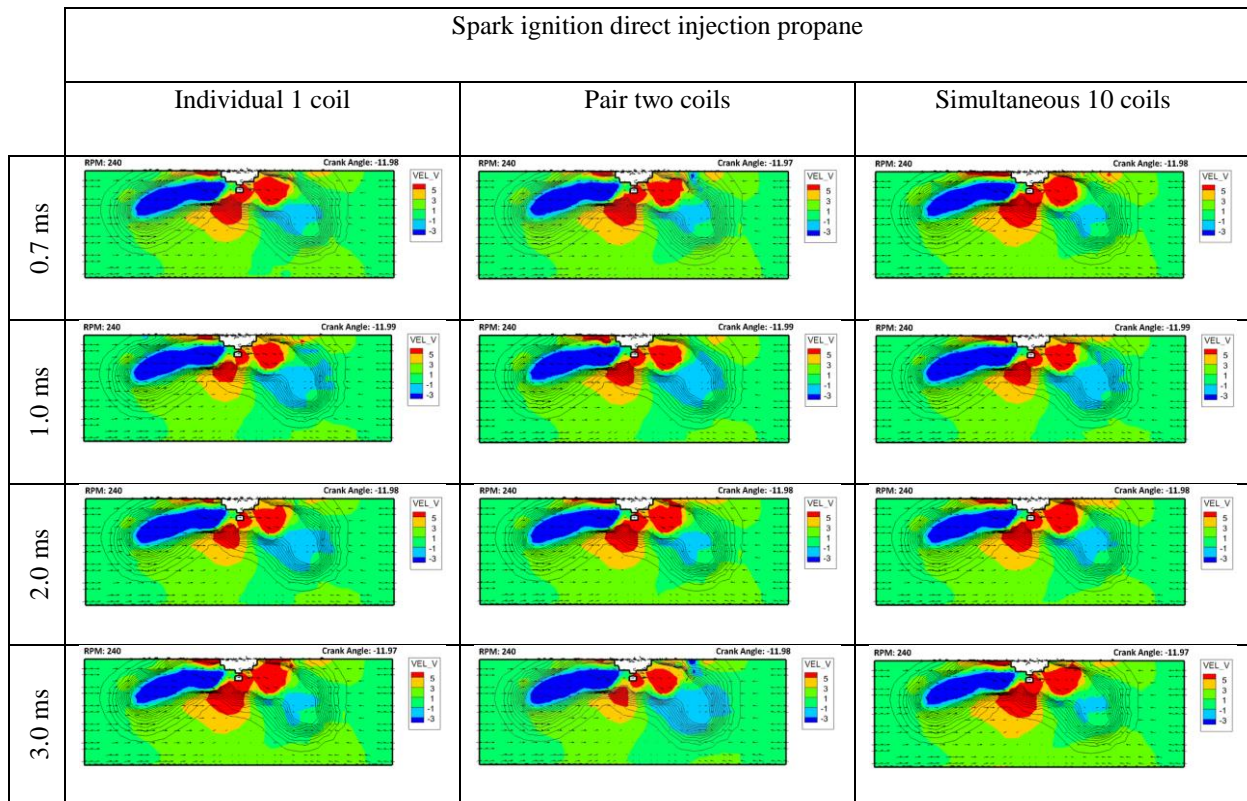
Fig. 4.2. Spark plasma propagation in the CVCC chamber using different ignition strategy (individual 1 coil, pair 2 coils, and simultaneous 10 coils)

Even with the longest discharge length and lowest current, the mixture won't ignite, according to Yang, Z's research findings [121]. As the duration time is increased, there is no appreciable improvement in the flame kernel development. Consequently, under these circumstances, a higher current level is needed for the best ignition.

4.2 Velocity distribution flow trend with varying discharge energy

The movement of the air flow pattern during compression and expansion is altered by discharge energy, which originates from the in-cylinder engine and passes via a section plane, as shown in Figure 4.3. According to the spark duration during the compression and expansion motions, this figure shows the flow pattern for the three different ignition schemes (one single coil, two pairs of coils, and ten simultaneous coils) in the RCEM. Crank angles from the spark period are converted based on the RCEM's running engine speed. After the spark phase at 15 °CA BTDC, the impact of streamflow speed on spark flame formation was investigated. The flow pattern was recorded near the end of the compression stroke (by approximately 11.98 °CA) to

introduce the streamflow situation. An earlier investigation found that the mean streamflow speed for all turbulence levels was not as good as the streamflow speed in the spark electrode distance [66]. In contrast, the spark gap exhibits the lowest turbulence strength when viewed from the outside in this manner. Superb streamflow speed at 11.98 °CA is shown by the red area around the spark plug, which is 5 m/s on average. A modest increase in flow velocity is evident in the broader red area surrounding the spark plug, which is the result of the spark duration being extended. Changes in ignition modes also reveal the same tendency when moving from the single coil mode to the pair and ten coils at the same time. One coil's discharge energy resulted in compression and expansion, as well as symmetrical motion in speed. This would explain why the flow rotation moved in the vicinity of the spark point. Fuel was fed into the combustion chamber and was reflected back by the RCEM engine's plain piston as the release energy increased, creating an opposing tumble vortex movement. As the tumbling flow increased, the centre consequently migrated in the direction of the cylinder's centre. It seems sense to deduce that there will be more turbulence in this combustion chamber the higher the flow velocity of a certain location. In cylinders, turbulence promotes more even mixing of the fuel and air. It is evident that increasing turbulence accelerates the spread of fire flames.



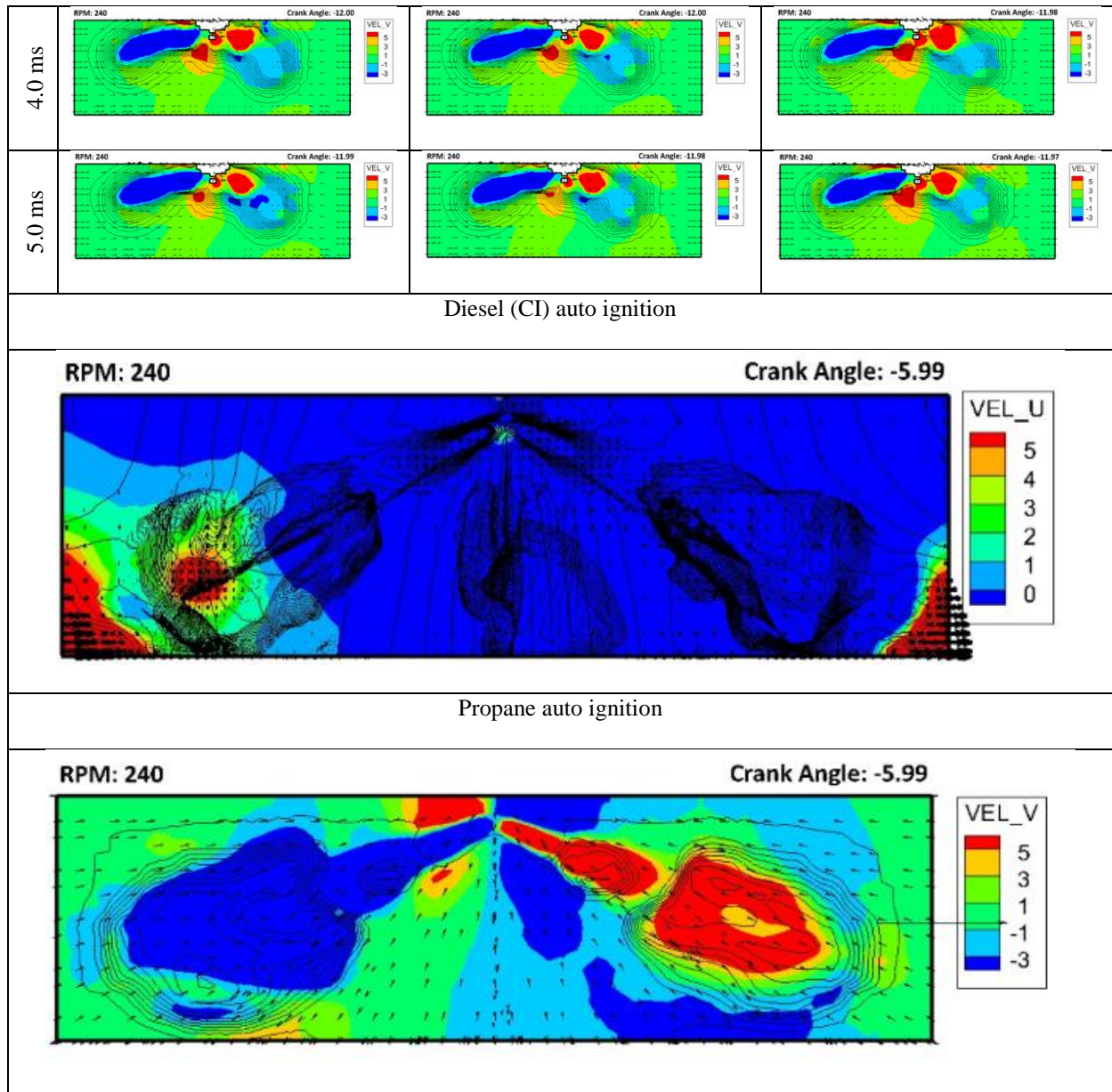


Fig. 4.3. Flow velocity motif of spark release duration study on RCEM fueled with diesel and propane DI through ignition strategies (individual, pair, and simultaneous) and spark period acquired at a crank angle of $\sim 11^\circ\text{CA}$ BTDC with SOI propane 20°CA BTDC, spark at 15°CA BTDC, speed of 240 RPM, slice z position of -0.004 m, and slice y position of 0.01 m, in comparison to diesel RCEM auto ignition

4.3 Flow characteristics inside a cylinder

The tumble ratio, turbulent kinetic viscosity, and TKE along the expansion and compression cycles are just a few of the metrics that are introduced and discussed in this section as they relate to the in-cylinder streamflow of the RCEM modified with spark and propane fuel.

4.3.1 Variations in the tumble ratio for the discharge energy

Formation, stability, and annihilation are the three phases that the tumbling ratio goes through. This early input stroke initiated the formation phase. Up until it hits TDC at 250 °CA, it will keep inclining downward. The in cylinder bore tumble ratio versus discharge energy is plotted in Figure 4.4. It is evident that while the spark plug discharge energy increases throughout the stabilization period, from 10 °CA BTDC to 15 °CA ATDC, the tumble ratio is little impacted.

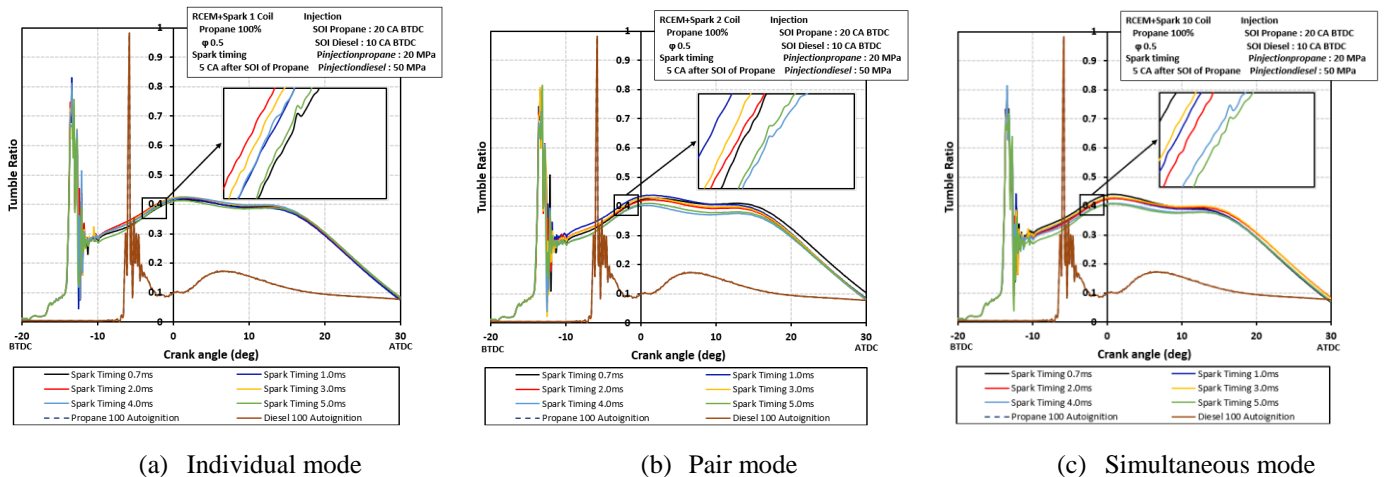


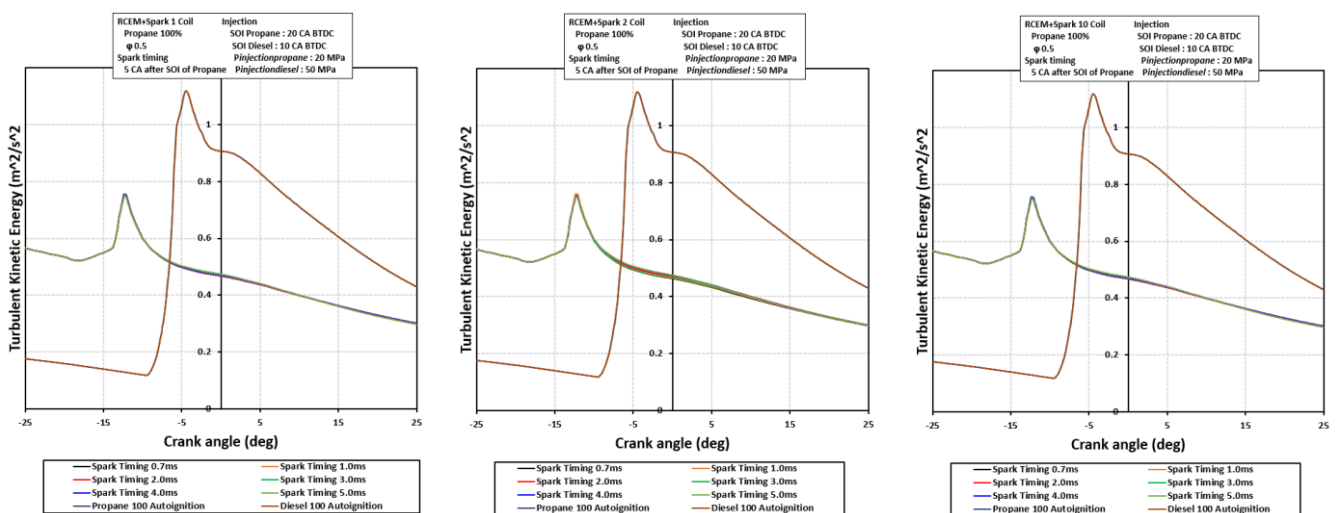
Fig. 4.4. The in-cylinder bore tumble ratio of spark discharge duration study on RCEM fueled with diesel and propane direct injection through ignition strategies (individual, pair and simultaneous) and spark durations ranging from 0.7 ms till 5.0 ms in comparison to diesel RCEM autoignition

The tumble ratio increases greatest at 15°CA BTDC, even though the pressure increased to the point where only tumbling vortices were formed and they only lasted briefly during the equilibrium cycle. Weak intake flow could be the reason of this. The impact of the tumble ratio in the in-cylinder bore on the discharge energy was investigated further. This indicates that extending the spark time, which reflects the increase in spark energy at the peak of the compression phase, has no discernible impact on the tumble ratio. Additionally, while moving, this tumbling streamflow was examined for several spark ignition methods. The tumble ratio rose very slightly with increasing spark timing until the compression stroke was completed. This shows that there is no appreciable effect of altering the spark period on the increase in

the tumble ratio. By comparing the outcomes with those of Ramesh and James [123], the tumble streamflow includes oscillations of the release energy on the start time of tumble streamflow. This effect was seen at the start of the intake cycle position up until the crank angle hit 25°CA ATDC. It was not long until this first development peaked at 0.98, fell to zero, and then peaked during crank angle at about 15°CA BTDC.

4.3.2 Energy fluctuation in a turbulent kinetic energy (TKE) pattern

Turbulent kinetic energy is the force responsible for motion caused by liquid flow, as determined by the root-mean-square (RMS) analysis of the velocity variation. The TKE is a helpful instrument for determining the turbulent viscosity in cylinder streamflow. Tumbling involution near the top of the compression cycle and frictional stresses, streamflow conditions near valve vortex shedding, and notable strain differences throughout the intake and exhaust phases are the two distinct sources of turbulent kinetic energy. For the purpose of assessing the impact of tumbling flow within a cylinder, one crucial parameter to take into account is the turbulent kinetic energy. Because turbulence intensity peaks while the flow is at its maximum and subsequently decreases during the compression phase, high level turbulent kinetic energy zones are important for combustion. The variation of the turbulent kinetic energy with respect to various discharge energies during the compression strokes is depicted in Fig. 4.5. The graph clearly demonstrates that, when the discharge energy increases (as a result of an increase in the number of coils), the average TKE increases as well. This could be caused by the air flow rate and speed increasing at higher release energy tiers.



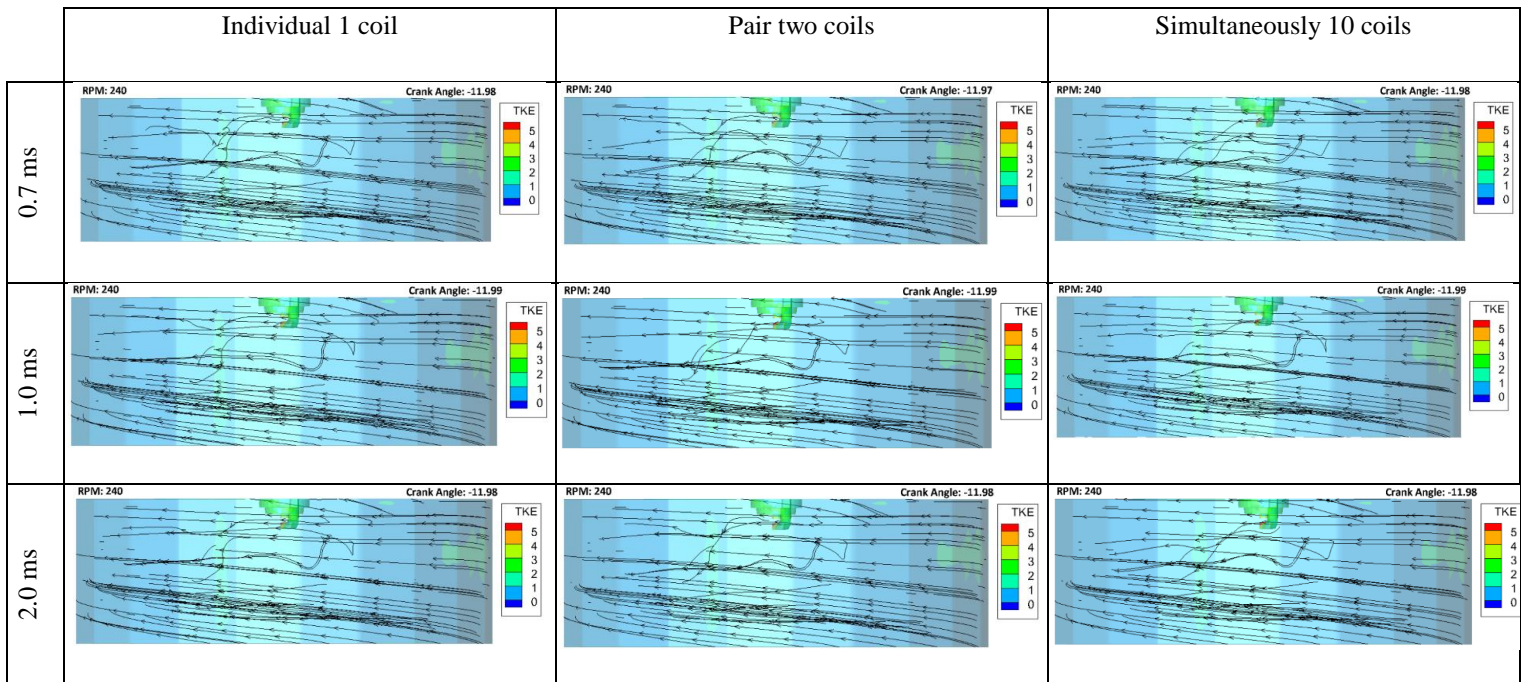
(a) Individual mode

(b) Pair mode

(c) Simultaneous mode

Fig. 4.5. TKE of spark release duration on RCEM fueled with diesel and propane direct injection with ignition strategies (individual, pair and simultaneous) and spark durations ranging from 0.7 ms till 5.0 ms in comparison to diesel RCEM auto ignition

The initial peak emerged at the last compression cycle point, at about 12°CA BTDC. Turbulence caused by direct fuel injection is the source of this highest peak. At the beginning of the expansion stroke, the piston enters a thicker area, creating a second peak. The TKE increases as a result of the increased engine velocity and spark discharge energy. When the ignition mode was switched from one single coil to ten simultaneous coils, the TKE increased on average by 0.926% (average increased TKE of 0.903 m²/s²), boosting the energy of the spark discharge. To be comprehensive, this TKE was also evaluated at six distinct spark durations, as illustrated in Fig. 4.6. These strategies work based on the energy of the spark discharge; a longer duration produces a higher spark energy and a higher TKE. The TKE of the propane RCEM modified with spark barely raised (7.20 °CA) as the spark time period grew from 0.7 ms (1.01 °CA) to 5.0 ms. The SOI of the propane used for direct injection in this simulation was set at 20 °CA BTDC. More precisely, the maximum turbulent kinetic energy of the propane RCEM using the spark ignition method was 2.638 m²/s², which was an increase of 4.44% over the basic RCEM driven by diesel. From this position until the compression stroke peak, the TKE may have increased as the spark discharge energy grew and the spark plasma created advanced. When fuel is injected into the injector nozzle, the turbulent flow is eliminated. The tumbling vortex is disrupted, increasing turbulent streamflow and leading to a greater TKE. The results of Addepalli and Mallikarjuna's investigation [124] on a big bore machine measuring 87.5 mm by 110 mm at different rotational speeds corroborate these observations. The machine's TKE climbed significantly at all three engine rotations, reaching a peak of almost 460 °CA at the start of the intake cycle. In this regard, the effect of engine speed on air velocity is not the only factor influencing the TKE; the spark release energy also plays a role. Greater TKE levels in the combustion chamber can help to achieve appropriate fuel-air mixing and ignition, which enhances combustion efficiency and lowers the generation of dangerous pollutants such particulate matter (PM) and unburned hydrocarbons (UHC).



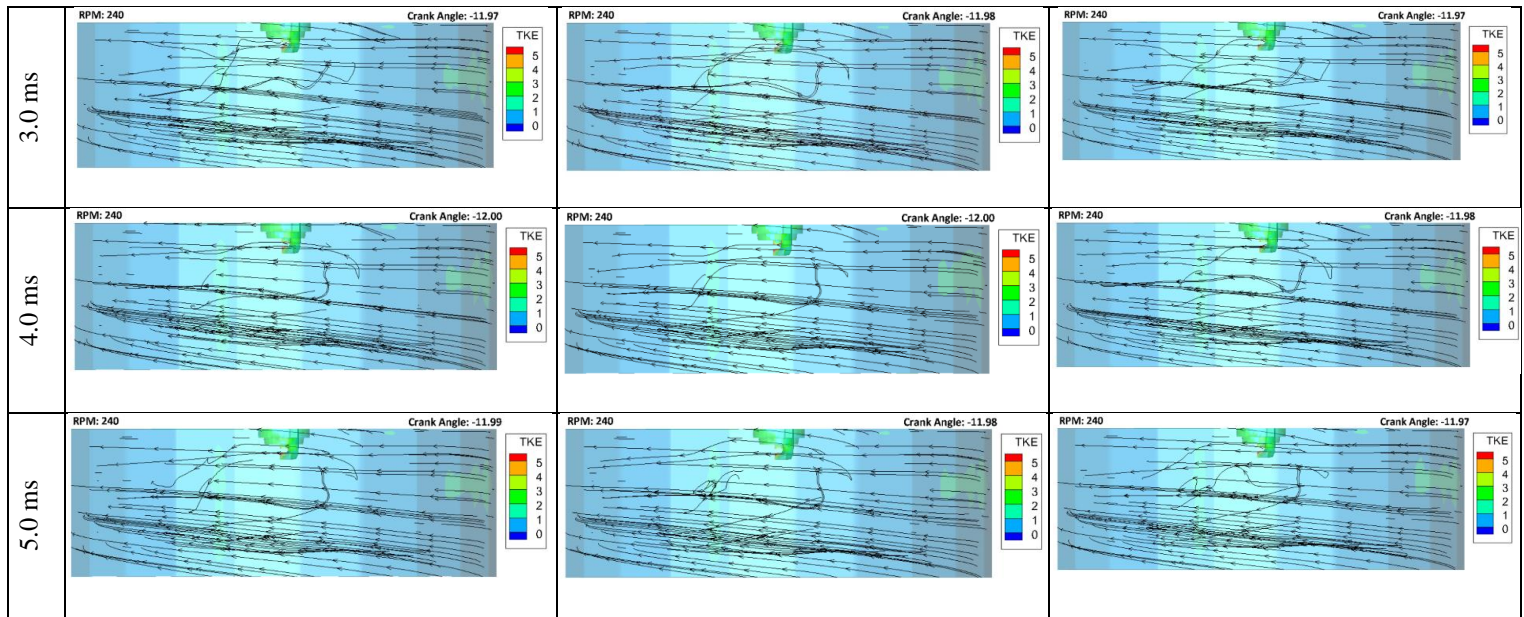


Fig. 4.6. Streamlines the TKE flow pattern's flow visualization of spark release duration on RCEM fueled with propane direct injection with different ignition strategies (individual, pair and simultaneous) and spark durations acquired at crank angle $\sim 11.97^\circ\text{CA}$ BTDC with SOI 20°CA BTDC, spark at 15°CA BTDC, speed of 240 RPM slice z position of -0.004 m , slice y position of 0.01 m

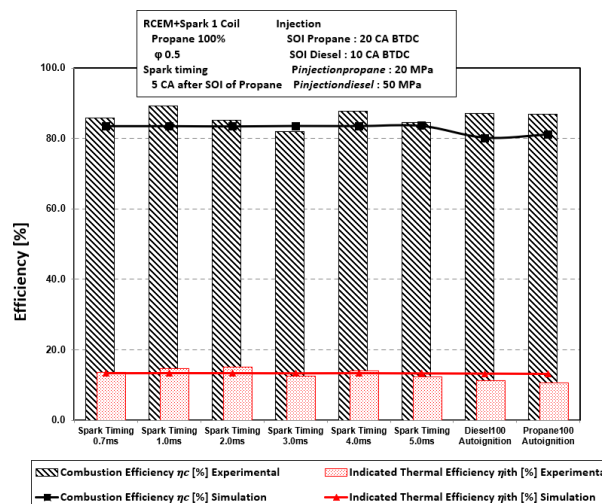
4.4 Impact of the spark released energy on combustion performance

A combustion-based investigation reveals a relationship between spark released energy and combustion features due to cycle diversities. Changes in the spark released energy are used to analyze the cycle characteristics and look at how they affect the input parameters.

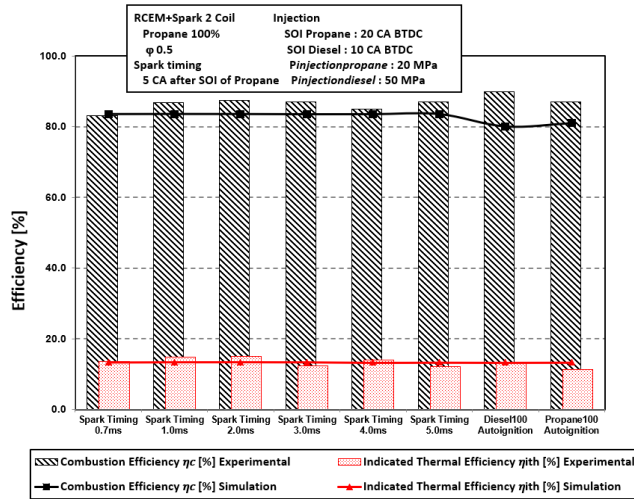
4.4.1 Combustion efficiency

Furthermore, established is the combustion efficiency, η_c , in respect to the properties of combustion. When all of the fuel's thermal power is used at TDC to increase the in-cylinder bore pressure, the best combustion occurs in a spark ignition machine. η_c is the percentage of heat that would be released through the fuel to the heat input (atmospheric conditions) at 1 atm and 298 K. The piston pulls more air into the cylinder as the engine rises to improve combustion efficiency. Selecting the appropriate energy for the spark discharge can result in stable combustion. Fig. 4.7 displays the RCEM's combustion efficiency for a range of spark

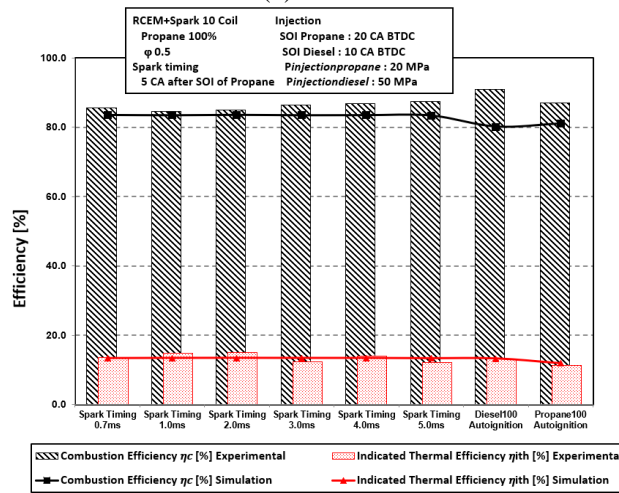
application techniques. For RCEM modified with spark, nearly all spark timing scenarios produced the same combustion capacity. The basic RCEM compression ignition engine with direct diesel injection is more efficient than the RCEM engine with spark. The thermal efficiency only marginally enhanced (7.20 °CA) when the propane RCEM adjusted with spark time period was raised from 0.7 ms (1.01 °CA) to 5.0 ms and the SOI of DI propane was 20 °CA BTDC. In comparison, diesel has a higher average thermal efficiency (14.26%) than propane. The higher heating value of diesel fuel than that of propane contributes to the improved thermal efficiency of direct injection diesel. Nonetheless, employing a spark application in a propane RCEM may enhance engine efficiency and combustion. Perhaps a longer ignition delay might provide enough mixing time. The thermal efficiency varies depending on the circumstances when the spark time increases. This circumstance could explain the engine's susceptibility to volatile propane fuel, which has a substantial impact on the combustion process. These results are in line with previous research by Masouleh [34], which observed cycle-to-cycle variation in a slow rotating machine and a relationship between the intake cycle and related turbulent flow motifs. 24,363,436 points are used in the RCEM model with a spark plug application, and 18,671,318 parts make up this mesh model. Using the spark model and the predetermined parameters, the case setup was carried out on the RCEM. For example, changing the energy amount in line with the coil configuration's counting led to different spark release temperatures in the ignition process.



(a) Individual mode



(b) Pair mode



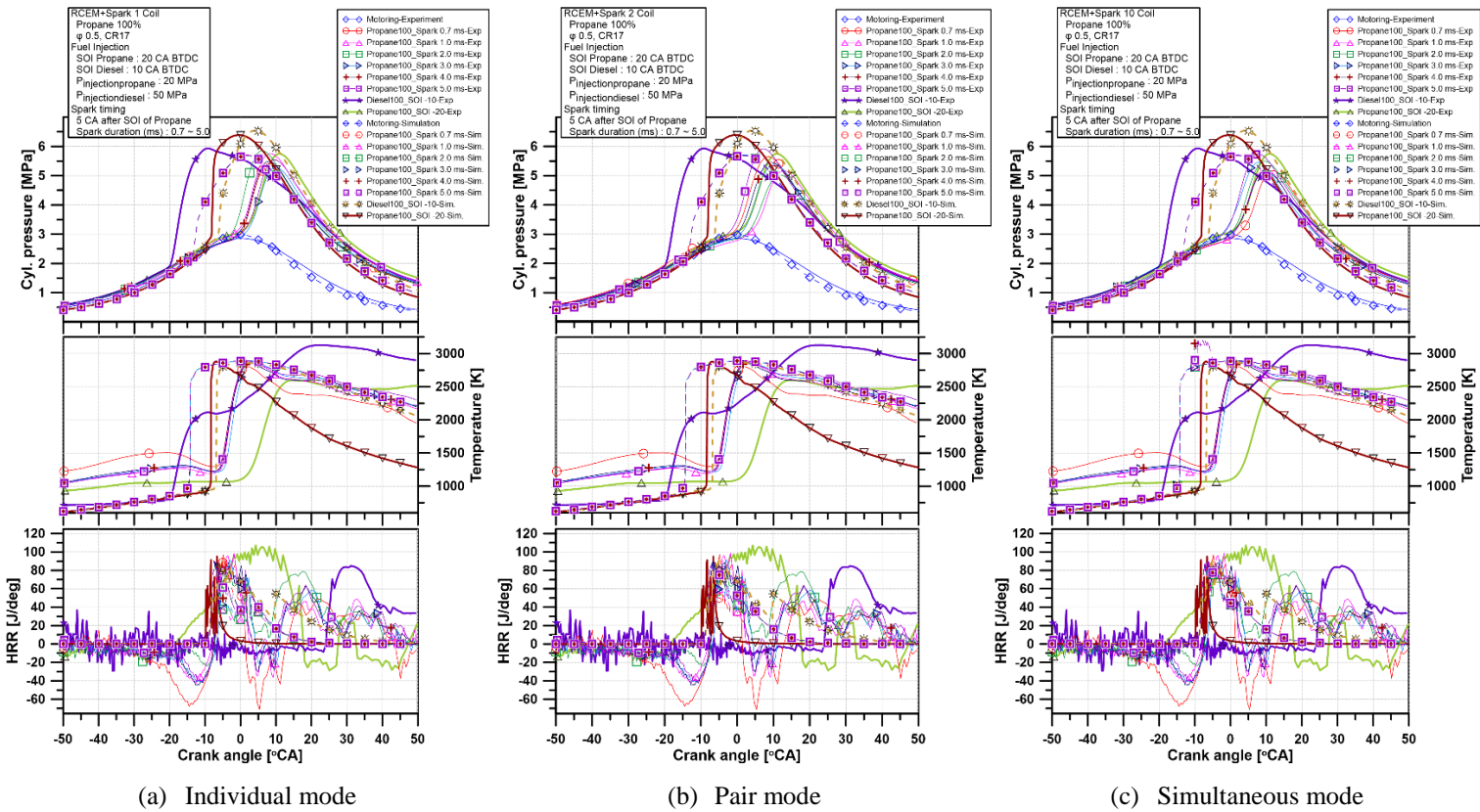
(c) Simultaneous mode

Fig. 4.7. Combustion efficiency of spark release duration study on RCEM fueled with diesel and propane direct injection with ignition strategies (individual, pair and simultaneous) and spark durations ranging from 0.7 ms till 5.0 ms in comparison to diesel RCEM auto ignition

4.4.2 Cycle performance analysis

The pressure inside the cylinder indicates the thermodynamic state of the charge. The rate of combustion can be further investigated by applying the first rule of thermodynamics and some basic assumptions. In this investigation, propane was injected via the RCEM bore at an equivalency ratio of 0.5 using various spark ignition modes in a diesel engine with a 17.0 compression ratio. Figure 4.8.a shows the influence of the three-spark method on the heat release rate (HRR), maximum temperature, and internal pressure during the full spark period interval (0.7–5 ms). The pressure measurements were gathered three times to guarantee certainty reading for every test circumstance. The matching cylinder pressures were simulated

using a range of test conditions. For any spark ignition technique, the main effects seen in simulations and experiments may be linked to the influence of spark period because the machine rotation, equivalency ratio, injection pressure, and SOI are constants. At a spark time of 1.0 ms, the single ignition approach and the simultaneous spark method yielded the highest peak cylinder pressure. The high-octane value of propane and the optimal RCEM in-cylinder pressure grew and were reached close to top dead center. In comparison, the pressure decreased by 0.183 MPa with the diesel engine. The maximum pressure was measured at a crank angle of 10.83 degrees, which is later than the diesel machine (-9.08 degrees). This situation is in line with previous research by Won Hyun Woo [125] and Yan Hu [126]. Propane has more volatility and a longer ignition delay than diesel, thus it mixes easier. In order to reduce the ignition delay during combustion, the spark ignition duration can be adjusted. Temperature and heat release rate are shown in Fig. 4.8(b) and (c) for spark durations of 0.7, 1.0, 2.0, 3.0, 4.0, and 5.0 ms. In an experimental setting employing diesel fuel with an SOI of 10 °C BTDC, the greatest in-cylinder temperature recorded was 3126 K. At roughly 2598 K, the propane fuel with SOI 20 °C A BTDC has the lowest maximum in-cylinder temperature. The reason for the difference in the in-cylinder temperatures between diesel and propane was that the latter had a lower heat value. Next, when a detailed comparison of the in-cylinder pressure, temperature, and propane and spark application is made, the results show that the spark applied at propane direct injection is nearly identical. The HRR is based on how much energy is lost via the cylinder walls and how much heat is released chemically during combustion. A behaviour pattern where the highest value decreases as the discharge energy increases is revealed by comparing different spark release energies at the same machine speed. The heat was released at nearly the same crank angle. This suggests that the flame formation process may not be directly impacted by the spark discharge duration, which Seima Tsuboi [29] also investigated. As a result, employing propane in a compression ignition engine raises the fuel's peak pressure, its amount blended at the starting point, and its rate of heat release.



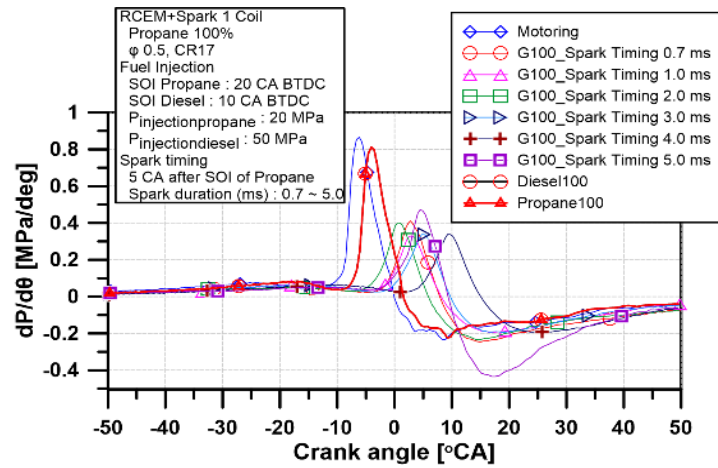
(a) Individual mode

(b) Pair mode

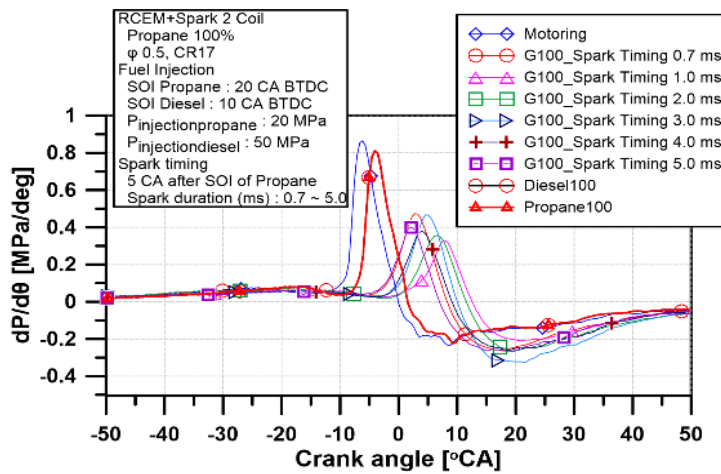
(c) Simultaneous mode

Fig. 4.8. Pressure, temperature, and IHR inside the bore of spark discharge duration study on RCEM fueled with diesel and propane direct injection with ignition strategy (individual, pair and simultaneous) for various spark durations from 0.7 till 5.0 ms in comparison to diesel RCEM auto ignition

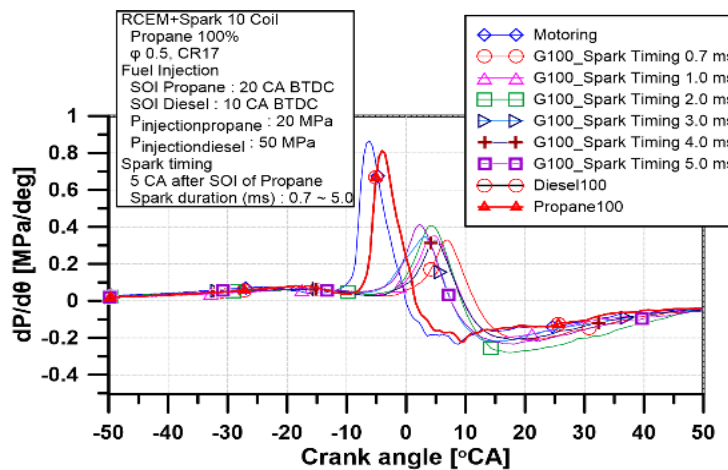
Propane fuel self-ignition problems are leading to an increasing trend of employing it in CI engines. Figure 4.9 shows the pressure rise rate (PRR) of the RCEM according to the spark ignition approach. Compared to diesel autoignition, the propane-powered RCEM with spark has a lower PRR. When a fuel with a low cetane number, such as propane, is employed, the fuel's greater rate of pressure rises in the cylinder bore results in engine noise and unburned hydrocarbon (UHC) emissions being inferior to diesel machines [12]. Furthermore, propane releases heat more quickly because to its quicker spark ignition. High reactivity fuels, such as diesel fuel, typically have a lower PRR than low reactivity fuels, such as propane fuel.



(a) Individual mode



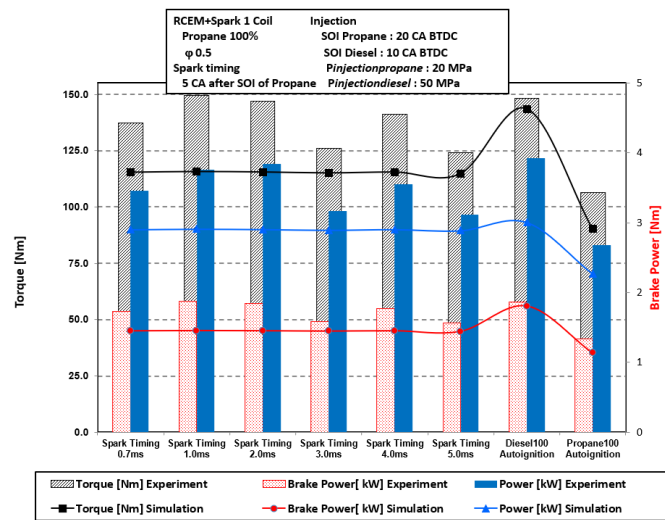
(b) Pair mode



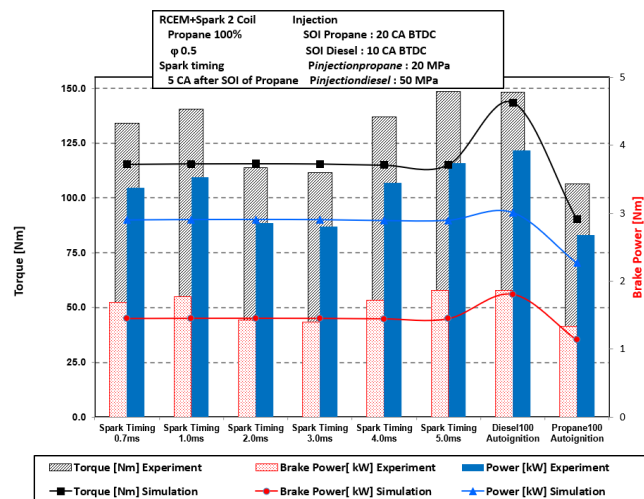
(c) Simultaneous mode

Fig. 4.9. PRR of spark release duration on RCEM fueled with diesel and propane direct injection with different ignition strategies (individual, pair, and simultaneous) and spark durations ranging from 0.7 till 5.0 ms in comparison to diesel RCEM auto ignition

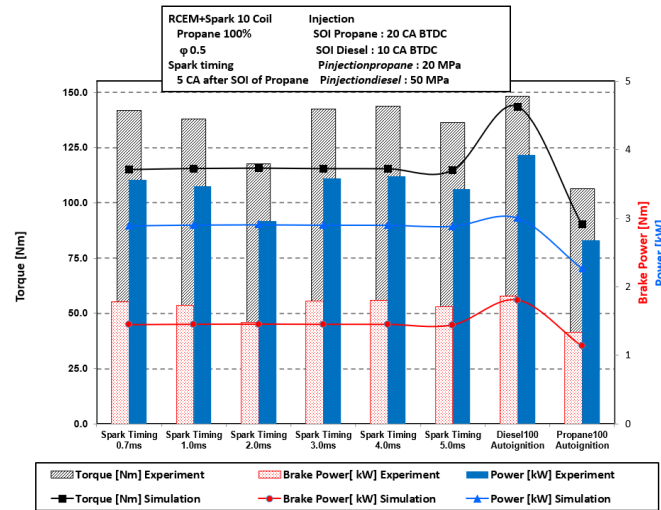
By comparing the energy of the electrical discharge at different spark periods, we found that the spark energy somewhat increases with pressure and temperature, and that the largest heat release nominals are obtained with a spark period of 1 ms. The timing of the spark has little bearing on the energy of the spark discharge. By increasing temperatures and HRR, a tiny disparity in combustion speed caused by an increase in coil quantity expedites the combustion process and speeds up the growth of flame propagation. Conversely, heat transport is impeded by higher peak temperatures and longer times at the CAD where these release energy amounts are maintained.



(a) Individual mode



(b) Pair mode



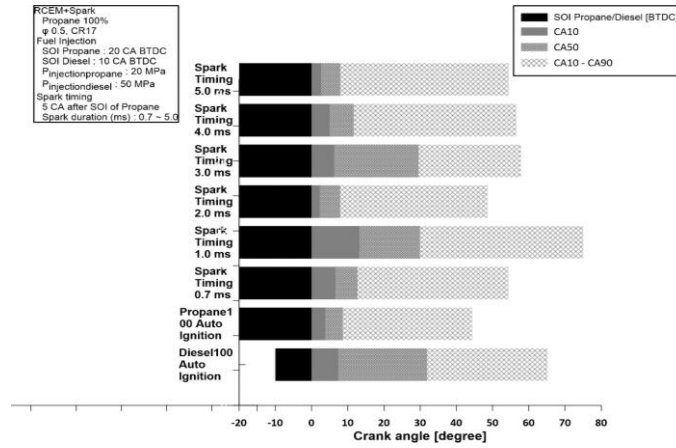
(c) Simultaneous mode

Fig. 4.10. Torque (Nm), indicated power (kW), and power (kW) of spark discharge duration study on RCEM fueled with diesel and propane direct injection with different ignition strategies (individual, pair, and simultaneous) and spark durations ranging from 0.7 till 5.0 ms in comparison to diesel RCEM auto ignition

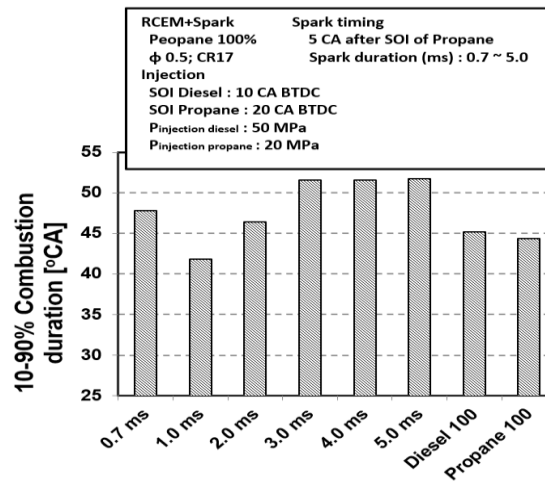
Furthermore, the analysis of the indicated power, torque, and power from models and experiments on the RCEM with spark is shown in Figure 4.10. An extended spark time approach yields higher power output. This motion makes more chemical heat and power possible. These results are consistent with research from the literature that indicates a higher mass flow rate will impact the heat in the spark area [127], resulting in a higher spark energy when the ideal temperature is reached and a faster expansion of the flame [128]. The temperature findings, heat release rate, and in-cylinder engine pressure all decreased with increasing machine speeds [129].

4.4.3 Combustion phasing period and ignition delay

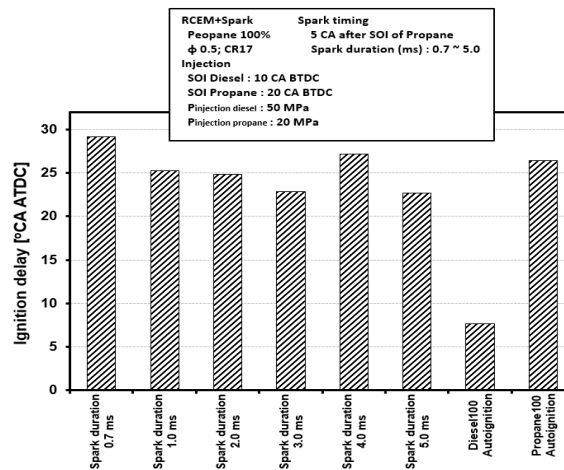
Heat release data could be utilized to predict the experiment timing. The combustion time might be determined by comparing the burning location's event to the CAD. It was expected that this investigation's intake temperature of 80 °C would result in uniform combustion with respect to propane's resistance to self-ignite in RCEM and have little impact on the maximum PRR, IMEP, and combustion phasing.



(a)



(b)



(c)

Fig. 4.11. (a) Combustion phasing, (b) Combustion duration, and (c) Ignition delay, of spark discharge duration study on RCEM fueled with diesel and propane direct injection with different ignition strategies (individual, pair, and simultaneous) and spark durations ranging from 0.7 till 5.0 ms in comparison to diesel RCEM auto ignition

Fig. 4.11(a) illustrates the RCEM's combustion phasing with the spark method, which differs from the original CI diesel autoignition. Compared to diesel DI, propane direct injection has a longer combustion phasing, with a spark timing of 15.0 ms. Propane's lower temperature, longer ignition delay, and greater mixing prior to combustion could all be contributing factors. Surprisingly similar combustion phases are used in each technique. The combustion phasing at TDC was suitably kept by the RCEM with the spark, much like diesel autoignition. A longer spark release duration of 5.0 ms was found to be able to somewhat suppress burns by increasing the probability of inflammation by visualised propagation of the spark plasma in a CVCC chamber. This result was in line with previous research by Zhenyi Yang [121], who found that varied release intervals for different energy levels give more power, which may play a major role in the transition from misfire to effective flame propagation. Fig. 4.11(b) shows the combustion time of the RCEM in the presence of a spark. The combustion duration (CA90) was found to be the time interval between the beginning of combustion (CA10), which occurs at around 10% of the fuel's accumulative thermal number, and the end of combustion (CA90), which occurs at 90% of the fuel's total heat number. The RCEM with a 5 ms spark period had the longest combustion period, which was measured on a 51.74 °CA. Propane burns more quickly due to its low temperature and extended ignition delay.

Among the various variables that might influence the duration of the ignition process are temperature, pressure, and equivalency ratio. When a diesel-fueled CI engine has an early ignition delay due to higher intake temperature, less time is allowed for the fuel to mix, resulting in higher emissions. For CI engines, propane is intriguing because of its high inhibition of auto-ignition, which prolongs the ignition delay and allows for additional blending prior to ignition. According to the data on the overall blending strengths, the scale of unblended air and fuel decreases as the ignition delay increases. Fig. 4.11(c) illustrates the ignition delay of the RCEM using different methods of spark application. The ignition delay for the RCEM over a 5 ms spark period was 8.2 ms, compared to the base diesel ignition delay of 6.3 ms. Extended ignition delays or limits that increase to auto-ignition may occur when low cetane propane is used to power the RCEM spark application. It was discovered that propane's strong auto-ignition ban in CI machines could be overcome with the use of a spark. This behaviour could be helpful for propane fuel since it gives the blending process an extra moment to complete itself after the injection cycle but before combustion starts, enabling combustion

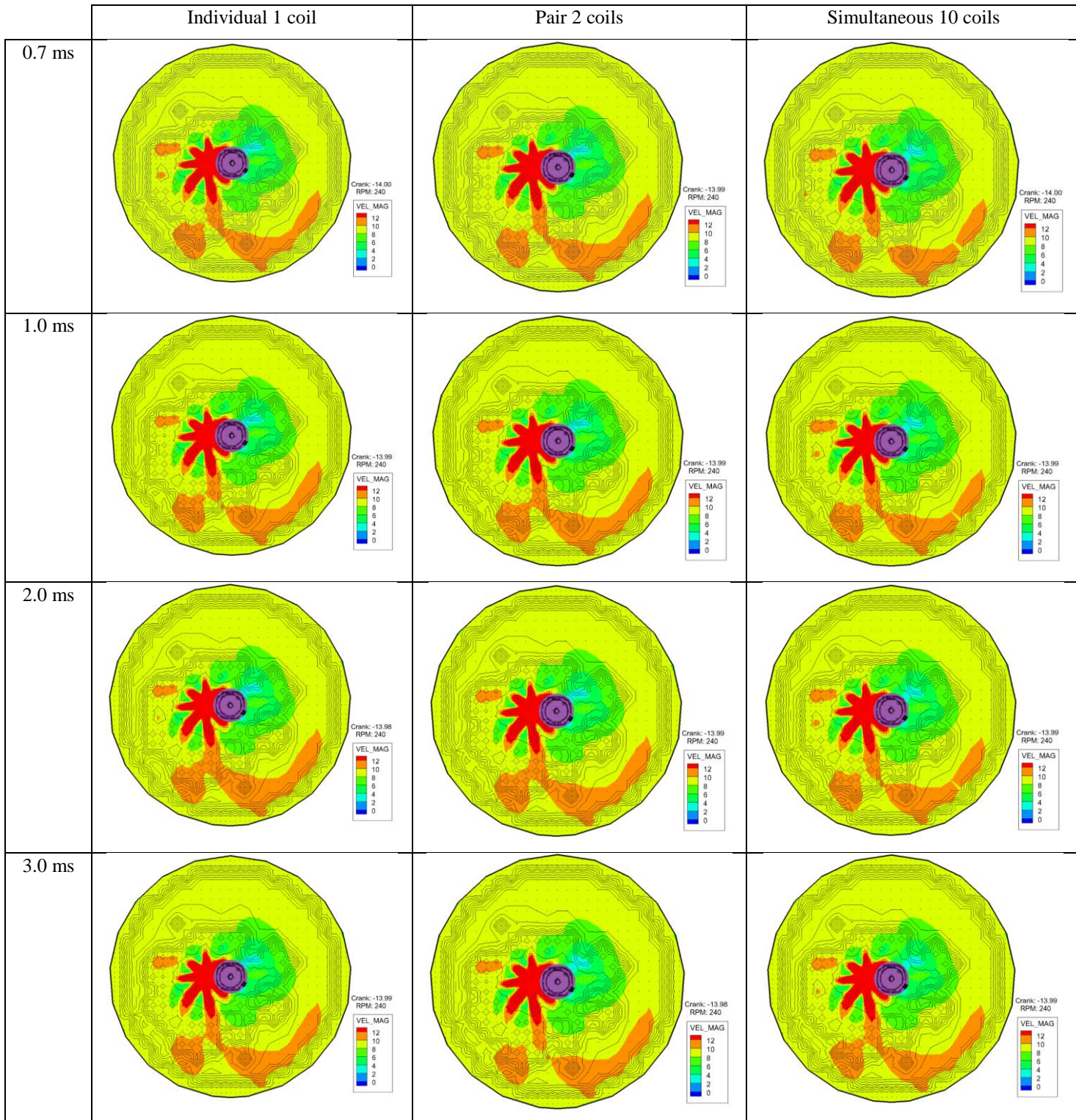
phasing to occur very close to TDC. On the other hand, a prolonged ignition delay may cause phased-delay combustion, which may result in an insufficient machine or ineffective thermal heating. In order to overcome the approach, a propane-powered compression ignition engine with a spark ignition method was used, as evidenced by the correlation between the charging period and release energy found by Zhenyi Yang [121] in a prior study [66]. Even at the lowest current and longest discharge length, the combination will not ignite. When the length time is increased, the creation of flame kernels does not significantly improve. This result implies that an extended-release period provides more energy availability, which may be the main cause of the transition from misfire to acceptable flame spread.

4.4.4 Spark discharge source flow

Previous study [130][131] has shown that the flow regime inside the cylinder at the spark plug discrepancy during the ignition period affects the emergence of the flame kernel and the subsequent combustion procedure. The results of the simulation have been spatially averaging almost the area, as Fig. 4.12 illustrates. These data show spatially screened value in comparison close to the spark plug with increasing spark discharge energy. The analysis strategy does not immediately penetrate the spark plug, in contrast to what was previously said. Despite this feature, the spark plug may still be projected at a same rotating velocity.

The large velocity magnitudes around the spark plug are consistent with the direction of the velocity flow. Turbulence scaling and modelling turbulent combustion are affected by the resolved-scale velocity slope. As proven by Petersen and Ghandhi [132], engine streamflows will likely experience turbulent dispersion in relatively small high-shear locations amid larger structures. This is consistent with the flow circulations shown in Figure 4.12 defies the surrounding flow by using a spark plug. The combustion room's red zone, as seen by the simulation imagery, corresponds to the streamflow circulation with the highest velocity. The blue zone reveals lower streamflow speed. Previous discussions on combustion phasing indicate that CA10 happened at 15 °CA BTDC, which is sometime after spark ignition. At -13.98 °CA BTDC, the average capture temperature, the centre, near the spark plug, burns first. The spark plug's in-cylinder streamflow turns out to be travelling clockwise, in line with the RCEM. All cycles have the same spark motion when it comes to the in-cylinder stream crossing the spark plug. The difference in flow rate caused by the energy influence of spark release is not very noticeable for any spark ignition strategy or time period. Consequently, a higher

velocity may cause the flame to form more quickly and expose the early kernel to greater velocities. Conversely, a lesser velocity causes slower early flame growth.



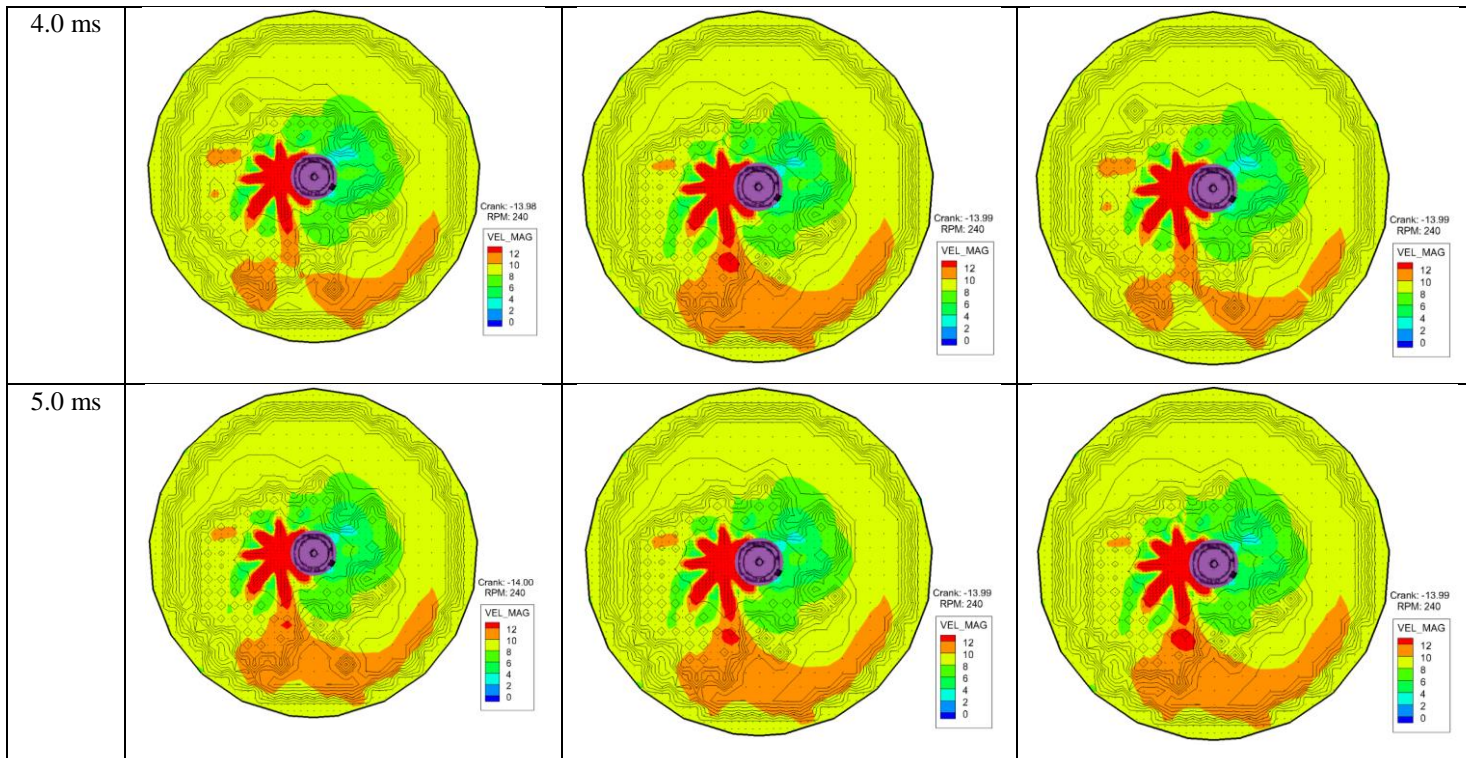


Fig. 4.12. Velocity magnitude flow area around the spark plug spark release duration on RCEM fueled with diesel and propane direct injection with different ignition strategies (individual, pair, and simultaneous) and various spark durations ranging from 0.7 till 5.0 ms captured at a crank angle of $\sim 3.98^\circ\text{CA}$ BTDC with a SOI of 10°CA BTDC, spark of 5°CA BTDC, speed of 240 RPM, and slice z position of -0.004 m, in comparison to diesel RCEM auto ignition

4.5 Summary

This study investigated the impact of spark released energy on the RCEM with several spark ignition and propane DI techniques using calculations and experiments. By varying the spark discharge time, CONVERGE computational fluid dynamics was utilized to investigate the evolution of spark plasma, turbulent kinetic energy, velocity distribution flow, and tumble motion flow. To increase the ignition released energy for six different ignition timing scenarios (0.7, 1.0, 2.0, 3.0, 4.0, and 5.0 ms), three spark ignition techniques using 50 to 200 mA were assessed. The following conclusions can be drawn from this study:

1. Multiply the current by the voltage to get the discharge energy release rate. Consequently, the simultaneous strategy—which was followed by the pair and the individual in that

order—produced the maximum released energy, coming in at about 190 mJ/s. This outcome is consistent with the energy provided by the in-cylinder released energy, which grows with the length of the discharge.

2. There was no discernible variation in the plasma size between the three igniting methods. The plasma size remained essentially unchanged even after selecting the simultaneous 10 coil option and increasing the released current to 200 mA. Therefore, there was no appreciable impact of pursuing the discharge spark time interval on the flame plasma formation phase.
3. The propane RCEM using the spark ignition method had the highest turbulent kinetic energy, measuring $0.903 \text{ m}^2/\text{s}^2$, which is a 0.926% increase over the RCEM powered by diesel. This might occur because the spark plasma advanced as a result of increasing the spark's released energy.
4. The thermal efficiency of the RCEM with spark rose slightly when the spark time period was raised from 0.7 ms (1.01 °CA) to 5.0 ms (7.20 °CA) with the SOI of propane DI set at 20 °CA BTDC. When compared to propane, diesel has a higher average thermal efficiency (14.26%). Because diesel fuel has a higher heating value than propane, it has a greater thermal efficiency than propane. A lower combustion period, more complex combustion phasing, and greater in-cylinder temperatures are the results of rising pressure and temperature.

5. EFFECT OF SPARK DISCHARGE DURATION ON LOW CARBON COMBUSTION AND EMISSION

In this chapter, the effects of spark discharge duration control strategies on low carbon combustion and emissions are investigated with a rapid expansion and compression machine research engine with spark application fueled by propane direct injection. An experimental system and simulation model were established to investigate in-cylinder combustion performance and emission characteristics.

5.1 Effects of spark discharge duration on the combustion of CI engines

An experiment on a rapid expansion and compression machine research engine with spark application powered by propane direct injection produced the experiment's findings. In this experiment, three variables that affect in-cylinder performance—cylinder pressure, temperature, and heat release rate—are evaluated to see how the energy released by spark affects the operation of an RCEM research engine that has been converted to run on spark and propane.

5.1.1 In-cylinder pressure for various spark duration timing

Propane with an equivalency ratio of 0.5 was introduced into the RCEM combustion chamber of a diesel engine with a CR of 17.0, and the spark duration was varied (0.7, 1.0, 2.0, 3.0, 4.0, and 5.0 ms). For every ignition technique, pressure values were taken three times in order to avoid readings that were unclear. The engine velocity, injection pressure, SOI, and equivalency ratio were fixed for this set of experiments and models. Therefore, for each spark ignition method, the main effects can be attributed to the timing of the sparks. The in-cylinder pressure is affected by the amount of energy lost through the bore walls and the percentage of chemical heat generated during combustion. With numerous ignition mechanisms and propane direct injection as fuel, the pressure inside the RCEM's in-cylinder is shown in Fig. 5.1. The spark duration was changed from 0.7 to 5.0 milliseconds. When the RCEM was driven by diesel at SOI 10 °CA BTDC, the maximum in-cylinder pressure was 5.9 MPa. The propane-fueled

RCEM had an average in-cylinder pressure of 5.7 MPa when SOI reached SOI 20 °CA BTDC. This pattern suggests that using spark as a method of ignition in conjunction with low-carbon propane combustion has an in-cylinder pressure equivalent to that of feeding an engine with diesel, which may reduce NO_x emissions. The reason for this decrease is that propane has a little higher liquid specific heat and a lower heating value than diesel. When the energy of several sparks released at a fixed machine rotation is evaluated, the longest discharge period results in a decreasing highest value. About the same crank angle was used to emit the heat. Accordingly, the length of the spark that is released, as studied by Seima Tsuboi et al. [29], might not directly affect how a flame forms. Propane increases the amount of fuel mixed at the beginning of combustion and raises the peak pressure, which speeds up the release of heat in a CI engine. The energy of the discharge was not significantly affected by the spark's timing. A slight change in combustion velocity caused by an increase in coil count sped up the combustion stage and the flame's evolution by raising temperatures. Heat transfer is impacted by these release energy levels, which are maintained at greater peak temperatures and longer crank angle durations.

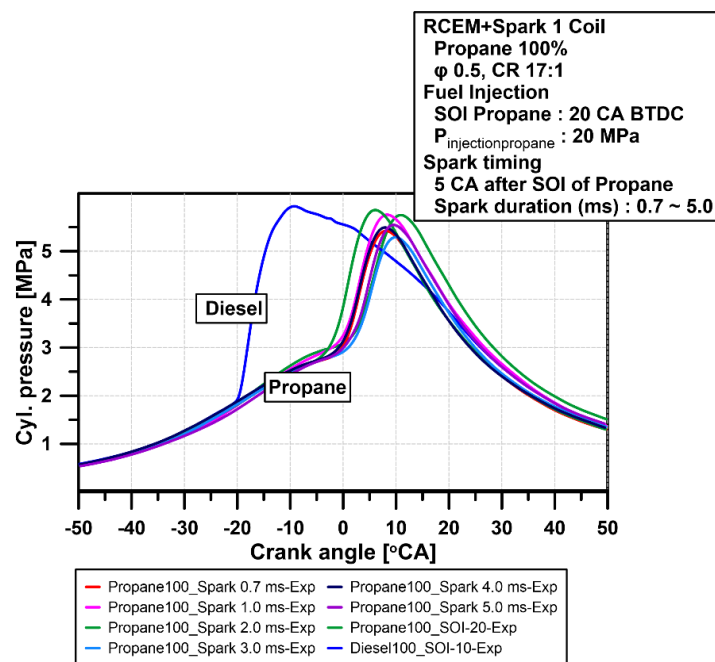


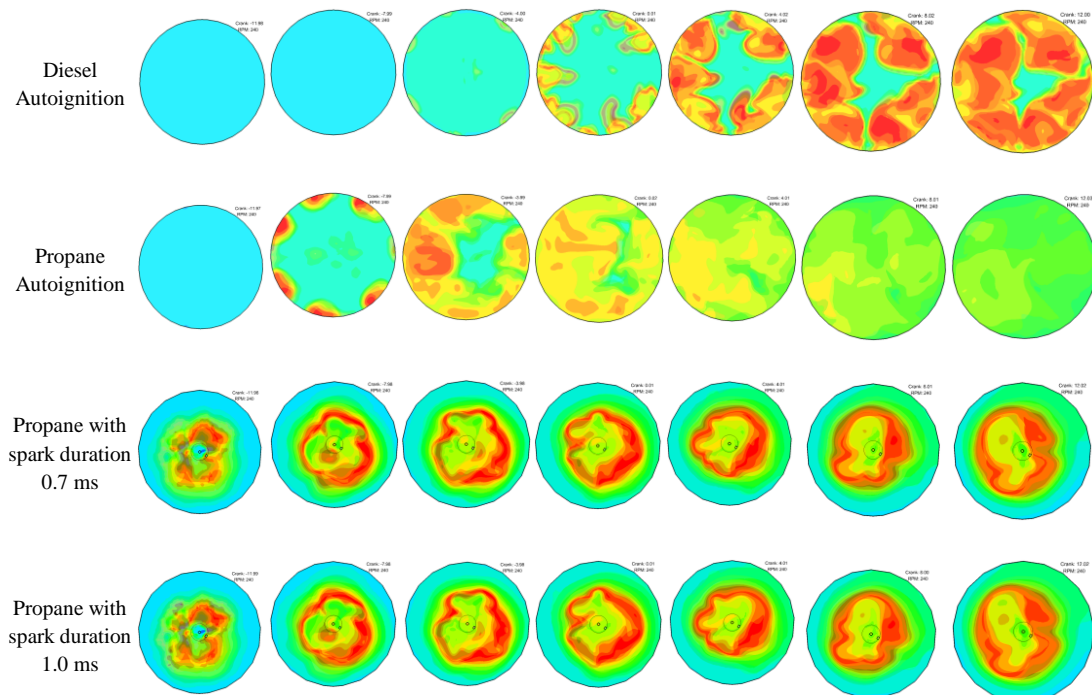
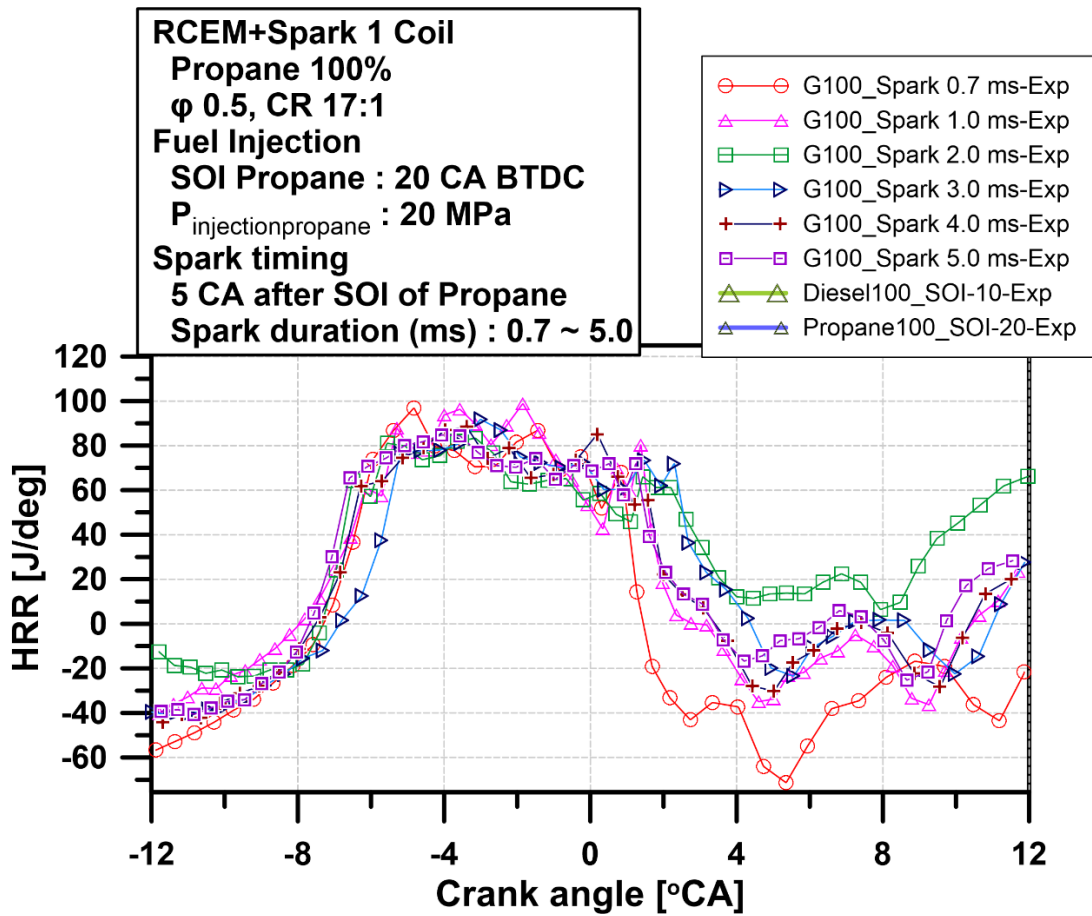
Fig. 5.1. In-cylinder pressure for varied spark durations between 0.7 and 5.0 ms in a propane-fueled RCEM with direct injection.

With a higher propane octane number, the maximum pressure of RCEM rose and approached TDC. The maximum pressure value was determined by measuring the 0.183 MPa pressure drop at CA of 10.83 degrees, which is later than that of the diesel engine (-9.08 degrees). This

situation is supported by the results of earlier studies conducted by Woo [125] and Hu [126]. Due to propane's greater volatility and longer ignition delay, diesel and propane can mix easily. Because of this, the ignited spark time might aid in lowering the ignition delay along the combustion state.

5.1.2 Heat release rate for various spark duration timing

The HRR is determined by the rate at which chemical energy heats up as a result of combustion processes and the rate at which thermal energy escapes through the cylinder walls. The effect of the spark length timing on the HRR across the course of the spark duration range (0.7–5 ms) is shown in Fig. 5.2. The largest pressure was obtained with the simultaneous spark approach at 1.0 ms of spark duration, and this was followed by the paired and single ignition techniques. By using high-octane propane, TDC was approached and the ideal RCEM pressure increased.



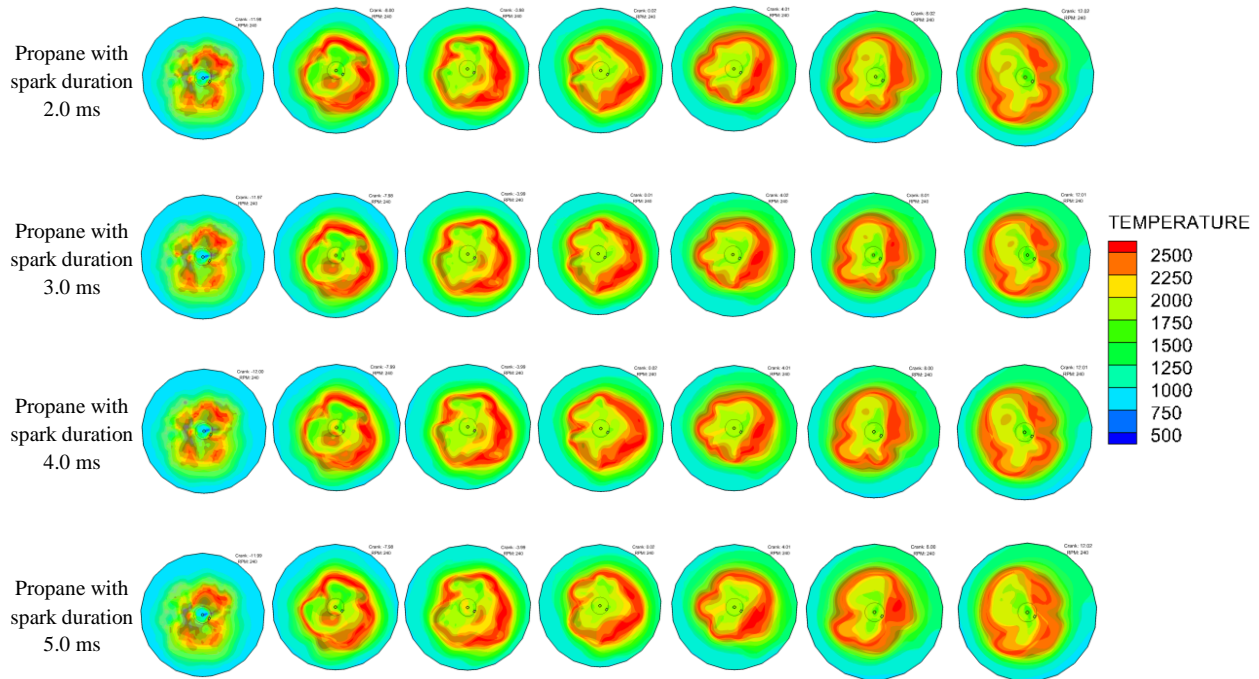


Fig. 5.2. Heat release rate and in-cylinder temperature distribution of the RCEM combustion chamber fueled with propane-DI with spark ignition strategy for spark durations from 0.7-5.0 ms, speed 240 RPM, slice z position – 0.004 m.

At SOI 20 °CA BTDC, the highest maximum HRR for RCEM fuelled with propane was around 90 J/deg. The HRR peaked between -8 and 4 °CA, as the HRR traces demonstrate. When the combustion processes of propane and diesel were thoroughly examined, the in-cylinder pressure and HRR were found to be almost identical. The heat release analysis indicates that the direct injection angle and injection time have an impact on the early phase of combustion. According to research by Splitter et al. [46] and Rajasegar et al. [43], direct injection considerably speeds up combustion. Delaying direct spark plug injection will therefore accelerate the early combustion phase.

5.1.3 In-cylinder temperature for various spark duration timing

The impact of cylinder peak temperature on heat transfer deficiencies and the generation of undesired emissions, most notably NO_x, is the reason for its significance [133]. A low intake temperature should naturally lead to a high input mass and inlet air density at a specific cylinder pressure as the cylinder temperature was determined using the ideal gas law. This is because a

lower inducted air mass results from a reduction in air density as the temperature of the inducted air rises. The effect of the spark duration timing on the in-cylinder temperature over the course of the entire spark period (0.7–5 ms) is shown in Fig. 5.3. The fuel with the highest cylinder temperature was diesel. Propane cylinder temperature varied from several spark duration fluctuations to about 2200 K. Unintentionally, the introduced fuels had different weights, but the measured fuel in the combustion chamber stayed consistent, therefore the injected fuel for both diesel and propane was changed to the same energy content. Thus, in this context, consuming less fuel led to a reduced IMEP, as found by Loeper et al. [92]. The combustion phasing change had an effect on the IMEP. The reduction of fuel consumed will lead to lower residual temperatures and lower combustion temperatures. Low-temperature combustion is what this is, usually occurring below 1800 K with minimal NO_x and soot emissions.

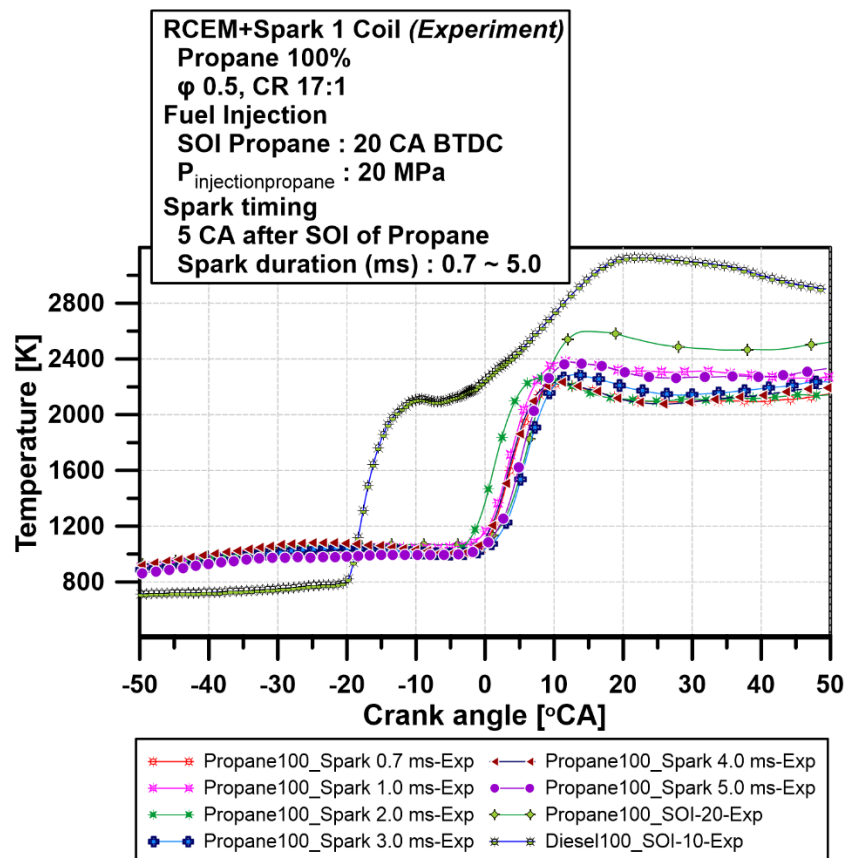


Fig. 5.3. In-cylinder temperature for varied spark length between 0.7 and 5.0 ms on a propane-fueled RCEM with direct injection.

We measured against the released energy at various spark timings and the maximum heat release values at the spark timing of 1 ms, and found that the spark grows with temperature and pressure. The spark's duration has a negligible effect on its released energy. The laminar flame

formation speed and combustion time are shortened by expanding temperatures and HRR when the number of coils is increased. This is achieved by creating a small gap in the combustion velocity. Conversely, longer times at the CAD during which these released energy levels are sustained have an impact on higher peak temperatures and heat transmission. These results supported earlier research, which shows that a higher flow rate will influence the thermal heat in the spark zone [127], leading to a stronger discharge of sparks when the flame front expands more quickly and the ultimate heat is attained [128]. In the example of propane-air combustion, Bonneau et. al. [134] discovered that the interactions of turbulent flow with quick and slow chemical reactions, compressible effects, walls, and heat losses altered heat flux signals.

A thorough summary of the findings on the impacts of spark duration on propane-fueled RCEMs shows that improving spark timing can enhance thermal efficiency as well as other combustion parameters like in-cylinder temperature, pressure, and release rate. The effects of spark timing on combustion are not monotonous; the pressure increase then quickens in accordance with the rate of heat release; the direct injection angle and injection time have an impact on the early phase of combustion based on the heat release; the temperature of the propane cylinder was slightly adjusted for multiple spark timings.

5.2 Effects of spark discharge duration on performance of CI engine

Assessing engine economics and overall performance requires consideration of engine thermal efficiency [135]. By modifying the fuel's properties or selecting the right igniting technique, it can be made better. Fig. 5.4 shows the IMEP and indicated thermal efficiency on a propane direct-injected RCEM as a function of spark timing length. When comparing diesel fuel to propane, higher IMEP and thermal efficiency were achieved. This is as a result of the IMEP using combustion heat being raised by the input heat calories. These results showed that increasing IMEP required more fuel to produce a certain amount of power.

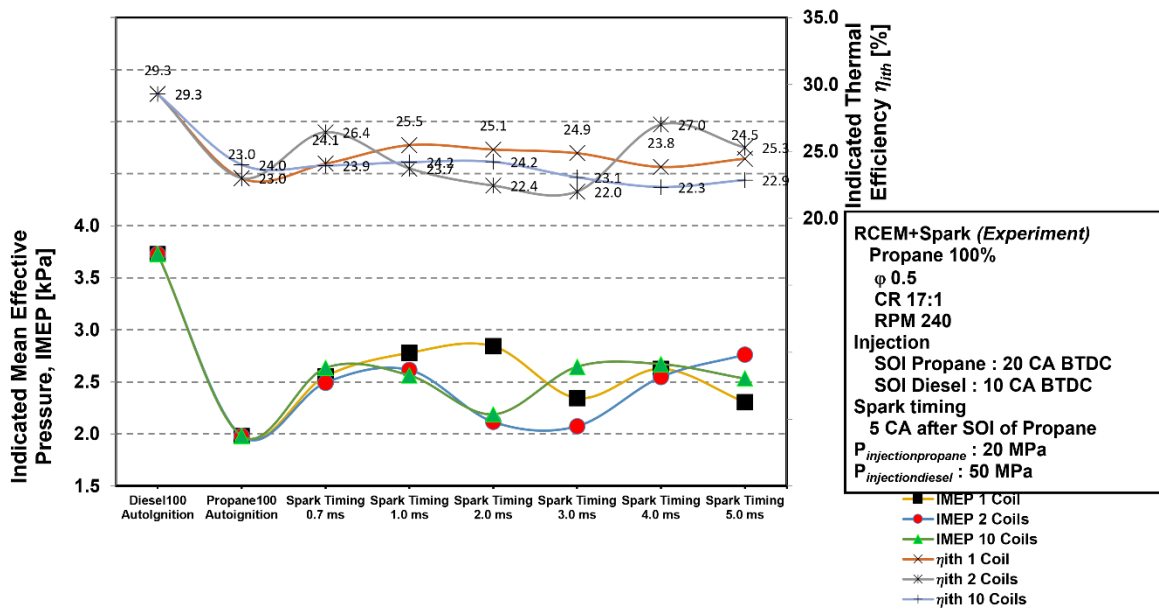


Fig. 5.4. The impact of spark lengths from 0.7 to 5.0 ms on the IMEP and indicated thermal efficiency for RCEMs powered by propane direct injection.

With a spark duration length increase from 0.7 ms (1.01 °CA) to 5.0 ms (7.20 °CA) at a direct injection propane SOI of 20 °CA BTDC, the propane RCEM modified with spark's thermal efficiency somewhat improved. As a result of its higher heating value, diesel fuel has a higher average thermal efficiency (14.26%) than propane. Applying a spark application to a propane RCEM modification can increase its efficiency by using a spark ignition method. There is adequate time for mixing with a longer ignition delay. Increasing the spark timing also changes the thermal efficiency in several situations. It seems that the combustion mechanism is affected by the volatile property of propane fuel. These responses are supported by Masouleh [34], who demonstrated that turbulent flow patterns fluctuated from cycle to cycle and were linked to a slow-rotating machine intake stroke, corroborates these answers. Longer spark durations were correlated with higher thermal efficiency. Furthermore, the trend in this finding is similar to that of Windarto, et. al.'s study [59], which showed that the simultaneous ignition approach for diesel fuelled by RCEM had a superior total discharged energy and that the selected strategy improved diesel efficiency more than propane.

Because propane fuel self-ignites, using it in a CI engine might be difficult. Fig. 5.5 shows the pressure rise rate (PRR_{max}) and BSFC as a function of spark duration on a propane direct injection fueled RCEM. The PRR of the diesel auto-ignition modified RCEM fueled by

propane with spark application is higher than the diesel PRR. Engines running on low cetane fuel, such as propane, usually release more unburned hydrocarbons into the atmosphere than those running on diesel [136], [137]. More heat is also released from propane since it burns with a faster spark. Previous studies have demonstrated that the pounding and PRR are operational limitations of the compression ignition technique that lead to noise escalation. But a high-sensitivity fuel, like diesel, often yields a lower PRR than a low-sensitivity fuel, like propane. It is possible that the homogeneous mixing process will take longer during compression. PRR_{max} thus tended to decline.

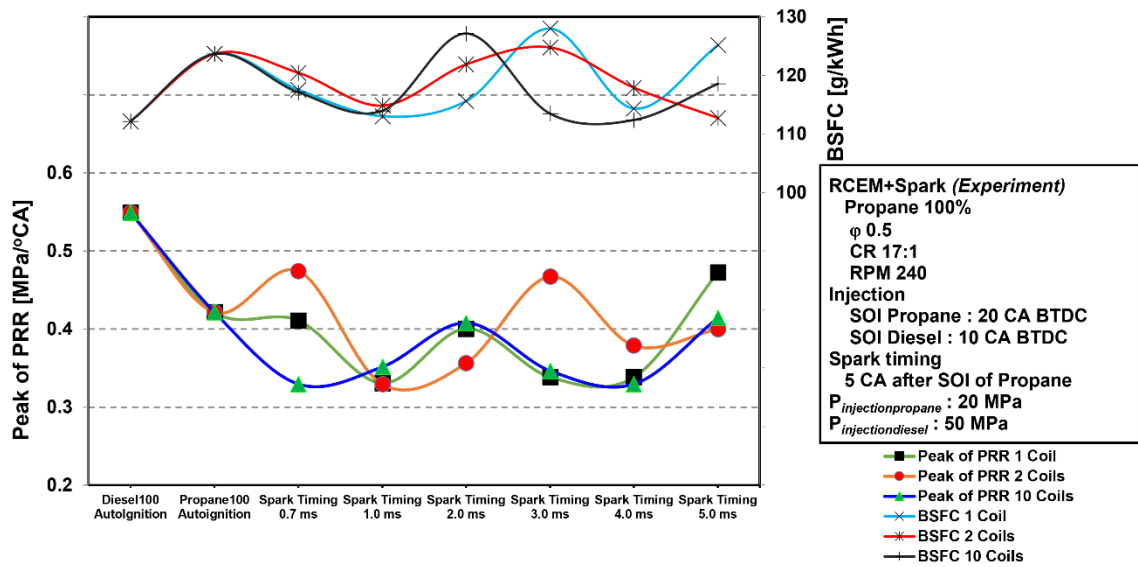


Fig. 5.5. The impact of spark lengths from 0.7 to 5.0 ms on the peak of pressure rise rate and BSFC for RCEMs powered by propane direct injection.

The author notes that when spark duration increases, BSFC tends to increase. The combined impacts of lower heating value and increased thermal efficiency are to blame for this. Propane autoignition and propane with spark application did not differ significantly, although extending the spark duration resulted in a rise in BSFC.

The CA 50 and PRR_{max} for the dataset shown in the earlier sections are shown in Fig. 5.6. When using spark ignition, the propane-fueled RCEM has a lower PRR than the diesel autoignition. Additionally, a higher proportion of fuel carbon leads to THC emissions, which rose quickly during the implementation of California Law 50 and continued to rise for propane fuel. PRR_{max} , however, falls with retarded CA 50. Consequently, bulk-gas emissions from

operations with low PRR_{max} may occur, particularly from cycles that run more slowly than usual.

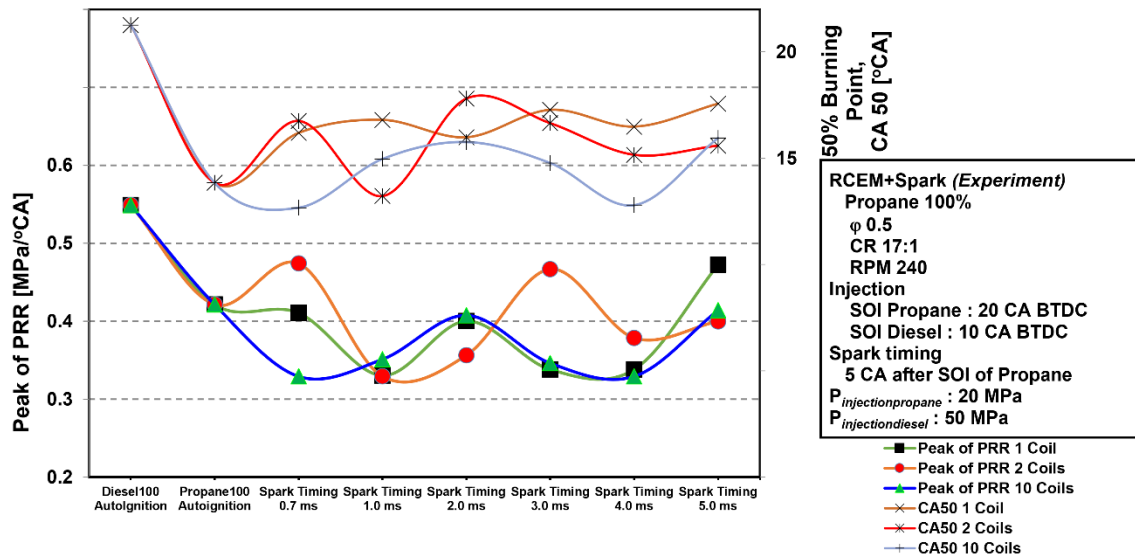


Fig. 5.6. The impact of spark lengths from 0.7 to 5.0 ms on the peak of pressure rise rate and CA 50 for RCEMs powered by propane direct injection.

A comprehensive summary of the findings regarding the impact of spark duration on the performance of RCEMs fueled by propane is as follows: while advancing spark timing increases thermal efficiency, it still has a higher thermal efficiency than propane; BSFC tends to increase with increasing spark duration; PRR_{max} decreases when CA 50 is retarded. Thus, it is possible to enhance the combustion process as a whole.

5.3 Effects of spark discharge duration on the emissions of an CI engine

In order to describe the RCEM model that uses a spark plug fuelled by propane direct injection, data on how spark discharge length influences pollutants were generated by simulation on CONVERGE. Using disparate experimental data on the pressure between the simulation results and experimental data, the physical representation is validated. The comparison of the simulation and experimental findings for driving pressure and crank angle is validated (Fig. 5.7).

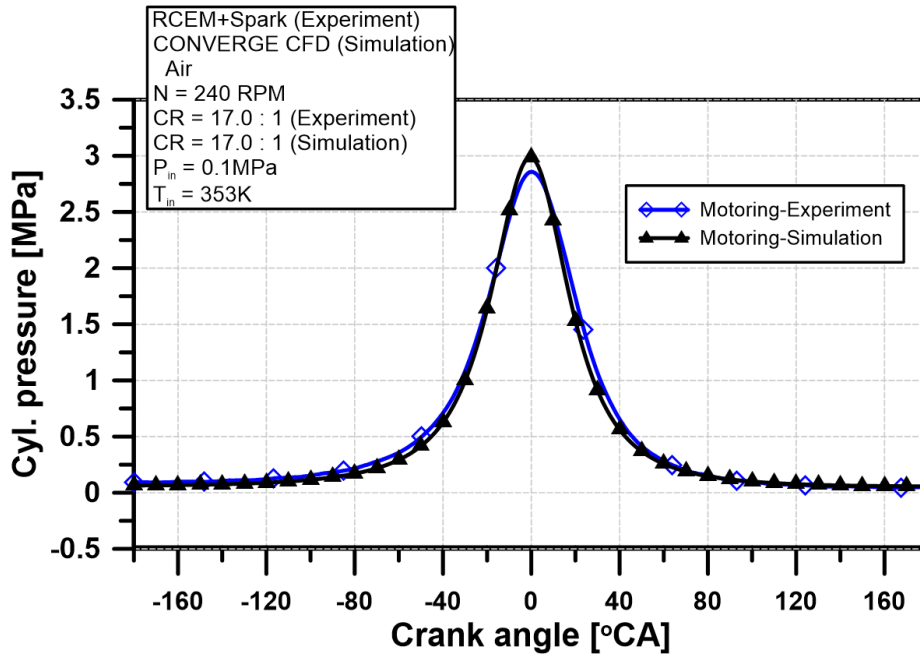


Fig. 5.7. Validation of in-cylinder pressure in RCEMs between simulation and experiment.

5.3.1 Hydrocarbon emissions (HC)

Partially burned fuel can result in unburned hydrocarbon. [138]. Insufficient combustion and wall quenching [139] are the main contributors of hydrocarbon emissions from combustion processes. A higher in-cylinder temperature can address these issues, which could be brought on by a quick burn rate that reduces heat transport [133]. At high combustion temperatures, the THC emissions are reduced by the high-efficiency combustion. Engine inefficiency can be predicted by computing the total hydrocarbon emissions of CI engines. Fig. 5.8 displays the THC pollutants of the diesel and propane fuel-powered simulated RCEM research engine. According to the figure, for every spark length of around 1.803%, the THC pollutants in diesel fuel are almost identical to those in propane fuel. Because of the much lower HRR and in-cylinder temperature, THC contaminants may increase. In one case, the reduced THC emission for propane is believed to be the result of full combustion of the homogenous fuel-air mixture due to a low carbon content. Higher homogenous ranges will be possible because of propane's improved fuel volatility (lower temperature evaporation), which will promote evaporation and mixing and reduce the liquid fuel thin film on the cylinder wall caused by impingement. During the cycle, there may be an improvement in the combustion in the cylinder bore. Certain fuels cannot burn entirely due to localized regions with non-homogeneous air-fuel mixing and extremely short combustion periods ranging from the very rich to the very low. THC emissions

will rise as a result. THC emissions increase in proportion to the amount of propane supplied up until auto-ignition. Previous studies [140], [141] have shown that substantial amounts of THC emissions are produced at low combustion temperatures, which makes it difficult to comply with emission standards. However, it seemed expected that the HC released from the crevice volume during the first step of the expanding operation would be oxidized because the timing of the spark was pushed back towards TDC. The shorter combustion time is what caused this to happen [142]. Multistage injection strategies that advance the commencement point of heat release and achieve a longer duration, as examined by Guo et. al. [143], are another element that can lower hydrocarbon emissions. In the successful optimization range of the direct start, the split injection technique with an injection timing of 1 ms is more advantageous.

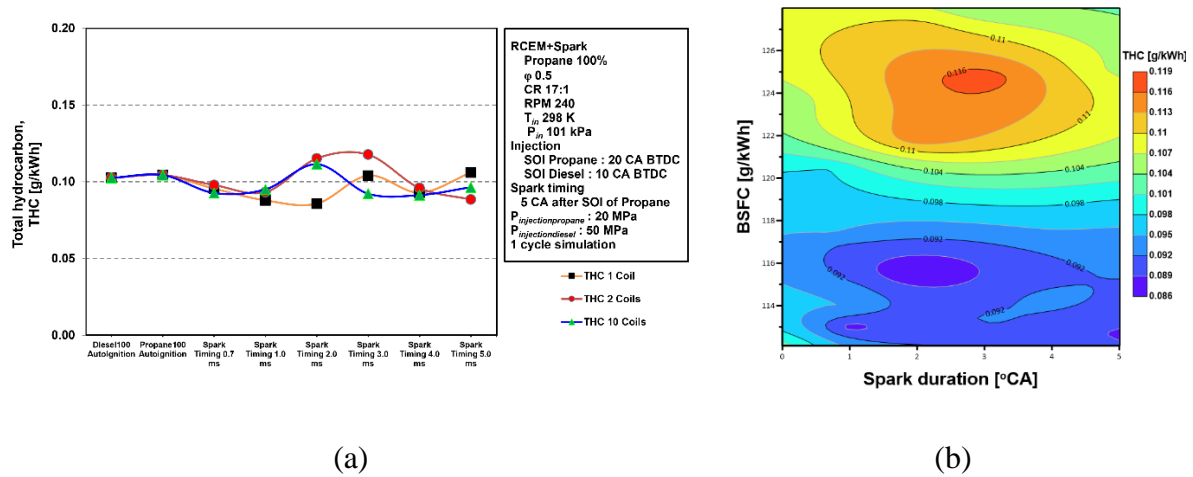


Fig. 5.8. (a) THC comparison on different spark ignition strategy on RCEM fueled with propane and (b) THC and BSFC comparison on different spark duration on RCEM fueled with propane.

5.3.2 Carbon monoxide emissions (CO)

Carbon monoxide is produced when there is insufficient fuel combustion in the engine. Incomplete burning happens when there is insufficient oxygen to finish combustion [144], [145], leaving a trace amount of CO produced by the engine cylinder's oil coating burning [146]. CO emission decreases with a rise in engine velocity [147]. The CO emission of the simulated RCEM research engine running on propane and diesel is displayed in Fig. 5.9. Diesel fuel emits 23.99% more CO emissions per kWh on average (0.085 g/kWh) than propane fuel. A low local equivalency ratio in relation to fuel mixing and temperature will result in higher CO emissions. According to another study by Changming Gong et. al. [148] the CO emissions

gradually rose as the equivalency ratio decreased for all compression ratios and at equivalency ratios higher than 0.25. These results are consistent with that finding.

Propane fuel had a shorter ignition delay than diesel fuel in a prior study [59], which led to insufficient combustion and increased CO levels. Propane, however, can be mixed well because it is more combustible than diesel. Propane, with its low cetane number and volatility, also has a significant auto-ignition characteristic. Elevated auto-ignition misfiring can occasionally lead to higher CO emissions. One possible good measure of combustion efficiency is the quantity of CO emissions in the exhaust. A decrease in CO emissions could therefore indicate increased combustion efficiency.

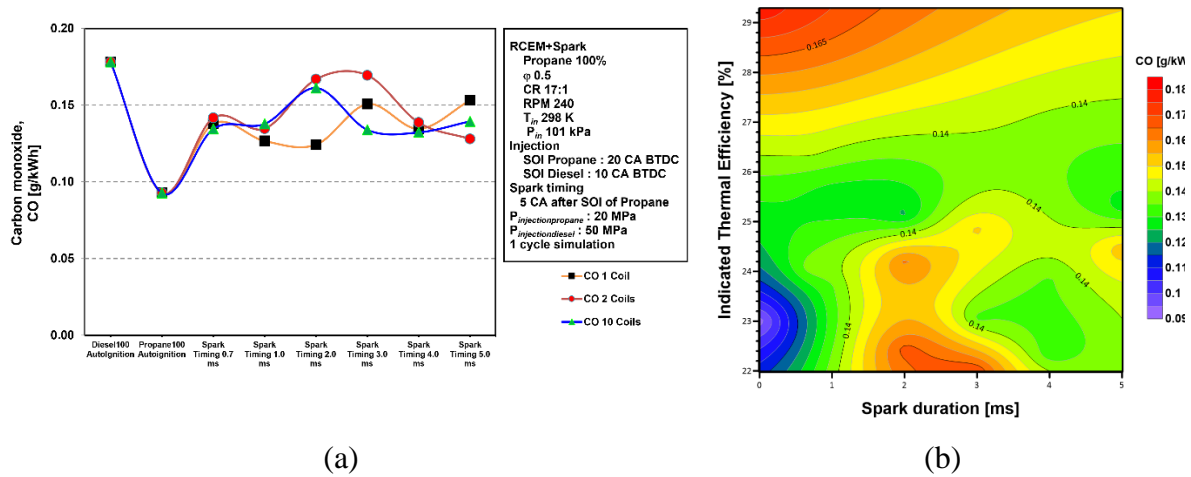
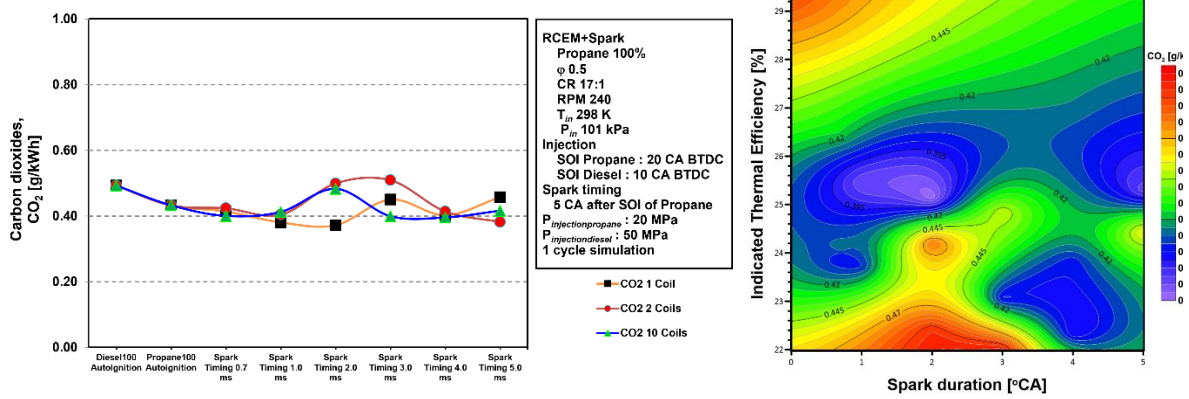


Fig. 5.9. (a) CO comparison on different spark ignition strategy on RCEM fueled with propane and (b) CO and indicated thermal efficiency comparison on different spark duration on RCEM fueled with propane.

5.3.3 Carbon dioxide emissions (CO₂)

The completion of the burning of the hydrocarbon fuel is indicated by the creation of CO₂ in engine exhaust. More CO₂ and less CO indicate better combustion quality and more efficient fuel use. fewer C/H ratios [149], [75] mean that using propane results in fewer CO₂ emissions. Insufficient combustion and instability may arise from low air-fuel ratios. Working close to such a mixture raises the ignition energy and slows down combustion. Figure 5.10 displays the CO₂ emissions of the diesel and propane-fueled simulated RCEM research engine. According to the figure, utilizing propane results in 12.19 percent fewer CO₂ emissions per kWh on average than diesel fuel. Improvements to the combustion process and increased fuel decarbonization could lead to a decrease in specific CO₂ emissions from propane fuel.



(a)

(b)

Fig. 5.10. (a) CO₂ comparison on different spark ignition strategy on RCEM fueled with propane and (b) CO₂ and indicated thermal efficiency comparison on different spark duration on RCEM fueled with propane.

5.3.4 Nitrogen oxides emissions (NO_x)

Combustion produces NO_x, which is primarily composed of NO (90–95%) and NO_x (5–10%) [150]. When a fire reaches a temperature higher than 1400 K or when there is high-temperature ignition, thermal NO is produced. When the burning temperature rises, NO generation increases rapidly and falls as the burning temperature falls [145]. Temperature has a dominant influence and fuel-rich mixes (with low λ) are more prone to produce NO_x [151]. The NO_x emissions of the engine running on diesel and propane are shown in Fig. 5.11. The graph indicates that at high average in-cylinder temperatures of 2200 K, high pressures, and short combustion times with spark durations of 0.7 to 5 ms, propane produces 32.20% less NO_x than diesel fuel. This approach is likely to produce significant pollutants because NO_x is formed during combustion at temperatures higher than 1800 K [152] or 1650 K [133]. As a result, when diesel is burned at a high temperature, the engine emits more NO_x emissions than when propane is used. It is expected that this burning will result in a consistent temperature throughout the combustion chamber, with the exception of the walls. This situation encourages lower NO_x emission because it will appear as though a lean mixture reaches maximum combustion temperature during the cycle when combined with the high volatility qualities of the low cetane fuel.

The impact of cetane number on NO_x pollution has been the subject of numerous studies. High cetane numbers have been linked to increased NO_x emissions [153], but they have also been

linked to decreased NO_x pollutants [154]. Propane, which has a low CN and a significantly longer igniting time than petrol, enables the research engine to run at higher loads with less smoke and fuel consumption than diesel fuel, according to earlier studies. In stratified combustion, when the mixture gets closer to the spark plug, it becomes heterogeneous, raising the flame temperature and consequently the NO_x emission [155]. The physical-chemical kinetics of the fuels and the history of the mixture temperature changes in the cylinder over time and space often have a major influence on the ignition timing and combustion phase [156].

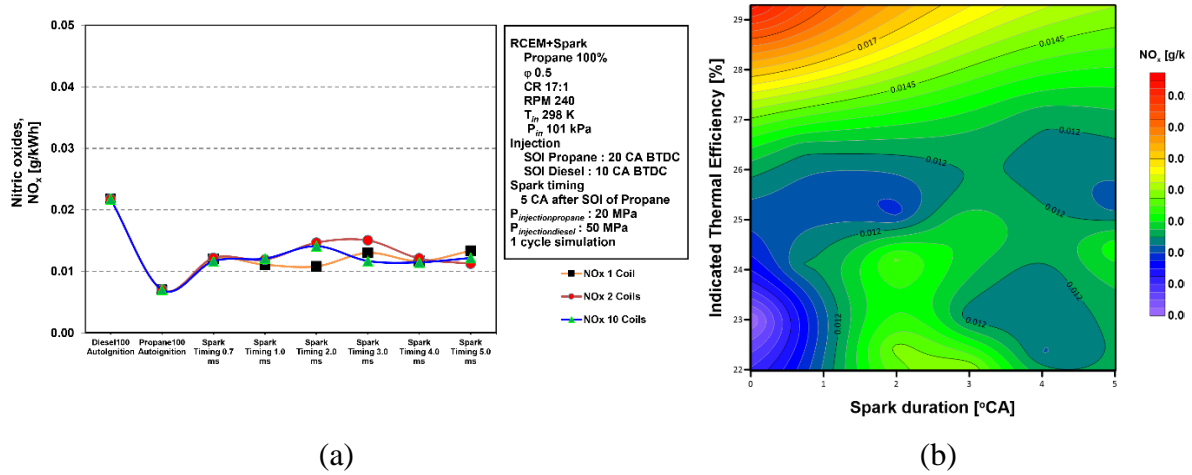


Fig. 5.11. (a) NO_x comparison on different spark ignition strategy on RCEM fueled with propane and (b) NO_x and indicated thermal efficiency comparison on different spark duration on RCEM fueled with propane.

NO_x emissions are decreased by using three-way catalysts, a lean NO_x trap, and selective catalytic reduction (SCR) [58]. Moreover, an exhaust bypass and a lean NO_x trap (LNT) are combined in an exhaust after-treatment system to lower NO_x [157]. In addition, engine internal NO_x emissions can be reduced by reducing the heat on the cylinder using injected water and EGR [158].

5.4 Summary

Using simulations and experiments, a thorough analysis of the impact of spark discharge length on low-carbon combustion of high-pressure direct-injection propane was conducted. The purpose of the plan and the experiments was to show the feasibility and promise of a new direct-injection propane and spark application. In order to examine the effects of combustion, performance, and emission at six ignition duration lengths (0.7, 1.0, 2.0, 3.0, 4.0, and 5.0 ms), three spark ignition methods were studied. Following a review of the data, the following findings were reached:

1. The discharge energy release rate was obtained by multiplying the current by the voltage. The most energy was released by the simultaneous ignition strategy, which was followed by the paired and individual ignition tactics. This result is consistent with the discharge typically, which include a longer discharge period and enhanced energy transfer from the in-cylinder discharged energy.
2. The size of the flame plasma varied little between the three ignition techniques. The plasma creation was basically unchanged, despite an increase in the discharge current through the use of an ignition method with ten coils operating simultaneously. As a result, extending the discharge spark length had no appreciable impact on the flame plasma generation stage.
3. When the spark duration was extended from 0.7 ms (1.01 °CA) to 5.0 ms (7.20 °CA) with the SOI of propane DI fixed at 20 °CA BTDC, the thermal efficiency of the RCEM modified with spark increased somewhat. Due to its higher heating value, diesel has an average thermal efficiency of 14.26% higher than propane. Temperature and pressure increase result in a shorter combustion period, more intricate combustion phasing, and greater in-cylinder temperatures. With the advancement of spark duration, the propane fuel produced an increased engine indicated thermal efficiency and a slightly higher brake-specific fuel consumption because of the combined effects of thermal efficiency and decreased heating value.
4. Propane emits more CO and HC but less NO_x than diesel pollutants. When comparing propane to diesel fuel, the spark ignition approach significantly improved standard emissions. In comparison to the corresponding values with diesel, HC, CO, CO₂, and NO_x were virtually equal by 1.8%, 23.99% less, 12.19% less, and 32.21% less, respectively, using propane fuel in some RCEM research engine modelling results.

6. OPTIMIZATION OPERATING PARAMETER OF SPARK DISCHARGE DURATION ON THE PERFORMANCE AND EMISSION CHARACTERISTICS

It is challenging to optimize of the objectives at once issues including conflicting dual objectives in compression ignition engines that are in a trade-off relationship (for example, using alternative fuel with low carbon content deflate HC and smoke pollutants but increases NO_x emissions). The purpose of chapter 6 is to conduct both experimental and numerical investigations to learn more about the spark discharge duration effect on performance and emission characteristics of low carbon propane combustion with high pressure direct injection is optimized and investigated. For a compression ignition propane engine, essential operational parameters were optimized using a genetic algorithm (GA) technique. The GA was used to identify the ideal circumstances that result in greater heat release rate, efficiency, and braking power as well as reduced emissions of BSFC, CO, and NO_x. Additionally, engine in-cylinder pressure and thermo-physical characteristics for varied spark durations were examined and contrasted. Finally, it was compared how the engines running on diesel and propane performed and what emissions they produced. The convergence of ANN and genetic algorithms is a novel aspect of this study as a promising approach for optimum operating parameter optimization of spark duration on low-carbon combustion of high-pressure direct-injection propane.

6.1 Modelling of artificial neural network

In this work Artificial Neural Network (ANN) is used to model the effect of the spark discharge duration effect on performance and emission characteristics of low carbon propane combustion with direct injection and genetic algorithm (GA) as an optimization technique to find the optimal operating parameter.

6.1.1 Data pre-processing

The accuracy of input variables can greatly increase the model's precision and decrease the requirement for huge data sets. After a thorough review of the literature input parameters for the model that have the greatest influence on the output variables were selected [159]. The use of diverse data can advance the learning and generalization capabilities of neural networks. As a result, Eq. (5) was used to normalize the input and output data within the range [0, 1].

$$x_n = \frac{y_{max}-y_{min}}{x_{max}-x_{min}}(x - x_{min}) + y_{min} \quad (5)$$

where x_n is the normalized value of variable x ; x_{max} and x_{min} are the maximum and minimum of x , respectively; y_{max} and y_{min} are the maximum and minimum of the normalized targets, respectively.

The sigmoid function is prevented by normalizing the parameters in Eq. (5) between 0.1 and 0.9 from becoming saturated and delays network learning as compared to normalizing the parameters between 0 and 1. But because input parameters exhibit significant nonlinearity and large deviations under extreme conditions, the accuracy of the model is found to be increased by logarithmic transformation before normalization since these unusual circumstances are uncommon and much more extreme than the rest in terms of magnitude [159].

6.1.2 Architecture of the ANN model

A common ANN model called a feed forward network has an output layer, an input layer, and a number of hidden layers. Inputs and outputs for each neuron in the network are weighted [160]. To make sure that each input contributes equally to the ANN, there are different numbers of neurons in the first and second hidden layers. Throughout the hidden layer of the network, the activation function was tan sigmoid, while in the output layer, it was linear [160]. The network has been trained using a common back-propagation approach. Levenberg-Marquardt method, a feedforward network training technique, is used because it can train small and medium-sized networks and cope with non-linear issues [161]. The process of "training" a network to produce the desired outcome involves modifying the weights of linkages among network layers. In accordance with Hristev [162], acquiring input signals, hidden layer weights and activation function are x_i , $w_{ji}^{(1)}$ and $\varphi^{(1)}$ respectively; whilst output layer weights and activation function are $y_j^{(1)}$, $w_j^{(2)}$ and $\varphi^{(2)}$ respectively. The computations in the first layer can thus be defined in Eq. (6) by combining the n inputs linearly and applying the bias b_j .

$$y_j^{(1)} = \varphi^{(1)}(v_j^{(1)}) = \varphi^{(1)}\left(\sum_{i=1}^n w_{ji}^{(1)} x_i + b_j^{(1)}\right); \quad j = 1, 2, \dots, m \quad (6)$$

Where w_i is the connected weights, x_i is the input, p is the total quantity of inputs, and b is the bias value for the neuron [163]. Fig. 6.1 depicts a general artificial neural network mathematical model that comprises the essential components for this sort of model in order to offer a clear understanding of the primary parts utilised to develop ANN models.

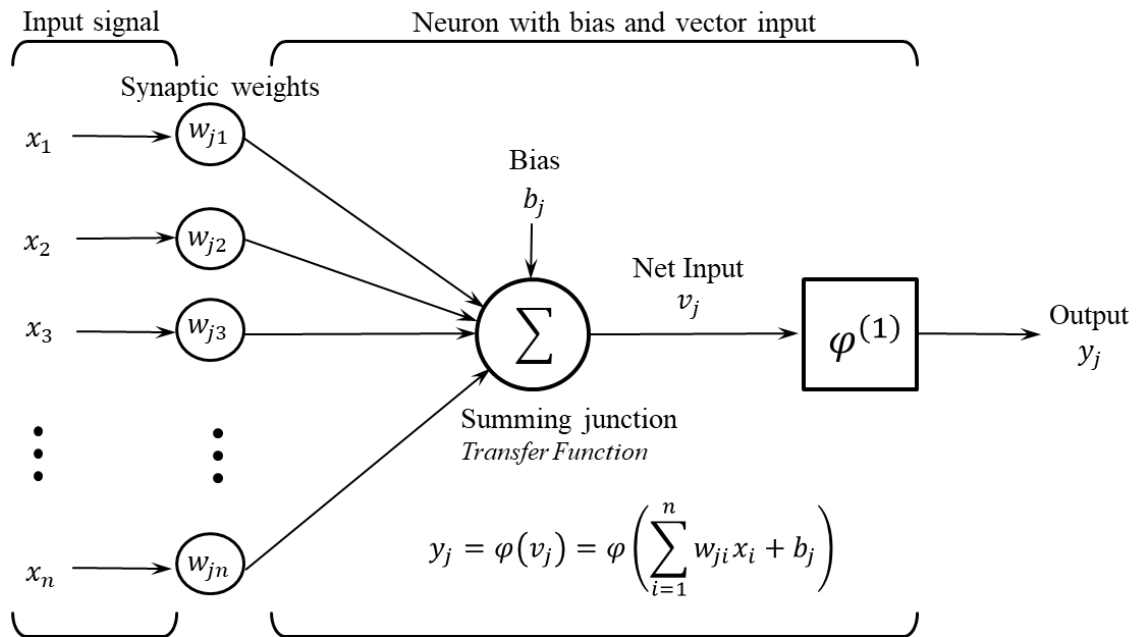


Fig. 6.1. A schematic diagram of main elements used to construct ANN models [163]

The selection of input and output parameters is significant because it affects how the process proceeds; if an incorrect variable was chosen that had little impact, the intended outcome would not be obtained. As a result, input parameters are chosen based on how they affect the process, and emphasis should be placed on those parameters that can be monitored and changed [164]. The five inputs of selected operating parameter are compression ratio (CR), fuel injection pressure (P_f), number of coil (n), start of injection (SOI), and spark duration timing (t). The experimental results and a thorough research of the literature were used to choose the inputs for this investigation. Meanwhile, heat release rate (HRR), turbulent kinetic energy (TKE), indicated mean effective pressure (IMEP), indicated thermal efficiency (η_{ith}), CO, and NO_x were the output parameters for the performance model. Figure 6.2 depicts a schematic illustration of ANN models.

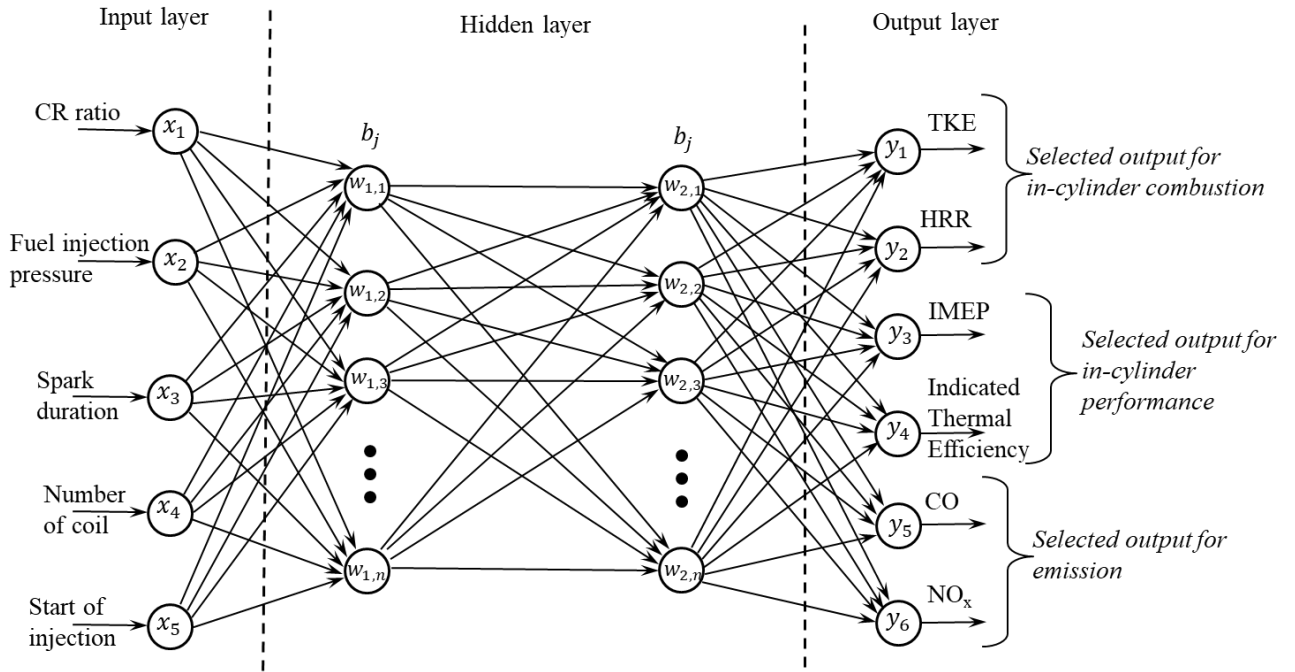


Fig. 6.2. ANN architecture with 5 inputs, 2 hidden layers, and 6 output in this study.

The accuracy of the model estimation outputs can be predicted by artificial neural networks, and this can be verified by correlation processing, network memory, and examination of the data [165]. The precision of the model projection could be increased by expanding the number of hidden neurons. While training duration and overfitting are likely to increase with a rise in hidden neurons. Kolmogorov's theorem [166] can be used to calculate the number of hidden neurons, as indicated in Eq. (7). Here, n_1 is 2 and n_2 is 5. Thus, the existence of 4 to 16 hidden neurons is determined.

$$X = \sqrt{n_1 + n_2 + 1} + a \quad (7)$$

where, X is the quantity of hidden neurons, n_1 denotes the quantity of hidden layers, n_2 denotes the quantity of input variables, and a denotes a constant that fluctuates between 1 and 10.

6.1.3 Assessment of ANN prediction

The estimated values are compared to the values obtained from experiments, and the neuron number for the most optimal closer value found is employed in further procedures. To assess the accuracy of ANN prediction, the coefficient of determination from Eq. (8), mean square error from Eq. (9), and standard error of prediction from Eq. (10) are employed [167], [165], [159].

$$R^2 = 1 - \frac{\sum_{i=1}^n (t_i - O_i)^2}{\sum_{i=1}^n (O_i)^2} \quad (8)$$

$$MSE = \frac{1}{N} (\sum_{i=1}^N (t_i - O_i)^2) \quad (9)$$

where t is the experimental result and O is the ANN estimated result.

$$SEP = \frac{\sqrt{\frac{1}{n} [\sum_{i=1}^n (x_{i,exp} - x_{i,pre})^2]}}{x_{mean}} \times 100 \quad (10)$$

where x_{mean} is the average value of the measured data, x_{exp} and x_{pre} are measured and predicted values (by ANN) respectively, and n is the number of data sets utilised for the ANN training.

6.2 Effects of spark discharge duration on performance of CI engine

Obtaining the global optimum can occasionally be challenging with traditional optimisation algorithms that use multi-objective optimisation and linear and non-linear programming. For addressing the engineering challenges, several optimisation approaches are proposed on evolutionary algorithms like genetic algorithms (GA), particle swarm optimisation, etc. Because GA uses stochastic processes for initialization, selection, cross-over, and mutation, it may solve issues with multiple objectives [168]. The GA was utilised to boost the ANN method's performance because it is a common optimizer. Many researchers used various optimizers, with GA being one of the best. The following are some benefits of utilising GA as an optimisation solution: (1) GA may explore and work with the solution space in numerous directions or simultaneously in parallel [169]; (2) GA utilises reintegration operators hence can combine beneficial qualities from other solutions [170] and (3) GA is a reliable method because it consistently produces similar optimum solutions across runs of the same issue [171].

Compression ratio (CR), fuel injection pressure (P_f), number of coils (n), start of injection (SOI), and timing of the spark (t), are the five real numbers that are taken into account in this study's ANN-GA approach, with heat release rate (HRR), turbulent kinetic energy (TKE), indicated mean effective pressure (IMEP), indicated thermal efficiency (η_{ith}), CO, and NO_x as the optimisation targets. As indicated in Eq. 11, the fitness function, a metric for identifying the chromosome with the capacity to live and produce progeny, is developed using the trained ANN model.

$$HRR = F(CR, P_f, n, SOI, t) \quad (11)$$

The process flow of the ANN genetic algorithm for optimising the effects of spark discharge energy on in-cylinder performance of a large bore compression ignition engine powered by direct injection propane is shown schematically in Fig. 6.3. As a result, the GA has so far demonstrated respectable performance in a range of optimisation issues. The GA was used in this study to identify the ideal circumstances that would increase the heat release rate (HRR), turbulent kinetic energy (TKE), indicated mean effective pressure (IMEP), indicated thermal efficiency (η_{ith}), and lower CO, and NO_x emissions.

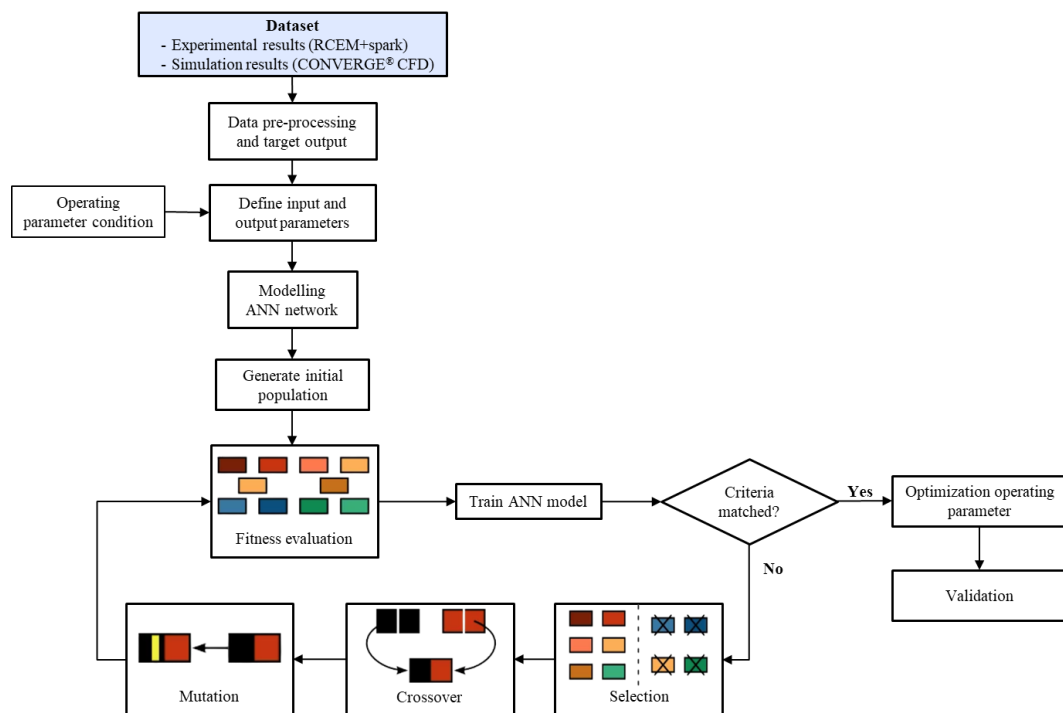


Fig. 6.3. Framework of research methodology in ANN genetic algorithm system

The process of creating the ANN model optimized with genetic algorithm was mostly based on the neural network toolbox of MATLAB R2017b, and the learning rate and training epochs of ANN model were set to 0.001 and 1000, respectively. Meanwhile, the network parameters used in the neural network architecture optimized with genetic algorithm after a thorough review of prior studies is given in Table 6.1. An ideal number of neurons is required since the overall number of neurons in buried layers has a substantial impact on the networks' capacity for prediction. For the first hidden layer, second hidden layer, and output layer, respectively, the selected activation functions are logsig, tansig, and purelin. The network is evaluated on validating data samples because neural networks might overfit and lose its generalisation.

Initial weights and bias for each neuron are permitted during network training with the training stopping when the validation MSE is determined to be lowest and begins to rise.

Table 6.1 Selected ANN network parameters generated on the MATLAB framework.

ANN Parameters	
Type of network	Feed – forward back propagation Levenburg – Marquardt
Function of training	(TRAINLM)
Function of learning	LEARNDGM
Function of performance	Mean squared error (<i>MSE</i>)
Function of transfer	Tan sigmoid
Selecting data	Training data set: 70% experimental data (chosen at random) Validation data set: 15% experimental data (chosen at random) Test data set: 15% experimental data (chosen at random)
Topology	In-cyl. performance model: 5 inputs, 6 outputs and 2 hidden layers with 16 neurons (4-16-16-3).
Limits	Epochs = 500 Min. gradient = 1.00×10^{-7} Max. fail = 7
Terminating rules	Whenever the validation error starts to rise, stop the network training

6.3 Data generation for artificial neural networks optimization

ANN training, validation, and testing data were generated by an experimental on rapid expansion and compression machine research engine with spark application fueled with propane direct injection. Heat release rate (HRR), turbulent kinetic energy (TKE), indicated mean effective pressure (IMEP), indicated thermal efficiency (η_{ith}), CO, and NO_x are just a few of the performance parameters that are introduced and discussed in this section as related to the spark release energy impact on combustion, in-cylinder performance, and emission of a RCEM modified with spark and fueled with propane.

6.3.1 Regression modelling

The mathematical formulae for the engine performance and emission parameters are provided for the input function of the GA toolbox. Regression analysis was used to create the models using experimental data for the selected compression ratio (CR), fuel injection pressure (P_f), number of coils (n), start of injection (SOI) and time of spark duration (t) for direct injection propane on RCEM with spark application. The 756 data sets were collected by engine testing

at different values of CR, P_f , n, SOI, and t as predictors or independent variables. The selected in-cylinder combustion and performance characteristics considered as responses (dependent variables) were HRR, TKE, IMEP, and η_{ith} , respectively. CO and NO_x were the selected emission components considered as responses. The in-cylinder combustion, performance and emission parameters can be stated mathematically as a regression equation, as seen in Eq. 12 [82].

$$f(x) = b_0 + \sum_{i=0}^{i=n} (b_i x_i + b_{ii} x_i^2) + \sum_{i < j}^{i=n} (b_{ij} x_i x_j + b_{ii} x_i^2) + \epsilon \quad (12)$$

where b_0 is the intercept's constant, ' b_i ' and ' b_{ii} ' are their respective coefficients, and ' b_{ij} ' is the result of the linear interaction between ' x_i ' and ' x_j '. As a result, the response includes terms for linear, squared, and cross products.

The regression analysis is carried out using Minitab software. A separate set of polynomial equations or models is developed for each response. Before the final coefficients and R² are calculated for the responses, the inconsistent terms are eliminated using the backward elimination procedure. Table 6.2 displays the predictor symbols for the regression model. Table 6.3 lists the independent factors in the regression model for the performance measures and the emitters.

Table 6.2. Symbol used in modelling for the variables in the regression formulas.

Parameter	Predictor symbol	Range
Compression ratio	x_1	17, 19
Fuel injection pressure	x_2	150, 200
Number of coils	x_3	1, 2, 10
Start of injection	x_4	-40, -35, -30, -25, -20, -15, -10, -5, 0
Spark duration timing	x_5	0.7, 1, 2, 3, 4, 5

Table 6.3. Regression model and corresponding R² values.

Response	Regression model	R ²
TKE	$0.6926 x_1 - 0.2933 x_5 - 0.02038 x_1^2 + 0.00387 x_2^2 + 0.000134 x_4^2 - 0.00502 x_1 x_2 + 0.04575 x_1 x_5 - 0.02471 x_2 x_5 + 0.000308 x_2 x_4 - 0.001657 x_5 x_3 - 0.000277 x_3 x_4$	99.84%
HRR	$6.612 x_1 - 1.042 x_2 + 0.703 x_3 - 0.952 x_4 - 0.1065 x_1^2 + 0.3564 x_5^2 - 0.007767 x_4^2 + 0.0908 x_1 x_2 - 0.1643 x_1 x_5 + 0.0822 x_1 x_3 + 0.04020 x_1 x_4 + 0.0392 x_2 x_5 - 0.0993 x_2 x_3 - 0.0819 x_5 x_3 - 0.00452 x_5 x_4 + 0.00324 x_3 x_4$	99.91%
IMEP	$0.26953 x_1 + 0.1398 x_5 + 0.0602 x_3 - 0.006481 x_1^2 - 0.01496 x_5^2 + 0.000064 x_4^2 - 0.001714 x_1 x_2 + 0.00056 x_1 x_3 - 0.002230 x_2 x_3 - 0.001157 x_5 x_3 - 0.000324 x_5 x_4 + 0.000707 x_3 x_4$	99.59%
η_{ith}	$5.330 x_1 - 2.662 x_2 - 2.176 x_5 + 0.130 x_3 - 0.1893 x_4 - 0.2348 x_1^2 - 0.0195 x_5^2 + 0.1620 x_1 x_2 + 0.1185 x_1 x_5 + 0.00542 x_1 x_3 + 0.00978 x_1 x_4 - 0.01367 x_2 x_3 + 0.00229 x_2 x_4 + 0.00312 x_5 x_3 - 0.00382 x_5 x_4$	99.81%
CO	$0.03042 x_1 - 0.00313 x_5 + 0.01108 x_4 - 0.000693 x_1^2 + 0.000357 x_2^2 - 0.000571 x_5^2 - 0.000923 x_1 x_2 - 0.000470 x_1 x_4 - 0.000184 x_2 x_4 - 0.000164 x_5 x_3 - 0.000155 x_5 x_4 + 0.000049 x_3 x_4$	96.92%
NO _x	$0.001844 x_1 + 0.00415 x_5 + 0.000612 x_4 - 0.000082 x_2^2 - 0.000105 x_5^2 + 0.000005 x_4^2 + 0.000014 x_1 x_2 - 0.000138 x_1 x_5 - 0.000036 x_1 x_4 + 0.000009 x_2 x_4 + 0.000037 x_5 x_4 + 0.000002 x_3 x_4$	90.84%

A training set and a validation set were created by randomly dividing the dataset. 70% of the data set is made up of the training set, and the remaining 30% is made up of the validation set, for a total of 756 data sets. The first was used to create a regression model that matched the replies, and the second was used to evaluate how well the models were working. Model performance metrics are regarded as the mean squared error (MSE) and the correlation coefficient (R²).

6.3.2 Validation of experimental data by simulation results

The physical representation is verified using different experimental data in terms of the pressure between the experimental data and simulation results. Table 6.4 provides a quick description of the models applied in this investigation. On a Windows computer with a 60 GHz Intel® Core i7™ 77003 processor and 32 GB of RAM, this simulation was conducted. At the input and outflow, 383 K and 1 bar of pressure, respectively, were set as the temperatures. Fig. 6.4 shows the model of the RCEM with spark plug application. This mesh model contains

18,671,318 elements and 24,363,436 points. The case set up was carried out on the RCEM with the spark model according to the parameters that were determined.

Table 6.4. CONVERGE key research processes.

Physical model	Physical process	Model
Turbulence Modelling	Renormalization group (RNG) $k - \epsilon$	Reynolds – averaged Navier – Stokes (RANS)
	Wall heat transfer	O'Rourke and Amsden
Modelling of ignition	Source	Energy
	Shape	Sphere
	Motion	Move with flow
Modelling of combustion	Chemistry	SAGE
	Emissions	Zeldovich (Extended)
	SOOT	SOOT Hiroyasu
Modelling of spray	Spray break up	KH (Kelvin-Helmholtz) RT (Rayleigh-Taylor)
	Collision	NTC
	Drop drag	Dynamic
	Spray-to-wall contact	Wall film
	Turbulent dispersion	O' Rourke
Modelling of reaction	Chemical Kinetics Solver	SAGE detailed chemistry solver

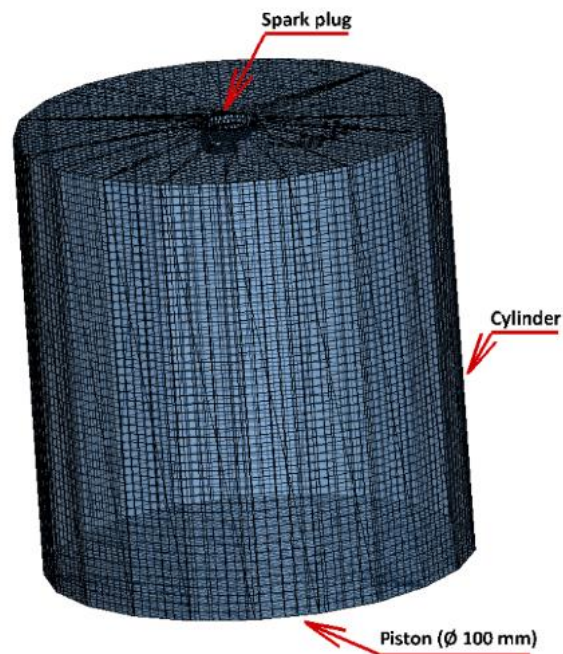
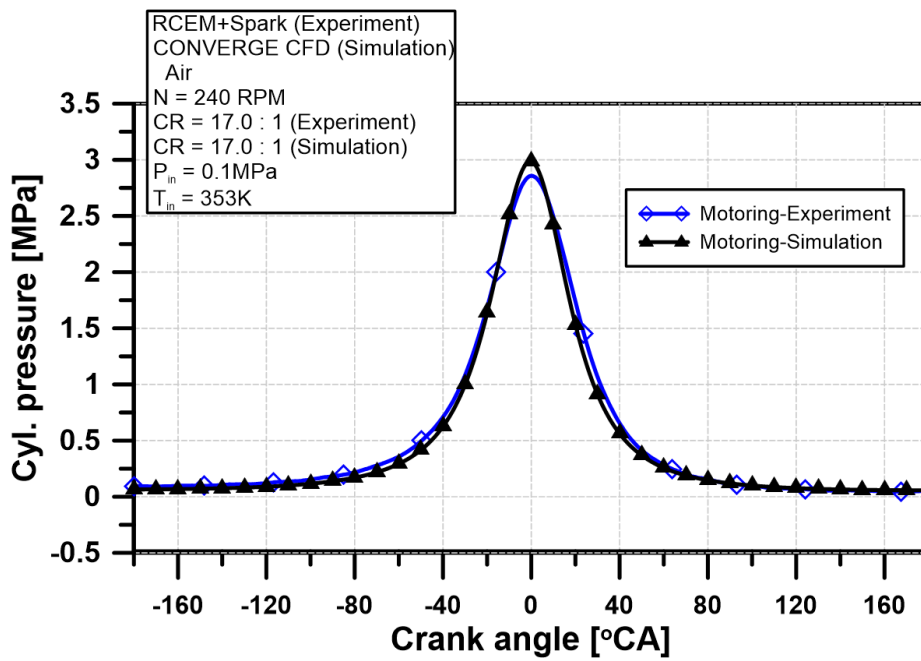


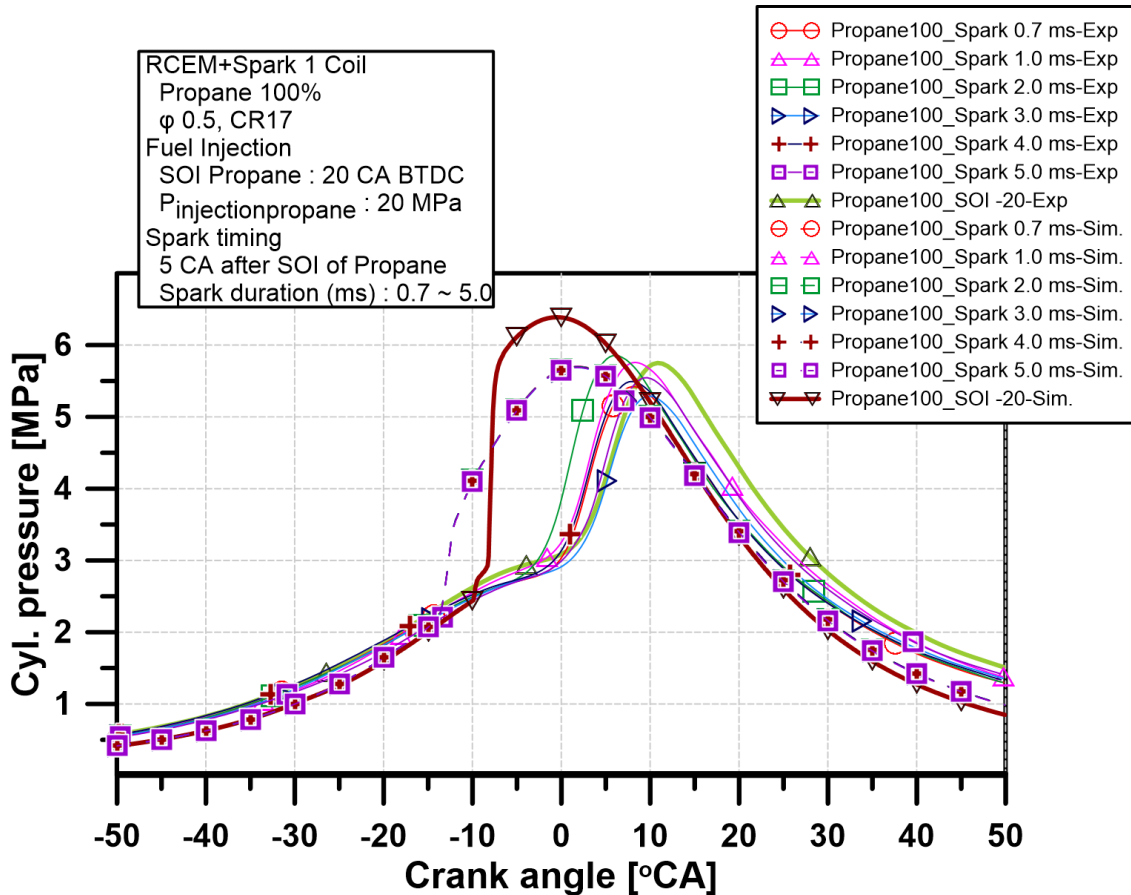
Fig. 6.4. RCEM with the spark model

Fig. 6.5 displays the validation of the simulated and experimental findings for driving pressure and crank angle. The comparison between the findings of the simulation and the experiment is shown in Fig. 7.5(a). In contrast, Fig. 7.5(b) shows the impact of the three-spark approach over

the course of the whole spark duration interval (0.7–5 ms) on maximum temperature, HRR, and internal pressure. To ensure that the readings for each test circumstance were accurate, three pressure measurements were taken. Propane's high-octane rating caused the in-cylinder pressure of the RCEM to rise to its ideal level, which was reached around the top dead center. The pressure dropped 0.183 MPa from the diesel engine. At a crank angle of 10.83 degrees, the highest pressure was recorded (-9.08 degrees).



(a)



(b)

Fig. 6.5. Validation of in-cylinder pressure in RCEMs using different ignition strategies and propane direct injection. (a) Motoring pressure; (b) In-cylinder pressure and spark times ranging from 0.7 to 5.0 milliseconds.

6.4 Optimization of in-cylinder combustion, performance and emission using genetic algorithm

Inferred mean effective pressure, suggested thermal efficiency, heat release rate, and turbulent kinetic energy all grow or decrease simultaneously at various levels of selected engine operating parameters, according to experimental and simulation findings. The column range of Table 7.2 displays the upper and lower boundaries for the remaining restrictions. After comparing the results of various targets while taking into account in-cylinder performances and emission operating settings, the optimization procedure is used to choose the optimum outcomes. The utilized GA algorithm by the MATLAB optimization toolbox has the properties presented in Table 6.5.

Table 6.5 Properties of GA algorithm in MATLAB.

Genetic algorithm parameters	
Number of input variables	5
Quantity of datasets	756
Bits required to encode 1 (one) gene	20
Bit count per chromosome	500
Lower limit range [CR Fp n SOI t]	[17 150 1 -40 0.7]
Upper limit range [CR Fp n SOI t]	[19 200 10 0 5]
Chromosome count in the population	300
Crossover operator	Two-point
Crossover probability	0.9
Mutation probability	Adaptive feasible
Pareto front population fraction	0.35
Maximum number of generation	100

6.4.1 Optimization of spark duration effect on the in-cylinder combustion

By comparing the released energy at various spark timings with our findings from a prior research [59], we found that the spark grows with temperature and pressure, with the largest heat release values occurring at the 1 ms spark timing. The length of the spark has a negligible effect on the energy it emits. The combustion velocity narrows as the number of coils rises, accelerating the creation of laminar flames and cutting down on combustion time by raising temperatures and HRR. The highest temperatures and the amount of time these released energy quantities are sustained at the CAD have an impact on higher peak temperatures and heat transmission, respectively.

The in-cylinder combustion parameters, specifically the turbulent kinetic energy and heat release rate, are taken into account while determining the optimization goals. Both of them are anticipated to have greater values in order to improve the engine's in-cylinder combustion process. For optimization in the GA toolbox, the polynomials models in Table 6.3 that were derived by regression analysis as fitness functions are stored as.m files. The best values are noted after a few iterations of runs that eliminate the impacts of initiation. The Pareto front is shown in Fig. 6.6, with the objectives of increasing TKE and HRR. The objective function space's Pareto front plot displays several sets of points for varying objective values. The software uses these criteria to find the ideal values of predictors for performance responses in order to balance two objectives. When all established result points have a broad distribution, the scores of the best predictors can be obtained via the stated objective space, but the majority of the final optimal Pareto front solutions are localized in the leading region with both higher TKE and HRR, indicating that the genetic algorithm prefers the optimized solutions in this region. For objectives 1 and 2, the locations between -5-0 and 20-25 were discovered to provide

the best level of predictors. Finally, it is discovered that the best values for CR, Fp, n, SOI, and t are 17.32, 200, 10, -19.98, and 3.44, respectively.

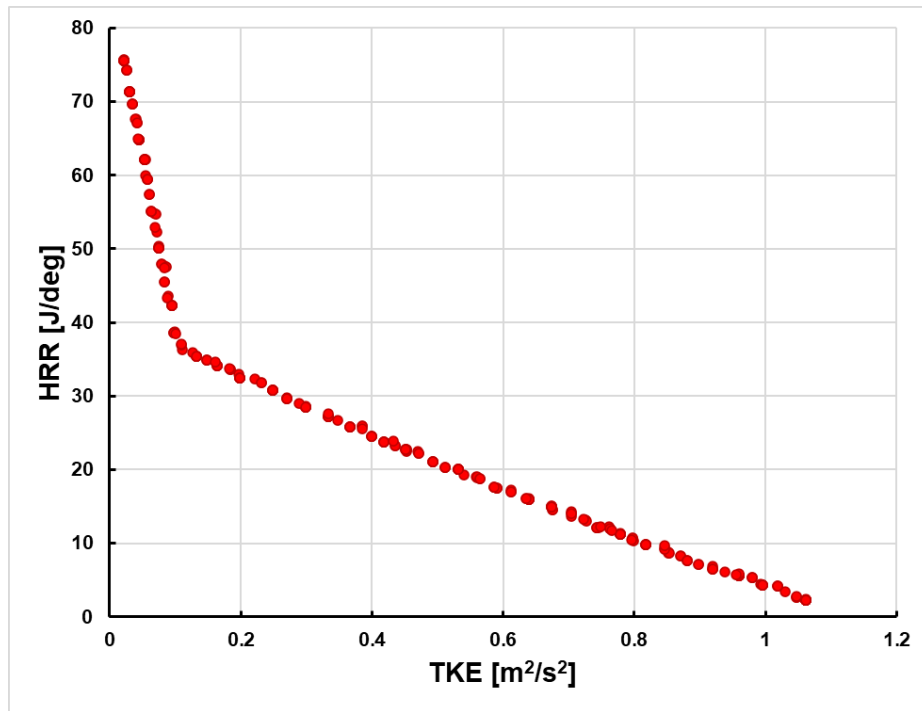


Fig. 6.6. Pareto front for optimization considering in-cylinder combustion.

6.4.2 Optimization of spark duration effect on the in-cylinder performance

The process for performing the optimization is the same as it was in the past. One of the two goals in this situation is to perform better or to the fullest. Therefore, increasing ITE and IMEP performance characteristics is one of the goals. In MatLab, all of the polynomials listed in Table 8 are employed as a fitness function. The Pareto front is depicted in Fig. 6.7, with objective 1 being to maximize ITE and IMEP. The Pareto front's goal space displays a collection of points that correspond to the best options. For objectives 1 and 2, the points of optimum values were located between 0 and 0.5 and 30 and 35, respectively. It is discovered that the ideal values for the input parameters CR, Fp, n, SOI, and t are 17.42, 199.99, 7.80, -21.38, and 3.05 respectively.

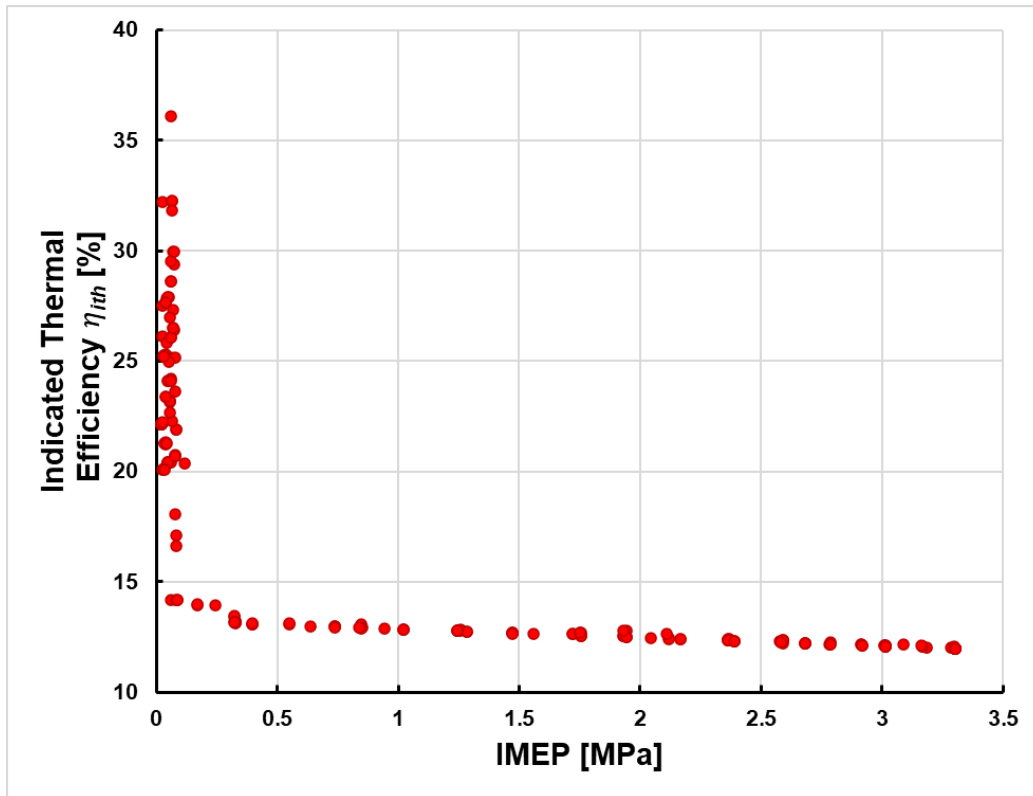


Fig. 6.7. Pareto front for optimization considering in-cylinder performance.

6.4.3 Optimization of spark duration effect on the emission

The engine operating parameters are optimized by taking into account all of the elements of exhaust pollution, including CO, CO₂, HC, NO_x, and smoke. Uncompleted fuel combustion or the dissociation of CO₂ produce carbon monoxide. The equivalency ratio is the main factor that affects CO emissions from internal combustion engines [26]. Significant amounts of CO will be present when the equivalency ratio is stoichiometric or highly fuel-lean due to CO₂ dissociation. As a result of the insufficient oxygen to complete the reaction to CO₂, CO is easily generated in fuel-rich engines. Thus, reducing CO is one of the optimization's goals. The second is to reduce NO_x. The Pareto front optimal solution in Fig. 6.8 compares the CO and NO_x emissions from all estimated scenarios and has two aim functions of minimizing CO and NO_x. Additionally, there is a link of some sort between the CO and NO_x emissions. The optimal values for the set of objectives are represented by the points that fall between 0.011 and 0.013 for objective 1 and between 0.02 and 0.03 for objective 2. To achieve a balance between the two goals, the Pareto front's points are applied. For the operating parameters CR, P_f, n, SOI, and t, the best values are discovered to be 17.95, 173.10, 9.64, -22.66, and 3.55, respectively.

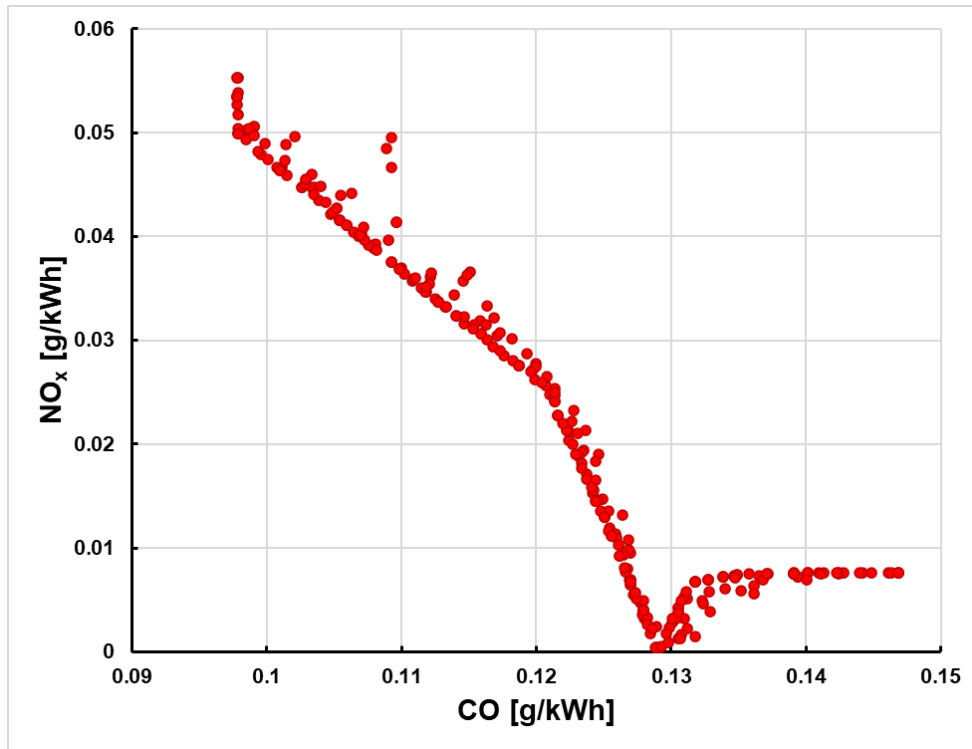


Fig. 6.8. Pareto front for optimization considering emission.

6.5 GA optimization of operating parameters optimization of spark duration effect

Utilizing the MATLAB software, the optimization is done by setting input parameters. It was possible to acquire the response of parameter combinations (HRR, TKE, IMEP, ITE, CO, and NO_x) for the entire set of compression ignition operating circumstances by optimizing each of the input parameters in order to meet the optimization aim and any pertinent constraints. For CR, F_p, n, SOI, and t, the optimized parameters have been chosen as shown in Table 6.6.

In order to ensure that the engine operates effectively across a suitable range of operating conditions, a number of restrictions are specified while choosing the best solution. These constraints aim to minimize abnormality situations and partial fuel combustion brought on by inappropriate parameter values. The optimal levels of CR, P_f, n, SOI, and t for enhancing performance and reducing emission contents of the propane direct injection are 17, 200 bar, 10, 20° bTDC, and 3 ms, respectively, after carrying out the multiple optimization runs by allocating different input parameters for in-cylinder combustion, performance, and emission.

Table 6.6. Optimum combination of selected operating parameter.

Respond of pareto front	CR	P_f	n	SOI	t
Objective of HRR and TKE	17.32	200	10	-19.98	3.44
Objective of $IMEP$ and η_{ith}	17.42	199.99	7.80	-21.38	3.05
Objective of CO and NO_x	17.95	173.10	9.64	-22.66	3.55

The dataset of neural networks obtained by selecting the experiment and simulation results based on the optimum combination of operating variables as mentioned before. The neural network was then trained by selecting a selection of neurons at random from the hidden layer. Then, the number of neurons was altered until the MSE value was reduced to a minimum. The number of neurons in the hidden layer with the lowest MSE was chosen as the optimal number. The input layer and output layer have 4 and 3 neurons, respectively, whereas the number of concealed neurons must be increased. A sensitivity test on MSE and R^2 against the total quantity of neurons that are hidden was undertaken to discover the ideal number of hidden neurons. Fig. 6.9(a) depicts the fluctuation of MSE with the total quantity of hidden neurons in the obtained network structure. With 16 hidden neurons, the MSE was reduced (0.00403). Fig. 6.9(b) depicts the correlation coefficient (R^2) between the anticipated and real values throughout the testing period. The highest R^2 value was 0.9976, obtained with 18 hidden neurons. Finally, the best number of neurons was determined to be 16 neurons, which is the least value of the MSE.

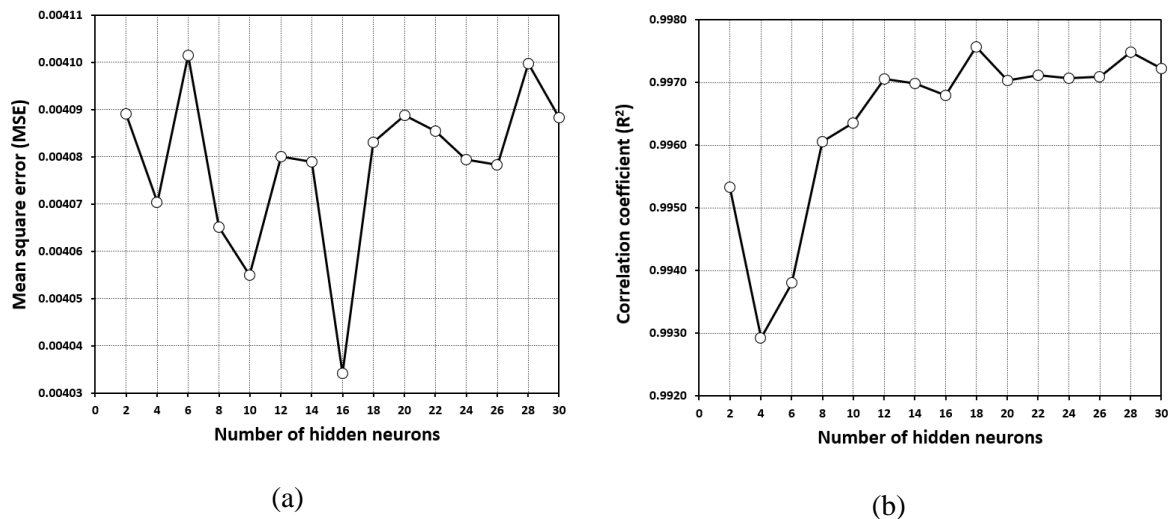


Fig. 6.9. Variation of MSE and R^2 in regard to the number of hidden neurons.

(a) Mean squared error (MSE); (b) Correlation coefficient (R^2)

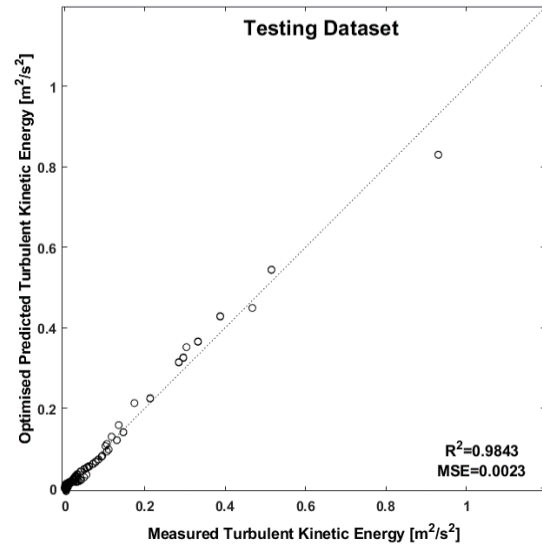
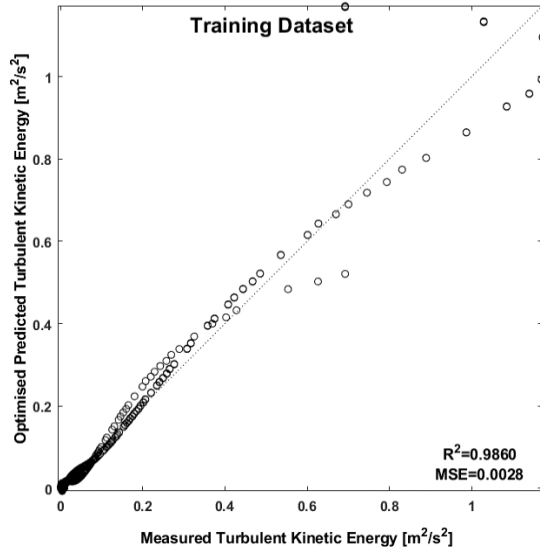
The variation of MSE with respect to the number of neurons in the hidden layer is shown in Table 6.7. The error was 0.047 when there were 5 total neurons in the hidden layer, and it dropped as the number of neurons increased until it reached a minimum of 24. As the number of neurons rose the *MSE* progressively increased. The smallest MSE was found to be 0.001 for training and validation datasets respectively. The neural network was further trained through a variety of training functions. The trained network's performance was evaluated. Mean squared error (MSE) is an indicator of performance used to evaluate network performance. A MSE of 5% has been chosen as the upper limit for the spark energy effect on the RCEM model in order to evaluate the testing performance of the developed ANN model. MSE for the training data were 0.0074, 0.0001, 0.0008, 0.0028, and 0.0134 for heat release rate (HRR), turbulent kinetic energy (TKE), tumble ratio, indicated power, and combustion efficiency (η_c) respectively whereas for the testing data these values were 0.9558, 0.9762, 0.9432, 0.9724, 0.9674 respectively. The created model was deemed to be acceptable because the MSE results for the test data were much lower than the established limit, as shown in Table 6.2.

Table 6.7 The R^2 coefficient and MSE calculated for the training and validation dataset based on the spark ignition strategy of the RCEM fueled with propane.

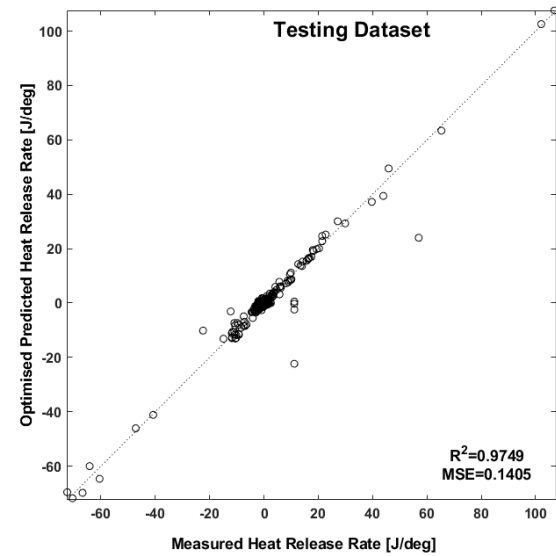
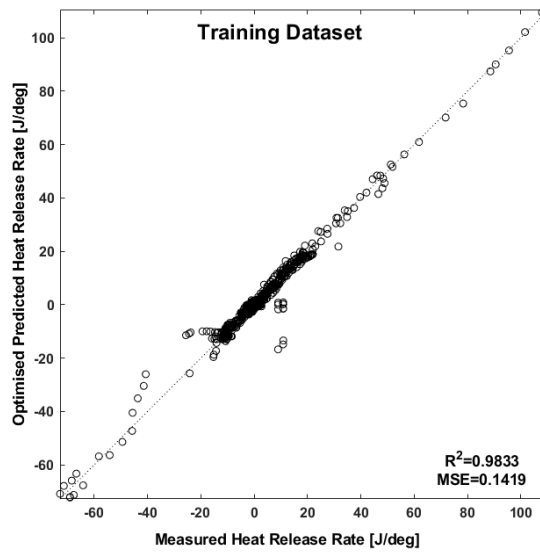
		Ignition strategy							Propane autoignition		
		Spark timing 0.7 ms	Spark timing 1 ms	Spark timing 2 ms	Spark timing 3 ms	Spark timing 4 ms	Spark timing 5 ms				
Training dataset	Correlation coefficient R^2	Turbulent kinetic energy	0.9855	0.9824	0.9728	0.9854	0.9762	0.9798	0.9925		
		Heat release rate	0.9724	0.9607	0.9433	0.9804	0.9662	0.9558	0.9774		
		Indicated mean effective pressure	0.9956	0.9872	0.9890	0.9997	0.9543	0.9716	0.8936		
		Indicated thermal efficiency	0.9044	0.9981	0.8184	0.9912	0.8212	0.9189	0.9642		
		Carbon monoxide	0.9768	0.9998	0.8859	0.9688	0.9223	0.9832	0.9643		
		Nitrogen oxides	0.9039	0.7948	0.9380	0.8550	0.9758	0.8393	0.9913		
	Mean Square Error <i>MSE</i>	Turbulent kinetic energy	0.0023	0.0028	0.0043	0.0030	0.0038	0.0056	0.0001		
		Heat release rate	0.0105	0.0074	0.0180	0.1419	0.0067	0.2696	0.0028		
		Indicated mean effective pressure	0.00001	0.00021	0.00664	0.00085	0.00052	0.00374	0.00376		
		Indicated thermal efficiency	0.85470	0.25715	0.85130	0.22339	0.82246	0.13430	0.47566		
		Carbon monoxide	0.00003	0.00001	0.00006	0.00006	0.00003	0.00002	0.00007		
		Nitrogen oxides	0.00003	0.00003	0.00001	0.00001	0.00001	0.00003	0.00003		
		Validation dataset	Correlation coefficient R^2	Turbulent kinetic energy	0.9658	0.9627	0.9534	0.9657	0.9567	0.9602	0.9727
				Heat release rate	0.9627	0.9511	0.9339	0.9706	0.9566	0.9462	0.9676
Indicated mean effective pressure	0.6430			0.9872	0.9890	0.9997	0.9543	0.9716	0.9999		
Indicated thermal efficiency	0.9633			0.9981	0.8184	0.9912	0.8212	0.9189	0.9642		
Carbon monoxide	0.9039			0.8364	0.8859	0.9688	0.9223	0.9832	0.9643		
Nitrogen oxides	0.9039			0.9624	0.9380	0.8550	0.9758	0.8393	0.9913		
Mean Square Error <i>MSE</i>	Turbulent kinetic energy		0.0023	0.0028	0.0043	0.0031	0.0038	0.0057	0.0001		
Heat release rate	0.0104	0.0074	0.0179	0.1405	0.0066	0.2669	0.0028				
Indicated mean effective pressure	0.00029	0.00025	0.00639	0.00075	0.00045	0.00355	0.00362				

		Indicated thermal efficiency	0.30678	0.24316	0.82985	0.20253	0.83665	0.12677	0.44941
		Carbon monoxide	0.01899	0.01774	0.02133	0.02090	0.01692	0.01908	0.00977
		Nitrogen oxides	0.01899	0.00013	0.00019	0.00020	0.00012	0.00019	0.00010

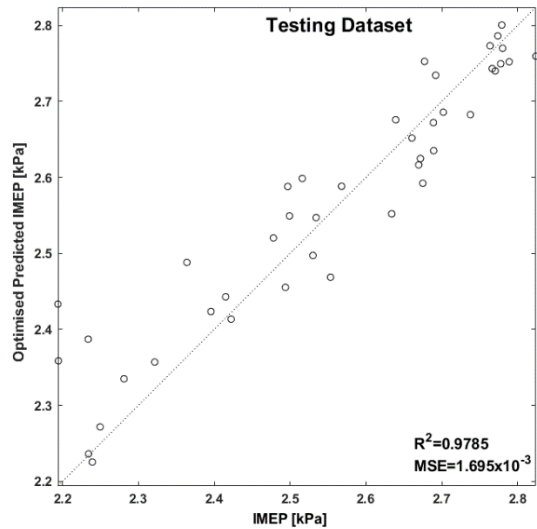
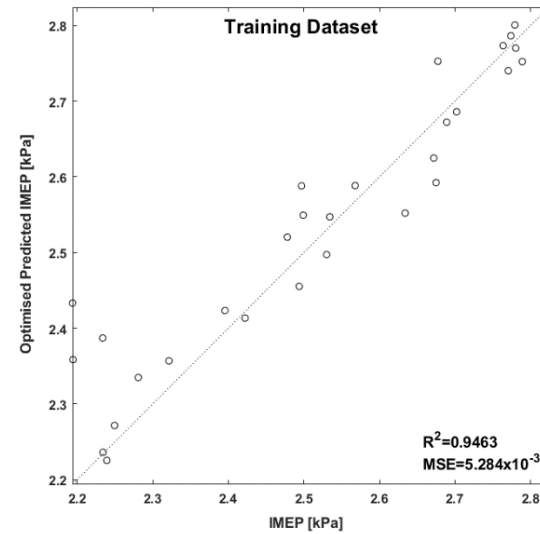
Fig. 6.10 depicts the contrast of the optimized ANN in-cylinder performance and emission with actual value from experimental and simulation results for the training and validation dataset. This is an achievement verification of the training optimized ANN model using previously unknown data. The prediction performance of the optimized ANN model is primarily assessed using the statistical metrics R^2 and MSE . The six anticipated parameters, heat release rate (HRR), turbulent kinetic energy (TKE), indicated mean effective pressure (IMEP), indicated thermal efficiency (η_{ith}), CO, and NO_x , correlate to R^2 values of 0.9833, 0.9860, 0.9463, 0.9873, 0.9998, and 0.9971, respectively, and MSE values of 0.1419, 0.0028, 5.284×10^{-3} , 0.0662, 0.002094, and 3.6301×10^{-6} . The R^2 of the testing dataset is similarly nearly 0.98, which is close to the R^2 of the training dataset. Meanwhile, the MSE of the training set is greater than the MSE of the testing dataset, which is reasonable given that the testing dataset is evaluated with unknown data. We discovered that the accuracy of forecasting of the conventional ANN model is more sensitive to the quality of the experimental datasets than the other two ANN models that employ extended datasets. These results are in accordance with previous research by Jiang [172], in which the quality of experimental data samples diminishes, the prediction accuracy of the ANN models drops as well; nevertheless, the decreasing pace is rather gradual, suggesting the durability of the upgraded models. Overall, because the R^2 and MSE of the validation dataset are comparable to that of the training dataset, there is no overfitting in the ANN model's establishment. Furthermore, it is evident through looking at the trend between the dashed line and the dot points that the points on each plot are mainly located around the dashed line. The findings reveal that the ANN model created in this work can predict five different types of parameters concurrently and with excellent accuracy. This suggests that in the future, instead of using the entire engine model, the ANN model may be used to predict these five combustion-related properties with high accuracy.



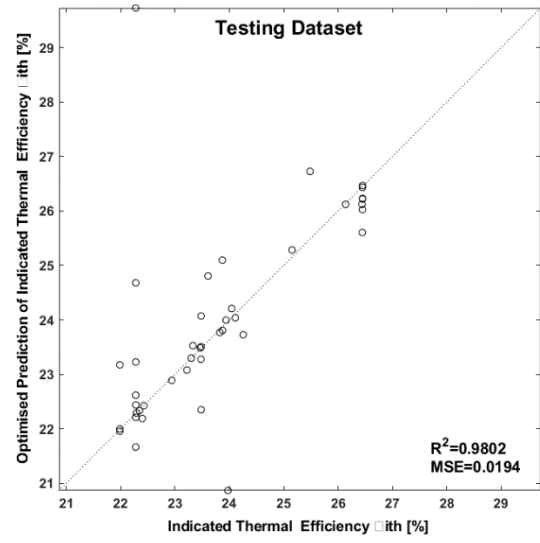
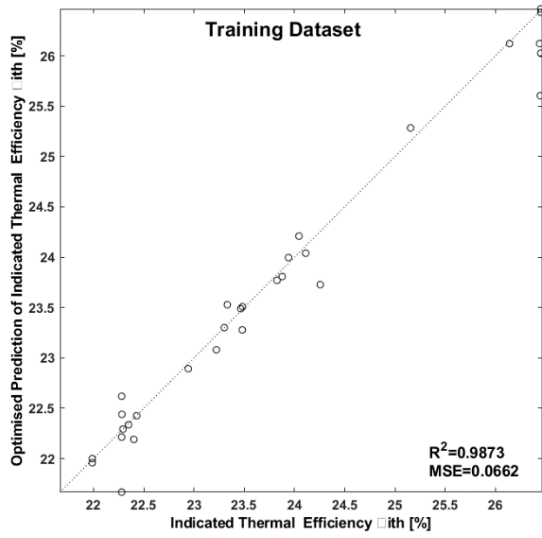
(a) TKE



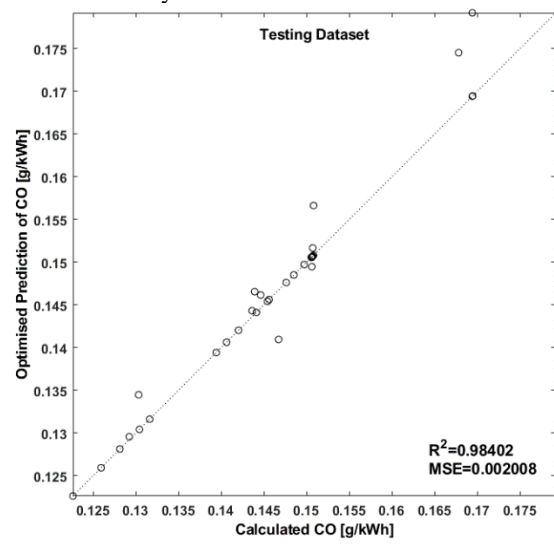
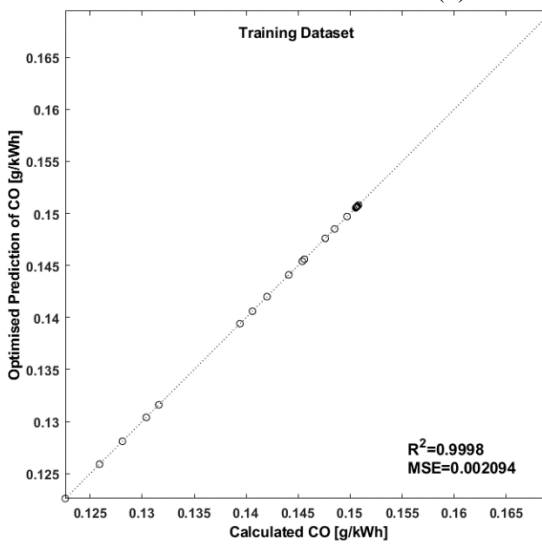
(b) HRR



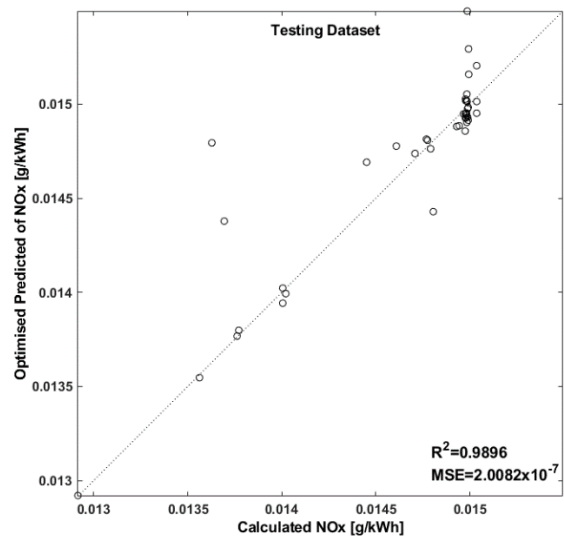
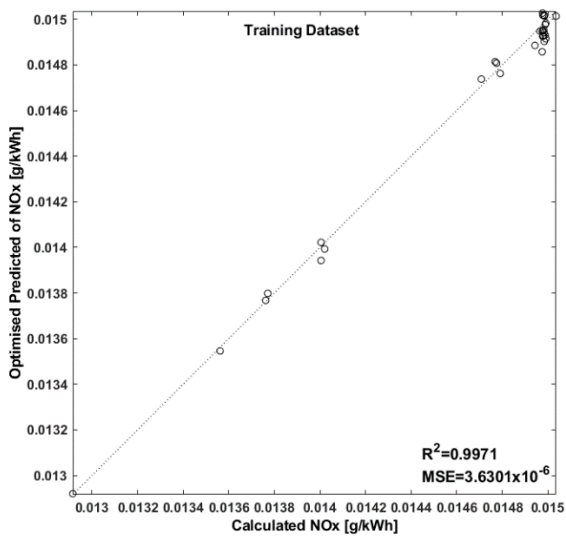
(c) IMEP



(d) Indicated thermal efficiency



(e) CO



(f) NO_x

Fig. 6.10. Comparing in-cylinder performance estimated by ANN and actual results from experimental and simulation results for the training and validation dataset: (a) TKE, (b) HRR, (c) IMEP, (d) Indicated thermal efficiency, (d) CO, and (e) NO_x.

6.6 Validation of the optimized results

The earlier sections demonstrated that a total of five parameters may be predicted using an ANN model for predicting spark release energy effects on in-cylinder performance of a large bore compression ignition engine, including heat release rate, turbulent kinetic energy, indicated mean effective pressure, indicated thermal efficiency (η_{ith}), CO, and NO_x. The comparatively minimal prediction errors indicated that the projected outcomes and actual values were in accord. It is interesting to validate the optimized results of the effect spark discharge energy effects on in-cylinder performance of a large bore compression ignition engine against the experimental results. The usual outcomes were chosen and displayed in Fig. 6.11, Fig. 6.12, Fig. 6.13, Fig. 6.14, Fig. 6.15, and Fig. 6.16. It is possible to evaluate how effectively the ANN model comprehends the input-output nonlinear connection by contrasting the anticipated outcomes with the experimental values of an optimised operating parameter input at compression ratio 17, 200 bar injection pressure, 10 coil numbers, SOI 20° bTDC, and 3 ms spark duration.

Fig. 6.11 shows the optimised values of TKE inside the bore of spark discharge effect on an ANN model, as well as the real values of the five optimum operating parameters that are incorporated in an ANN model's output responses. The overall forecast trend is positive, and the ANN model is quite precise in forecasting turbulent kinetic energy.

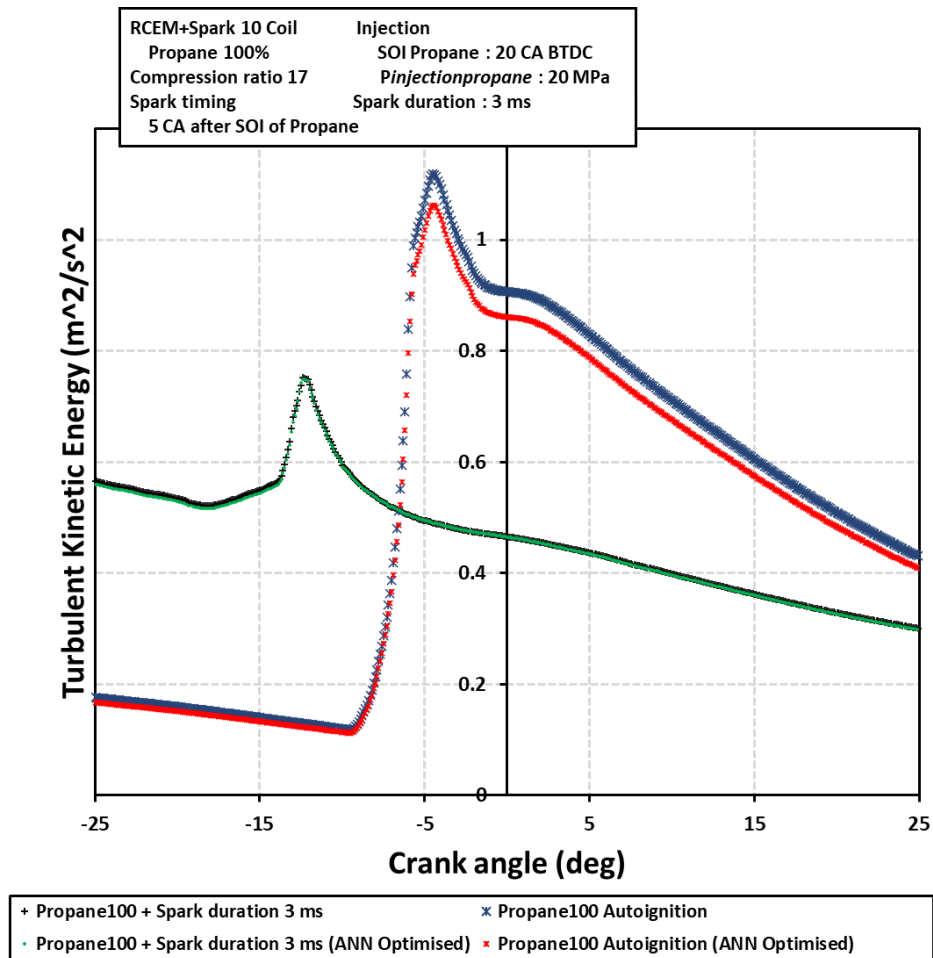


Fig. 6.11. Comparison of ANN optimised results with experimental results of turbulent kinetic energy on RCEM fueled with propane direct injection at spark duration 3 ms.

A propane direct injection-fueled RCEM with an optimized ANN-based estimate method is shown in Fig. 6.12 along with the experimental findings of HRR inside the bore of spark discharge effect. At the same machine speed, while comparing various spark release energies, a behavior pattern emerges where the greatest value decreases as the discharge energy rises. It is also noteworthy that the HRR curves at various spark timings are highly overlapping. This is because the timing of the spark has little effect on the energy of the discharge. Overall, this indicates the ANN estimated the engine combustion behavior in red dashed line essentially corresponds the continuous line shown by the real values, indicating that the inherent link between input and output ANN model with high prediction.

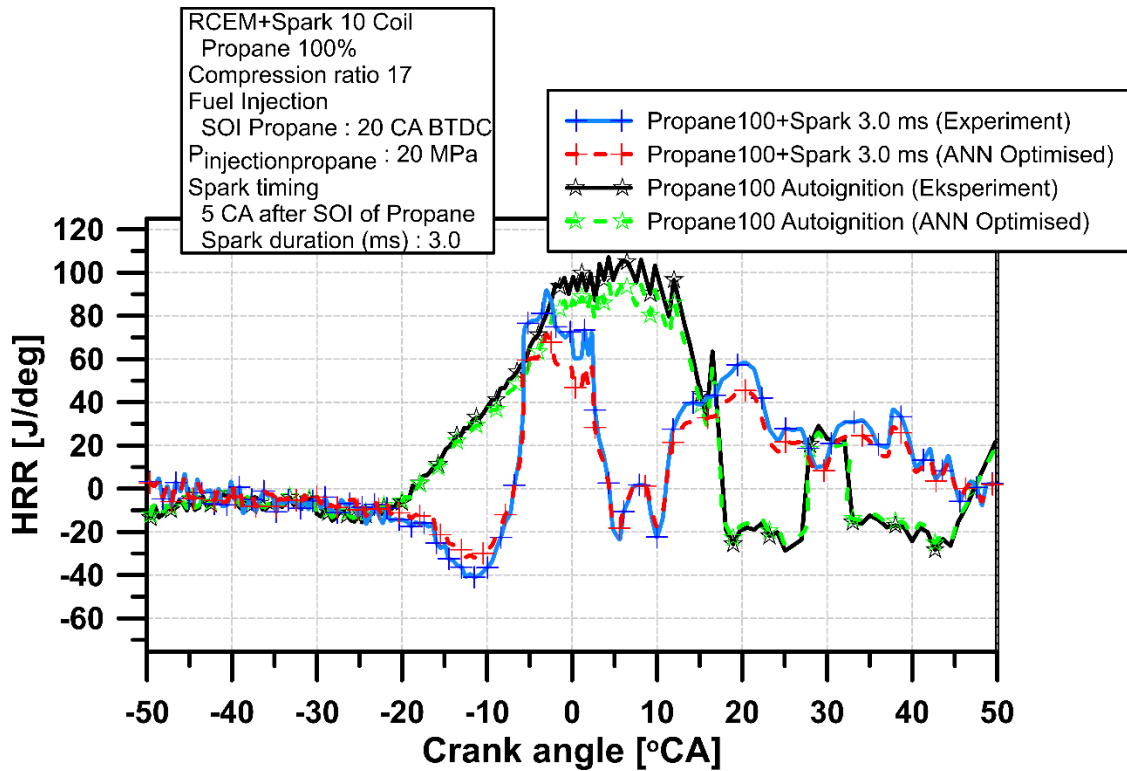


Fig. 6.12. Comparison of experimental findings from HRR of spark duration effect on RCEM powered by propane direct injection and ANN-optimized results.

Fig. 6.13 depicts a comparison of optimised IMEP values based on the artificial neural network optimised model with the actual data with ignition strategy for various spark durations from 0.7 ~ 5.0 ms. Higher IMEP was obtained for propane fuel. This is because of input heat calorie could improve the IMEP by utilizing combustion heat. Based on the findings, rising of IMEP led to greater fuel consumption quantity for producing a higher power output. Moreover, as indicated by the red dashed lines and continuous solid lines slightly overlap. This implies that the ANN model may be used to forecast IMEP. Therefore, The ANN model may be utilised as an analytical tool for further in-cylinder performance investigation, as well as to aid in multi-dimensional modelling and improvement of effective propane combustion.

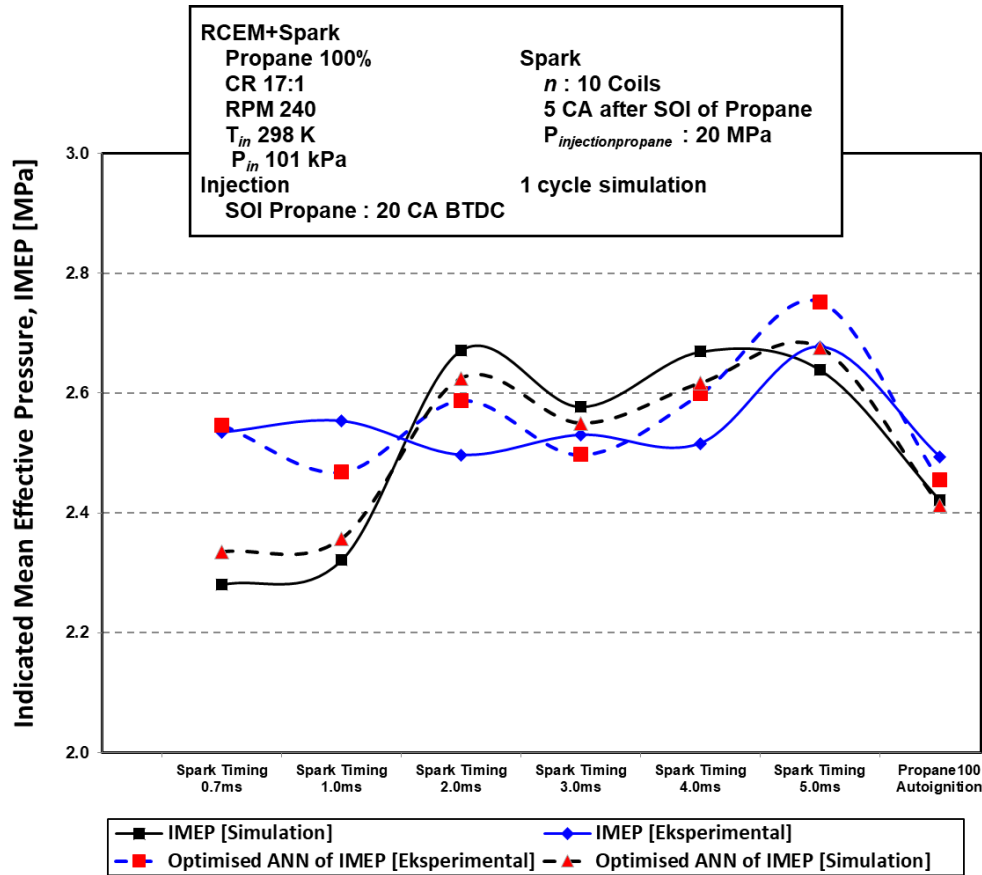


Fig. 6.13. Comparison of IMEP experimental data with ANN-optimized results for the spark discharge effect on RCEMs using propane direct injection and varied spark durations from 0.7 to 5.0 ms.

The experimental findings of the specified thermal efficiency inside the bore of the spark discharge effect on the RCEM powered by propane direct injection are compared in Fig. 6.14 with the optimum results. It can be found that longer spark duration approach yields a higher power output. This movement allows for additional chemical heat and power. The thermal efficiency of propane RCEM modified with spark application somewhat improved when the spark duration length was extended from 0.7 ms (1.01 °CA) to 5.0 ms (7.20 °CA) when the SOI of direct injection propane was 20 °CA BTDC. The efficiency can be enhanced by adopting a spark ignition approach in a propane RCEM modified with a spark application. A longer ignition delay gives enough time for mixing. Additionally, when the spark timing is increased, under many circumstances, increasing the spark timing alters the thermal efficiency. This related to volatile characteristic of propane fuel, which gives impact the combustion mechanism significantly. These findings support by Masouleh [34], when it was discovered

that a slow-rotating machine's intake stroke was connected to turbulent flow patterns that changed from cycle to cycle. Increased thermal efficiency was also linked to longer spark durations. The estimation of the tendency of the indicated thermal efficiency is appropriate according to an ANN model. Therefore, the optimized ANN model results can be used as a tool for analyzing in-cylinder performance as well as assisting in the development of large bore engines.

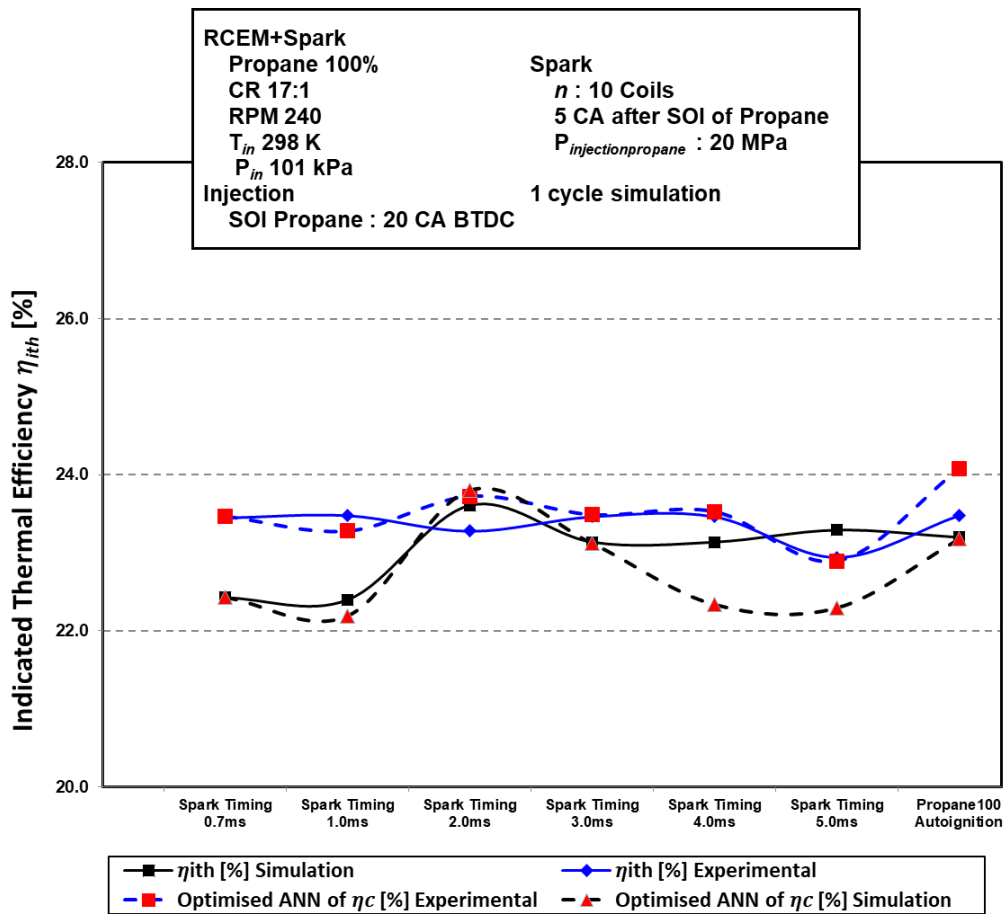


Fig. 6.14. Comparison of experimental and ANN-optimized results of the spark duration effect on a propane-fueled, direct-injection RCEM for varied spark durations ranging from 0.7 to 5.0 milliseconds.

The CO emission as spark duration effect on RCEMs powered by propane direct injection and using an ignition strategy is compared in Fig. 6.15 between results from ANN optimization and experimental findings. CO are related to temperature and the fuel mixing effect. In other words, insufficient combustion of fuel is the primary cause of CO, which will rise if the local equivalency ratio gets too lean. Based on the previous paper [59] compared ignition delay

between diesel and propane fuel, resulted that propane had a shorter ignition delay. Shorter ignition delays lead to greater insufficient combustion and higher CO. In this research, propane is more flammable than diesel fuel, which is good for advancing premixing. But propane will have a strong auto-ignition attribute due to its volatility and low cetane number. Sometimes, misfiring due to increased auto-ignition results in greater CO emissions. The amount of CO emissions in the exhaust product may be a good indicator of combustion effectiveness. Consequently, a drop in CO emissions might be a sign of improved combustion efficiency.

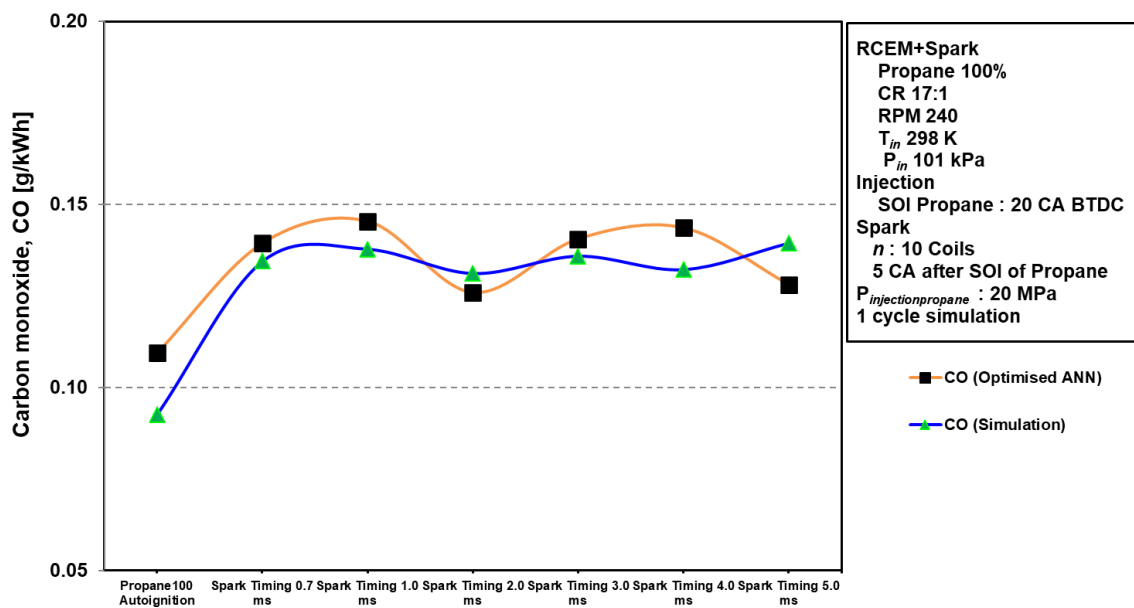


Fig. 6.15. CO comparison of experimental and ANN-optimized data on a propane-fueled, direct-injection RCEM for varied spark durations ranging from 0.7 to 5.0 ms

Fig. 6.16 shows comparison of ANN optimized results with experimental results of NO_x emission of spark discharge effect on RCEM fueled with propane direct injection with ignition strategy. The production of thermal NO is triggered by high-temperature ignition, or when the burn temperature exceeds 1400 K. The development rate of the NO_x grows quickly as the burning temperature rises, while the growth rate of this element reduces as the burning temperature falls [145]. Propane has a low cetane number and a substantially longer ignition delay than gasoline, allowing the research engine to operate at greater loads with less smoke and less fuel consumption than diesel fuel. The mixture becomes heterogeneous in a stratified combustion as it gets closer to the spark plug, which raises the flame temperature and, as a result, the NO_x emission [155].

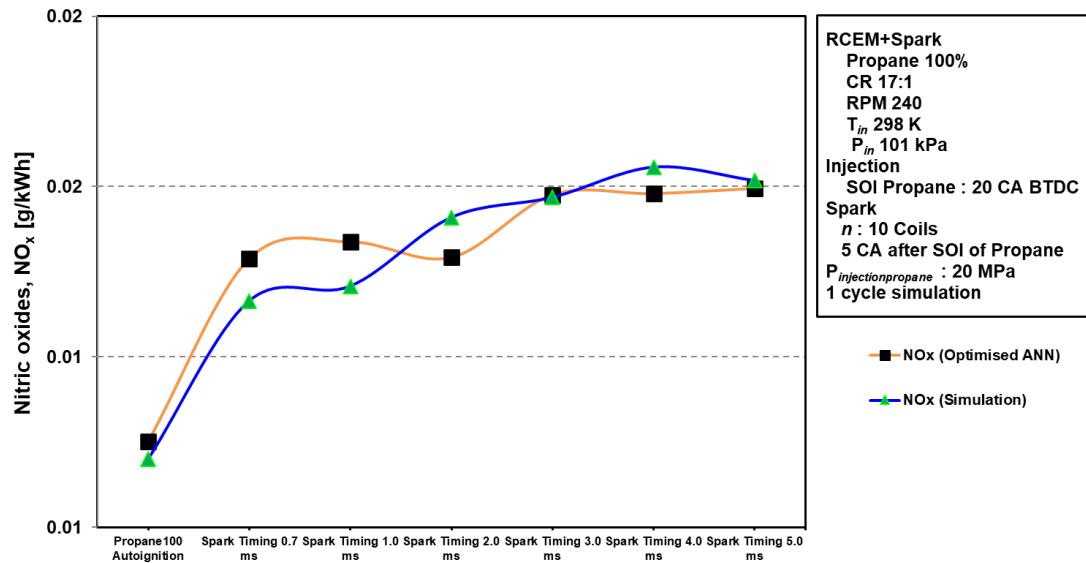


Fig. 6.16. Comparison of ANN optimised results with experimental results of NO_x of spark duration effect on RCEM fueled with propane direct injection with ignition strategy

The performance and emission parameters of the spark duration effect on direct injection propane were accurately predicted using the validated optimized ANN model. Due to the significant nonlinearity of NO_x emission, the error percentage is as expected high. However, it is found that the optimized ANN model's overall predictive power is fairly strong. The comparison of experimental and simulation findings with ANN-optimized outcomes is shown in Table 6.8. The reported maximum prediction errors for NO_x emission are 7%, indicating good agreement between ANN and multi-zone models in both parameters.

Table 6.8. Comparison between ANN optimised results with experimental and simulation results.

Parameters	ANN optimised results	Experimental/ Simulation results	% Difference
TKE	102.883	103.029	0.14
HRR	93.669	93.704	0.37
IMEP	2.539	2.540	0.04
η_{ith}	22.906	22.601	1.35
CO	0.133	0.134	0.74
NO _x	0.015	0.014	7.14

6.7 Summary

This section thoroughly investigated an artificial neural network method optimized using genetic algorithm that combines the ANN with Levenberg-Marquardt back propagation training algorithm to forecast effectively in-cylinder performance of a large bore compression ignition engine fueled with propane. A total of 756 dataset for each parameter obtained from experimental and simulation results were used for the ANN training, validation, and testing. The proposed ANN architecture contained 2 hidden layers with 16 neurons, respectively, and had operating parameters, including compression ratio (CR), fuel injection pressure (P_f), number of coil (n), start of injection (SOI), and spark duration timing (t) as the input parameters and the heat release rate (HRR), turbulent kinetic energy (TKE), indicated mean effective pressure (IMEP), indicated thermal efficiency (η_{ith}), CO, and NO_x as the output. It has been shown that the ANN can predict the impact of spark duration on in-cylinder performance after being properly trained. The impacts of operating parameters on the performances were also studied. Following is a summary of the key findings:

1. A polynomial equation models was established based on the regression analysis of the input variables and output variables. Based on the experimental data samples, it is feasible to construct the nonlinear relationship between operating parameters and response performance indicators.
2. The optimum combination of the operating parameters is decided by carrying out multi-objective optimisation using genetic algorithm tool. It is carried out by conventional method by considering individually performance and emissions. The optimum values of compression ratio, fuel injection pressure, number of coils, start of injection, and spark duration timing were found to be 17, 200 bar, 10 coils, 22 °CA bTDC, and 3 ms respectively.
3. The genetic algorithm ANN model demonstrated high accuracy on predicting optimum operating parameters, having the MSE for the training data were 0.0074, 0.0001, 0.0008, 0.0028, and 0.0134 for heat release rate (HRR), turbulent kinetic energy (TKE), tumble ratio, indicated power, and combustion efficiency (η_c) respectively whereas for the testing data these values were 0.9558, 0.9762, 0.9432, 0.9724, 0.9674 respectively. The created model was deemed to be acceptable because the *MSE* values for the test data were far below the stipulated limit.
4. The testing dataset shows that the ANN model can pick up on trends between inputs and target responses, suggesting that ANN can learn on connection between in-cylinder performance patterns.

7. SUMMARY AND CONCLUSION

This thesis work has addressed and achieved all of the intended goals. Through the use of simulation and experimentation, the experimental method's shortcoming in the context of hardware optimization was resolved. Through the use of simulation and experimentation, the impacts of spark discharge time on compression ignition engine performance and emission characteristics on the burning of propane fuel were thoroughly examined. The best factors to increase engine efficiency and emission characteristics were also found from the results.

The importance results were summarized below:

This work utilized simulations and experiments to examine the impact of spark discharge energy on the performance of the in-cylinder characteristics of gasoline RCEMs using direct injection spark ignition. Using CONVERGE computational fluid dynamics, the flow of tumble motion, velocity distribution flow, turbulent kinetic energy, and spark flame formation in response to variations in the spark discharge energy are examined. In accordance with six specific examples of ignition timing variation, three spark ignition strategies—ranging from 50 mA to 200 mA—are used to increase the ignition discharge energy (0.7 ms, 1.0 ms, 2.0 ms, 3.0 ms, 4.0 ms, and 5.0 ms).

The SOI of propane DI was set at 20 °CA BTDC, and when the spark time period was raised from 0.7 ms (1.01 °CA) to 5.0 ms (7.20 °CA), the thermal efficiency of the RCEM with spark rose somewhat. In actuality, diesel has a higher average thermal efficiency (14.26%) than propane. Because diesel fuel has a higher heating value than propane, it has a greater thermal efficiency. Increases in pressure and temperature lead to higher in-cylinder temperatures, a more complex combustion phasing, and a shorter combustion time.

Three different ignition approaches produced plasmas with negligible differences in size. The plasma size did not significantly change, even when the released current was increased to 200 mA by selecting the simultaneous 10 coil option. Therefore, there was no appreciable difference in the flame plasma growth phase when the discharge spark timing period was pursued. With the use of spark ignition, the propane RCEM produced the highest turbulent kinetic energy of $0.903 \text{ m}^2/\text{s}^2$, which is a 0.926% increase over the initial diesel-fueled RCEM. This might occur as a result of the spark plasma moving forward due to increased spark produced energy.

Compared to diesel, propane emits more CO and HC but less NO_x. In comparison to diesel fuel, the propane fuel's spark ignition approach significantly improved standard emissions. According to the RCEM research engine modelling results, when propane fuel was used instead of diesel, the corresponding values for HC, CO, CO₂, and NO_x were almost the same at 1.8%, 23.99%, 12.19%, and 32.21%, respectively.

The optimum combination of the operating parameters is decided by carrying out multi-objective optimisation using genetic algorithm tool. It is carried out by conventional method by considering individually performance and emissions. The optimum values of compression ratio, fuel injection pressure, number of coils, start of injection, and spark duration timing were found to be 17, 200 bar, 10 coils, 22 °CA bTDC, and 3 ms respectively.

The genetic algorithm ANN model demonstrated high accuracy on predicting optimum operating parameters, having the MSE for the training data were 0.0074, 0.0001, 0.0008, 0.0028, and 0.0134 for heat release rate (HRR), turbulent kinetic energy (TKE), tumble ratio, indicated power, and combustion efficiency (η_c) respectively whereas for the testing data these values were 0.9558, 0.9762, 0.9432, 0.9724, 0.9674 respectively. The created model was deemed to be acceptable because the *MSE* values for the test data were far below the stipulated limit.

Additionally, the relationship observed between the energy released during spark plug combustion, the in-cylinder flow characteristics, and the advancement of the combustion cycle in the vicinity of the spark plug indicates that the creation of a robust flow distribution surrounding the spark plug may expedite the formation of flames and expose the kernel development to a broader spectrum of variable velocities through an increase in spark discharge energy. Additionally, raising the spark discharge energy raises engine pressure and enhances the tumble ratio. It is necessary to conduct more research on renewable fuels with the best spark discharge characteristics. This could make it possible to improve engine performance based on big data from combustion state, alternative fuels, and the impact of cycle-to-cycle variation, among other things, using the technique described in this paper in conjunction with machine learning techniques. The goal is to reduce exhaust pollutant emissions and boost overall engine lean combustion efficiency in future high-efficiency engines. It is thought that more investigation is required on the ideal spark discharge phenomenon on renewable fuels. If the

methodology outlined in this paper is combined with machine learning approaches, future high-efficiency marine engines may operate more effectively, produce less exhaust pollutants, and have a higher total engine lean combustion efficiency.

Spark energy discharge in the establishment of a compression ignition engine could expedite plasma production and enable a wider range of spark durations. Reliable ignition and acceptable ignition delays were achieved by using spark plug ignition. Further investigation into the optimal spark discharge characteristics of renewable fuels is needed. In future high-efficiency engines, the suggested approach may enhance engine performance by lowering exhaust emissions and raising lean combustion efficiency.

The optimized ANN model can be used in the context of the current investigation and provided with thousands of datasets from the outcomes of experiments and simulations. The GA and ANN tools have been found to be appropriate for use in engine applications. The quantity of experimental runs can be greatly decreased when ANN modelling is used during the engine testing phase. The model can forecast the combustion and emission behavior of an engine under various operating situations once the best ANN model has been identified. Future generations of artificial neuron networks will be able to train on a wide range of factors, such as emission analysis, and compare their prediction accuracy to that of existing machine learning models.

REFERENCES

- [1] R. D. Reitz *et al.*, “IJER editorial: The future of the internal combustion engine,” *International Journal of Engine Research*, vol. 21, no. 1, pp. 3–10, Jan. 2020.
- [2] G. Kalghatgi, *Fuel/engine interactions*. Warrendale, Pa. (400 Commonwealth Dr., Wallendale PA USA) : Society of Automotive Engineers, 2014.
- [3] G. T. Kalghatgi, “Developments in internal combustion engines and implications for combustion science and future transport fuels,” *Proceedings of the Combustion Institute*, vol. 35, no. 1, pp. 101–115, Jan. 2015.
- [4] P. Bielaczyc and J. Woodburn, “Trends in Automotive Emission Legislation: Impact on LD Engine Development, Fuels, Lubricants and Test Methods: a Global View, with a Focus on WLTP and RDE Regulations,” *Emission Control Science and Technology*, vol. 5, no. 1, pp. 86–98, Mar. 2019.
- [5] G. Kalghatgi, H. Levinsky, and M. Colket, “Future transportation fuels,” *Progress in Energy and Combustion Science*, vol. 69, pp. 103–105, Nov. 2018.
- [6] J. Herdzik, “Decarbonization of Marine Fuels—The Future of Shipping,” *Energies 2021, Vol. 14, Page 4311*, vol. 14, no. 14, p. 4311, Jul. 2021.
- [7] S. J. Yeo, J. Kim, and W. J. Lee, “Potential economic and environmental advantages of liquid petroleum gas as a marine fuel through analysis of registered ships in South Korea,” *Journal of Cleaner Production*, vol. 330, p. 129955, Jan. 2022.
- [8] A. C. Polk, C. D. Carpenter, K. K. Srinivasan, and S. R. Krishnan, “An investigation of diesel-ignited propane dual fuel combustion in a heavy-duty diesel engine,” *Fuel*, vol. 132, pp. 135–148, 2014.
- [9] P. Dimitriou and R. Javaid, “A review of ammonia as a compression ignition engine fuel,” *International Journal of Hydrogen Energy*, vol. 45, no. 11, pp. 7098–7118, Feb. 2020.
- [10] U. Oester and J. S. Wallace, “Liquid propane injection for diesel engines,” *SAE Technical Papers*, 1987.
- [11] S. R. Krishnan, K. K. Srinivasan, and M. S. Raihan, “The effect of injection parameters and boost pressure on diesel-propane dual fuel low temperature combustion in a single-cylinder research engine,” *Fuel*, vol. 184, pp. 490–502, Nov. 2016.
- [12] K. A. Hodges, A. Aniello, S. R. Krishnan, and K. K. Srinivasan, “Impact of propane energy fraction on diesel-ignited propane dual fuel low temperature combustion,”

- Fuel*, vol. 209, no. April, pp. 769–775, 2017.
- [13] M. Cardone, E. Mancaruso, R. Marialto, L. Sequino, and B. M. Vaglieco, “Characterization of Combustion and Emissions of a Propane-Diesel Blend in a Research Diesel Engine,” *SAE Technical Papers*, vol. 2016-April, no. April, 2016.
- [14] G. Nikolaou, “LPG for Marine Engines. The Marine Alternative Fuel,” p. 144, 2017.
- [15] Z. Ahmad, O. Kaario, C. Qiang, and M. Larmi, “Effect of pilot fuel properties on lean dual-fuel combustion and emission characteristics in a heavy-duty engine,” *Applied Energy*, vol. 282, p. 116134, Jan. 2021.
- [16] Y. Putrasari and O. LIM, “A study of a GCI engine fueled with gasoline-biodiesel blends under pilot and main injection strategies,” *Fuel*, vol. 221, pp. 269–282, Jun. 2018.
- [17] M. Aydin, A. Irgin, and M. B. Çelik, “The impact of diesel/LPG dual fuel on performance and emissions in a single cylinder diesel generator,” *Applied Sciences (Switzerland)*, vol. 8, no. 5, pp. 1–14, 2018.
- [18] J. Lee *et al.*, “A study of emissions reduction through dual-fuel combustion with propane in a compression ignition engine,” *SAE Technical Papers*, vol. 11, 2013.
- [19] M. Y. E. Selim, “Sensitivity of dual fuel engine combustion and knocking limits to gaseous fuel composition,” *Energy Conversion and Management*, vol. 45, no. 3, pp. 411–425, Feb. 2004.
- [20] D. B. Lata and A. Misra, “Analysis of ignition delay period of a dual fuel diesel engine with hydrogen and LPG as secondary fuels,” *International Journal of Hydrogen Energy*, vol. 36, no. 5, pp. 3746–3756, Mar. 2011.
- [21] A. C. Polk, C. D. Carpenter, K. K. Srinivasan, and S. R. Krishnan, “An investigation of diesel-ignited propane dual fuel combustion in a heavy-duty diesel engine,” *Fuel*, vol. 132, no. September, pp. 135–148, 2014.
- [22] J. Kang, S. Chu, J. Lee, G. Kim, and K. Min, “Effect of operating parameters on diesel/propane dual fuel premixed compression ignition in a diesel engine,” *International Journal of Automotive Technology 2018 19:1*, vol. 19, no. 1, pp. 27–35, Oct. 2017.
- [23] A. Tilz, C. Kiesling, G. Meyer, A. Nickl, G. Pirker, and A. Wimmer, “Experimental investigation of the influence of ignition system parameters on combustion behavior in large lean burn spark ignited gas engines,” *Experimental Thermal and Fluid Science*, vol. 119, no. May, p. 110176, 2020.

- [24] Z. Yang *et al.*, “Effects of Spark Discharge Energy Scheduling on Flame Kernel Formation under Quiescent and Flow Conditions.” SAE International , 2019.
- [25] D. Jung, K. Sasaki, and N. Iida, “Effects of increased spark discharge energy and enhanced in-cylinder turbulence level on lean limits and cycle-to-cycle variations of combustion for SI engine operation,” *Applied Energy*, vol. 205, no. April, pp. 1467–1477, 2017.
- [26] Heywood JB, *Internal combustion engine fundamentals*. McGraw-Hill Education, 1988.
- [27] B. Sforzo, J. Kim, J. Jagoda, and J. Seitzman, “Ignition probability in a stratified turbulent flow with a sunken fire igniter,” *Journal of Engineering for Gas Turbines and Power*, vol. 137, no. 1, 2015.
- [28] S. Yu *et al.*, “The Effect of High-Power Capacitive Spark Discharge on the Ignition and Flame Propagation in a Lean and Diluted Cylinder Charge,” in *SAE Technical Papers*, 2016.
- [29] S. Tsuboi, S. Miyokawa, M. Matsuda, T. Yokomori, and N. Iida, “Influence of spark discharge characteristics on ignition and combustion process and the lean operation limit in a spark ignition engine,” *Applied Energy*, vol. 250, no. April, pp. 617–632, 2019.
- [30] T. Badawy, X. C. Bao, and H. Xu, “Impact of spark plug gap on flame kernel propagation and engine performance,” *Applied Energy*, vol. 191, pp. 311–327, Apr. 2017.
- [31] J. Kim, B. Sforzo, J. Seitzman, and J. Jagoda, “High energy spark discharges for ignition,” in *48th AIAA/ASME/SAE/ASEE Joint Propulsion Conference and Exhibit 2012*, 2012.
- [32] M. Kim, Y. Kim, J. Kim, and H. H. Song, “Development of quasi-dimensional turbulence model for spark-ignition engine with physical analysis of tumble: Energy-based tumble model focusing on energy intake and turbulence production,” *Applied Energy*, vol. 252, p. 113455, Oct. 2019.
- [33] M. El-Adawy, M. R. Heikal, A. R. A. Aziz, M. I. Siddiqui, and H. A. Abdul Wahhab, “Experimental study on an IC engine in-cylinder flow using different steady-state flow benches,” *Alexandria Engineering Journal*, vol. 56, no. 4, pp. 727–736, Dec. 2017.
- [34] M. Ghaderi Masouleh, K. Keskinen, O. Kaario, H. Kahila, S. Karimkashi, and V. Vuorinen, “Modeling cycle-to-cycle variations in spark ignited combustion engines by

- scale-resolving simulations for different engine speeds,” *Applied Energy*, vol. 250, pp. 801–820, Sep. 2019.
- [35] M. Kaplan, “Influence of swirl, tumble and squish flows on combustion characteristics and emissions in internal combustion engine-review,” *International Journal of Automotive Engineering and Technologies*, vol. 8, no. 2, pp. 83–102, 2019.
- [36] A. Kalpakli Vester, Y. Nishio, and P. H. Alfredsson, “Unravelling tumble and swirl in a unique water-analogue engine model,” *Journal of Visualization*, vol. 21, no. 4, pp. 557–568, Aug. 2018.
- [37] N. Pavel *et al.*, “Laser ignition - Spark plug development and application in reciprocating engines,” *Progress in Quantum Electronics*, vol. 58, pp. 1–32, Mar. 2018.
- [38] L. E. Gettel and K. C. Tsai, “Flame kernel development with the multiple electrode spark plug,” *Combustion and Flame*, vol. 54, no. 1–3, pp. 225–228, Dec. 1983.
- [39] J. Kim, B. Sforzo, J. Seitzman, and J. Jagoda, “High Energy Spark Discharges for Ignition,” 2012.
- [40] C. Bae and J. Kim, “Alternative fuels for internal combustion engines,” *Proceedings of the Combustion Institute*, vol. 36, no. 3, pp. 3389–3413, Jan. 2017.
- [41] R. D. Reitz *et al.*, “IJER editorial: The future of the internal combustion engine,” *International Journal of Engine Research*, vol. 21, no. 1. SAGE Publications Ltd, pp. 3–10, 01-Jan-2020.
- [42] A. T. Hoang, “Combustion behavior, performance and emission characteristics of diesel engine fuelled with biodiesel containing cerium oxide nanoparticles: A review,” *Fuel Processing Technology*, vol. 218, p. 106840, Jul. 2021.
- [43] R. Rajasegar and A. Srna, “Effect of Spray Collapse on Mixture Preparation and Combustion Characteristics of a Spark-Ignition Heavy-Duty Diesel Optical Engine Fueled with Direct-Injected Liquefied Petroleum Gas (LPG),” in *SAE Technical Paper 2023-01-0323*, 2023.
- [44] J. Shin and S. Park, “Numerical analysis for optimizing combustion strategy in an ammonia-diesel dual-fuel engine,” *Energy Conversion and Management*, vol. 284, p. 116980, May 2023.
- [45] X. Zhen and Y. Wang, “An overview of methanol as an internal combustion engine fuel,” *Renewable and Sustainable Energy Reviews*, vol. 52, pp. 477–493, Dec. 2015.
- [46] D. Splitter, V. Boronat, F. D. F. Chuahy, and J. Storey, “Performance of direct injected

- propane and gasoline in a high stroke-to-bore ratio SI engine: Pathways to diesel efficiency parity with ultra low soot,” *International Journal of Engine Research*, vol. 22, no. 12, pp. 3475–3488, Dec. 2021.
- [47] K. J. Morganti, T. M. Foong, M. J. Brear, G. Da Silva, Y. Yang, and F. L. Dryer, “The Research and Motor octane numbers of Liquefied Petroleum Gas (LPG),” *Fuel*, vol. 108, pp. 797–811, Jun. 2013.
- [48] D. F. Chuahy, D. Splitter, V. Boronat, and S. W. Wagnon, “Enabling high compression ratio in boosted spark ignition engines: Thermodynamic trajectory and fuel chemistry effects on knock,” *Combustion and Flame*, vol. 222, pp. 446–459, Dec. 2020.
- [49] Y. Seo, J. Kim, E. Park, J. Lee, M. Cho, and S. Han, “Analysis of Energy Consumption of Novel Re-Liquefaction System Integrated with Fuel Supply System (FSS) for LPG-Fuelled LPG Carrier to Conventional Systems,” *Energies*, vol. 15, no. 24, 2022.
- [50] T. Kar, T. Fosudo, A. Marchese, B. Windom, and D. Olsen, “Effect of fuel composition and EGR on spark-ignited engine combustion with LPG fueling: Experimental and numerical investigation,” *Fuel*, vol. 327, no. July, p. 125221, 2022.
- [51] L. Bilgili, “A systematic review on the acceptance of alternative marine fuels,” *Renewable and Sustainable Energy Reviews*, vol. 182, p. 113367, Aug. 2023.
- [52] K. Kim, J. Kim, S. Oh, C. Kim, and Y. Lee, “Lower particulate matter emissions with a stoichiometric LPG direct injection engine,” *Fuel*, vol. 187, pp. 197–210, Jan. 2017.
- [53] A. K. Ramalingam, M. Kriek, S. Pischinger, and K. A. Heufer, “Understanding the Oxidation Behavior of Automotive Liquefied Petroleum Gas Fuels: Experimental and Kinetic Analyses,” *Energy and Fuels*, vol. 34, no. 2, pp. 2323–2333, Feb. 2020.
- [54] D. A. DelVescovo, J. Li, D. A. Splitter, F. D. F. Chuahy, and P. Zhao, “Genetic algorithm optimization of a chemical kinetic mechanism for propane at engine relevant conditions,” *Fuel*, vol. 338, p. 127371, Apr. 2023.
- [55] A. Vardhan, R. S. Rajput, A. C. Tiwari, and R. Randa, “Performance and Emission Analysis of Modified Compression Ignition Engine from Diesel Engine to Variable Load using Petrol and LPG Fuel,” *Chemical Engineering and Processing - Process Intensification*, vol. 181, p. 109115, Nov. 2022.
- [56] H. Kokabi, M. Najafi, S. A. Jazayeri, and O. Jahanian, “Hydrogen and propane implications for reactivity controlled compression ignition combustion engine running

- on landfill gas and diesel fuel,” *International Journal of Hydrogen Energy*, vol. 46, no. 62, pp. 31903–31915, Sep. 2021.
- [57] E. Arslan and N. Kahraman, “Comparison of natural gas and propane addition to combustion air in terms of engine performance in compression ignition engine,” *Fuel*, vol. 312, p. 122952, Mar. 2022.
- [58] S. Baek, K. Kim, J. Cho, C. L. Myung, and S. Park, “Assessment of gaseous, particulate, and unregulated emissions from diesel compression ignition and LPG direct injection spark ignition minibus vehicles under the world harmonized vehicle cycle on a chassis dynamometer,” *Fuel*, vol. 294, p. 120392, Jun. 2021.
- [59] C. Windarto, A. Setiawan, N. H. X. Duy, and O. Lim, “Investigation of propane direct injection performance in a rapid compression and expansion machine: Pathways to diesel marine engine efficiency parity with spark discharge duration strategies,” *International Journal of Hydrogen Energy*, Jun. 2023.
- [60] E. Elnajjar, M. Y. E. Selim, and M. O. Hamdan, “Experimental study of dual fuel engine performance using variable LPG composition and engine parameters,” *Energy Conversion and Management*, vol. 76, pp. 32–42, Dec. 2013.
- [61] A. Chakraborty, S. Biswas, S. Meitei, A. Sengupta, D. Kakati, and R. Banerjee, “Examining the significance of the ignition characteristics of hydrogen and liquefied-petroleum-gas on the reactivity controlled compression ignition and its interspersed profiles induced in an existing diesel engine: A comparative perspective,” *Energy Conversion and Management*, vol. 268, p. 115976, Sep. 2022.
- [62] F. Leach, G. Kalghatgi, R. Stone, and P. Miles, “The scope for improving the efficiency and environmental impact of internal combustion engines,” *Transportation Engineering*, vol. 1, no. April, p. 100005, 2020.
- [63] H. Zhu *et al.*, “A preliminary study of the discharge current and spark energy for the multi-coil offset strategy,” in *SAE Technical Papers*, 2019, vol. 2019-April, no. April.
- [64] M. Zheng and S. Yu, “Advanced Ignition Systems for Future Future Clean Combustion Engines: Review,” *Journal of Automotive Safety and Energy*, vol. 6, no. 4, pp. 295–313, 2015.
- [65] C. Willman, B. Scott, R. Stone, and D. Richardson, “Quantitative metrics for comparison of in-cylinder velocity fields using particle image velocimetry,” *Experiments in Fluids*, vol. 61, no. 2, p. 62, Feb. 2020.
- [66] A. Nishiyama, M. K. Le, T. Furui, and Y. Ikeda, “The relationship between in-cylinder

- flow-field near spark plug areas, the spark behavior, and the combustion performance inside an optical S.I. Engine,” *Applied Sciences (Switzerland)*, vol. 9, no. 8, pp. 1–13, 2019.
- [67] D. A. Eichenberger and W. L. Roberts, “Effect of unsteady stretch on spark-ignited flame kernel survival,” *Combustion and Flame*, vol. 118, no. 3, pp. 469–478, Aug. 1999.
- [68] M. Elkelawy *et al.*, “Influence of lean premixed ratio of PCCI-DI engine fueled by diesel/biodiesel blends on combustion, performance, and emission attributes; a comparison study,” *Energy Conversion and Management: X*, vol. 10, p. 100066, Jun. 2021.
- [69] G. T. Kalghatgi, P. Risberg, and H. E. Ångström, “Advantages of Fuels with High Resistance to Auto-ignition in Late-injection, Low-temperature, Compression Ignition Combustion,” *SAE Technical Papers*, Oct. 2006.
- [70] R. Ianniello, G. Di Blasio, R. Marialto, C. Beatrice, and M. Cardone, “Assessment of direct injected liquefied petroleum gas-diesel blends for ultra-low soot combustion engine application,” *Applied Sciences (Switzerland)*, vol. 10, no. 14, 2020.
- [71] S. Woo, J. Lee, and K. Lee, “Investigation of injection characteristics for optimization of liquefied petroleum gas applied to a direct-injection engine,” *Energy Reports*, vol. 9, pp. 2130–2139, Dec. 2023.
- [72] A. Boretti, “Advances in Diesel-LNG Internal Combustion Engines,” *Applied Sciences 2020, Vol. 10, Page 1296*, vol. 10, no. 4, p. 1296, Feb. 2020.
- [73] L. P. Wyszynski, C. R. Stone, and G. T. Kalghatgi, “The volumetric efficiency of direct and port injection gasoline engines with different fuels,” *SAE Technical Papers*, 2002.
- [74] J. Cho, K. Kim, S. Baek, C. L. Myung, and S. Park, “Abatement potential analysis on CO₂ and size-resolved particle emissions from a downsized LPG direct injection engine for passenger car,” *Atmospheric Pollution Research*, vol. 10, no. 6, pp. 1711–1722, Nov. 2019.
- [75] R. Ryskamp, “Emissions and Performance of Liquefied Petroleum Gas as a Transportation Fuel: A Review,” p. 36, 2017.
- [76] M. A. Burnett and M. S. Wooldridge, “An experimental investigation of flame and autoignition behavior of propane,” *Combustion and Flame*, vol. 224, pp. 24–32, Feb. 2021.

- [77] Z. Yang *et al.*, “Impacts of Spark Discharge Current and Duration on Flame Development of Lean Mixtures Under Flow Conditions,” *ASME 2018 Internal Combustion Engine Division Fall Technical Conference, ICEF 2018*, vol. 1, Jan. 2019.
- [78] S. V. Channapattana, A. A. Pawar, and P. G. Kamble, “Optimisation of operating parameters of DI-CI engine fueled with second generation Bio-fuel and development of ANN based prediction model,” *Applied Energy*, vol. 187, pp. 84–95, 2017.
- [79] J. Liu, B. Ma, and H. Zhao, “Combustion parameters optimization of a diesel/natural gas dual fuel engine using genetic algorithm,” *Fuel*, vol. 260, p. 116365, Jan. 2020.
- [80] Y. Li, M. Jia, X. Han, and X. S. Bai, “Towards a comprehensive optimization of engine efficiency and emissions by coupling artificial neural network (ANN) with genetic algorithm (GA),” *Energy*, vol. 225, p. 120331, Jun. 2021.
- [81] M. S. P, G. V, P. P, G. A, and D. G, “Prediction efficiency of artificial neural network for CRDI engine output parameters,” *Transportation Engineering*, vol. 3, p. 100041, Mar. 2021.
- [82] S. V. Channapattana, A. A. Pawar, and P. G. Kamble, “Optimisation of operating parameters of DI-CI engine fueled with second generation Bio-fuel and development of ANN based prediction model,” *Applied Energy*, vol. 187, pp. 84–95, Feb. 2017.
- [83] D. Babu, V. Thangarasu, and A. Ramanathan, “Artificial neural network approach on forecasting diesel engine characteristics fuelled with waste frying oil biodiesel,” *Applied Energy*, vol. 263, p. 114612, Apr. 2020.
- [84] J. Seo, B. Yun, J. Kim, M. Shin, and S. Park, “Development of a cold-start emission model for diesel vehicles using an artificial neural network trained with real-world driving data,” *Science of the Total Environment*, vol. 806, p. 151347, 2022.
- [85] A. T. Le, D. Q. Tran, T. T. Tran, A. T. Hoang, and V. V. Pham, “Performance and combustion characteristics of a retrofitted CNG engine under various piston-top shapes and compression ratios,” *Energy Sources, Part A: Recovery, Utilization, and Environmental Effects*, pp. 1–17, Aug. 2020.
- [86] S. Foroutani, G. Salehi, H. Fallahsohi, K. Lary, and A. M. Arasteh, “Artificial Neural Network Modeling and Numerical Simulation of Syngas Fuel and Injection Timing Effects on the Performance and Emissions of a Heavy-Duty Compression Ignition Engine,” *ACS Omega*, vol. 6, no. 48, pp. 32379–32394, Dec. 2021.
- [87] F. Jaliliantabar, B. Ghobadian, G. Najafi, and T. Yusaf, “Artificial neural network modeling and sensitivity analysis of performance and emissions in a compression

- ignition engine using biodiesel fuel,” *Energies*, vol. 11, no. 9, 2018.
- [88] X. H. Fang, N. Papaioannou, F. Leach, and M. H. Davy, “On the application of artificial neural networks for the prediction of NO_x emissions from a high-speed direct injection diesel engine,” *International Journal of Engine Research*, vol. 22, no. 6, pp. 1808–1824, Jun. 2021.
- [89] A. S. El-Shafay, U. F. Alqsair, S. M. Abdel Razek, and M. S. Gad, “Artificial neural network prediction of performance and emissions of a diesel engine fueled with palm biodiesel,” *Scientific Reports*, vol. 12, no. 1, pp. 1–15, 2022.
- [90] X. Niu, C. Yang, H. Wang, and Y. Wang, “Investigation of ANN and SVM based on limited samples for performance and emissions prediction of a CRDI-assisted marine diesel engine,” *Applied Thermal Engineering*, vol. 111, pp. 1353–1364, Jan. 2017.
- [91] H. Taghavifar and L. P. Perera, “Data-driven modeling of energy-exergy in marine engines by supervised ANNs based on fuel type and injection angle classification,” *Process Safety and Environmental Protection*, vol. 172, pp. 546–561, Apr. 2023.
- [92] P. Loeper *et al.*, “Experimental Investigation of Light-Medium Load Operating Sensitivity in a Gasoline Compression Ignition (GCI) Light-Duty Diesel Engine,” *SAE Technical Papers*, vol. 2, Apr. 2013.
- [93] K. Darrow, R. Tidball, J. Wang, and A. Hampson, “Technology Characterization – Reciprocating Internal Combustion Engines,” *Catalog of CHP Technologies*, no. 2, 2015.
- [94] K. L. Kelly and J. Gonzales, “What Fleets Need to Know About Alternative Fuel Vehicle Conversions, Retrofits, and Repowers,” Oct. 2017.
- [95] S. Unnasch and L. Goyal, “Life Cycle Analysis of LPG Transportation Fuels under the Californian LCFS,” *Life Cycle Associates Report LCA.8103.177.2017*, Prepared for WPGA., pp. vii–ix, 2017.
- [96] J. A. Onwudili and D. J. Nouwe Edou, “Process modelling and economic evaluation of biopropane production from aqueous butyric acid feedstock,” *Renewable Energy*, vol. 184, pp. 80–90, Jan. 2022.
- [97] R. M. Baldwin, M. R. Nimlos, and Y. Zhang, “Techno-Economic, Feasibility, and Life Cycle Analysis of Renewable Propane (Final Report),” Oct. 2022.
- [98] A. Barkhordari, S. I. Mirzaei, A. Falahat, D. A. Krawczyk, and A. Rodero, “Experimental Study of a Rotating Electrode Plasma Reactor for Hydrogen Production from Liquid Petroleum Gas Conversion,” *Applied Sciences (Switzerland)*, vol. 12, no.

- 8, 2022.
- [99] IEA-AMF, “Liquefied petroleum gas, LPG.” [Online]. Available: https://www.iea-amf.org/content/fuel_information/lpg. [Accessed: 23-Jun-2023].
- [100] M. Rood Werpy, A. Burnham, and K. Bertram, “Propane vehicles : status, challenges, and opportunities.,” Jun. 2010.
- [101] J. Thomas, B. West, T. Alleman, M. Melendez, and M. Shirk, *History of Significant Vehicle and Fuel Introductions in the United States*, no. September. 2017.
- [102] M. Setiyo, S. Soeparman, N. Hamidi, and S. Wahyudi, “Techno-economic analysis of liquid petroleum gas fueled vehicles as public transportation in Indonesia,” *International Journal of Energy Economics and Policy*, vol. 6, no. 3, pp. 495–500, 2016.
- [103] Y. Putrasari and O. Lim, “Dimethyl Ether as the Next Generation Fuel to Control Nitrogen Oxides and Particulate Matter Emissions from Internal Combustion Engines: A Review,” *ACS Omega*, vol. 7, no. 1, pp. 32–37, 2022.
- [104] N. K. Miller Jothi, G. Nagarajan, and S. Renganarayanan, “Experimental studies on homogeneous charge CI engine fueled with LPG using DEE as an ignition enhancer,” *Renewable Energy*, vol. 32, no. 9, pp. 1581–1593, Jul. 2007.
- [105] K. Ravi, J. Pradeep Bhasker, and E. Porpatham, “Effect of compression ratio and hydrogen addition on part throttle performance of a LPG fuelled lean burn spark ignition engine,” *Fuel*, vol. 205, pp. 71–79, Oct. 2017.
- [106] N. Jamsran and O. Lim, “A Study on the Autoignition Characteristics of DME–LPG Dual Fuel in the HCCI Engine,” <https://doi.org/10.1080/01457632.2016.1142816>, vol. 37, no. 17, pp. 1488–1497, Nov. 2016.
- [107] Y. Ohno, *DME Handbook*. Tokyo, Japan: Japan DME Forum Ohmsha Ltd., 2006.
- [108] Y. Ohno, *DME Handbook—Supplement*. Tokyo, Jaolan: Japan DME Forum Ohmsha Ltd., 2011.
- [109] “LPG supply growth outstripping demand, infrastructure | Oil & Gas Journal.” [Online]. Available: <https://www.ogj.com/pipelines-transportation/article/14173824/lpg-supply-growth-outstripping-demand-infrastructure>. [Accessed: 23-Jun-2023].
- [110] A. Burnham, M. Mintz, M. Rood, and A. Burnham, “Status and Issues for Natural Gas in the United States Alternative Fuel and Advanced Vehicle,” no. February, 2015.
- [111] A. Koen Rademaekers *et al.*, *Study on Energy Prices, Costs and Subsidies and their*

- Impact on Industry and Households Contract details European Commission-DG Energy*. 2018.
- [112] Z. Zhang *et al.*, “Characteristics of trans-critical propane spray discharged from multi-hole GDI injector,” *Experimental Thermal and Fluid Science*, vol. 99, pp. 446–457, Dec. 2018.
- [113] “D1835 Standard Specification for Liquefied Petroleum (LP) Gases.” [Online]. Available: <https://www.astm.org/d1835-20.html>. [Accessed: 24-Jun-2023].
- [114] Richards; K.J.; Senecal; P.K.; and Pomraning; E, *CONVERGE Manual v3.0*. Middleton: Convergent Science, Inc., 2013.
- [115] D. Jung and N. Iida, “An investigation of multiple spark discharge using multi-coil ignition system for improving thermal efficiency of lean SI engine operation,” *Applied Energy*, vol. 212, no. September 2017, pp. 322–332, 2018.
- [116] K. Kim, J. Han, and S. Im, “Evaluation of the Ignition Effect in Constant Volume Combustion Chamber Based on Matching Effect of High Voltage (MEHV) Method,” *Energies 2020, Vol. 13, Page 5084*, vol. 13, no. 19, p. 5084, Sep. 2020.
- [117] J. P. Holman, *Experimental Methods for Engineers*, Eighth Edi., vol. s1-VIII, no. 193. New York: McGraw-Hill Education, 1853.
- [118] A. Gharehghani, A. Kakooe, A. M. Andwari, T. Megaritis, and A. Pesyridis, “Numerical investigation of an RCCI engine fueled with natural gas/dimethyl-ether in various injection strategies,” *Energies*, vol. 14, no. 6, 2021.
- [119] Willard W. Pulkrabek, *Engineering Fundamentals Of The Internal Combustion Engine 2Nd Ed*. Prentice-Hall Of India Pvt. Limited, 2013.
- [120] W. N. W. Mansor and D. B. Olsen, “Computational modeling of diesel and dual fuel combustion using CONVERGE CFD software,” *ARPJ Journal of Engineering and Applied Sciences*, vol. 11, no. 23, pp. 13697–13707, 2016.
- [121] Z. Yang *et al.*, “Impacts of spark discharge current and duration on flame development of lean mixtures under flow conditions,” *ASME 2018 Internal Combustion Engine Division Fall Technical Conference, ICEF 2018*, vol. 1, 2018.
- [122] C. ye, Z. Yang, S. Yu, M. Xu, and M. Zheng, “A Study of Energy Enhanced Multi-Spark Discharge Ignition in a Constant-Volume Combustion Chamber.” SAE International , 2019.
- [123] P. Ramesh and E. James Gunasekaran, “Investigation of flow field pattern in a GDI engine at different speeds using numerical techniques,” *SAE Technical Papers*, vol. 12,

- 2013.
- [124] A. A. Reddy and J. M. Mallikarjuna, "Parametric Study on a Gasoline Direct Injection Engine - A CFD Analysis," *SAE Technical Papers*, vol. 2017-January, no. January, Jan. 2017.
- [125] H. Woo WON and A. Sci, "A Method and System for Combining the Advantages of Gasoline Compression Ignition (GCI) Engine Technologies into Hybrid Electric Vehicles (HEVs)," *Applied Sciences 2021, Vol. 11, Page 9934*, vol. 11, no. 21, p. 9934, Oct. 2021.
- [126] Y. Hu, Z. Huang, L. Wang, X. Sun, and W. Chen, "Experimental study on combustion and emissions of a compression ignition engine fueled with gasoline," *Advances in Mechanical Engineering*, vol. 14, no. 7, pp. 1–8, Jul. 2022.
- [127] M. A. M. Johar, M. F. M. Said, M. A. Abas, Z. A. Latiff, M. F. Ali, and N. M. I. N. Ibrahim, "Flow analysis of intake port geometry of spark ignition engine using simulation," *AIP Conference Proceedings*, vol. 2059, no. 1, p. 020048, Jan. 2019.
- [128] C. Shi, C. Ji, S. Wang, J. Yang, Z. Ma, and P. Xu, "Assessment of spark-energy allocation and ignition environment on lean combustion in a twin-plug Wankel engine," *Energy Conversion and Management*, vol. 209, no. December 2019, p. 112597, 2020.
- [129] D. Lou, Y. Ren, Y. Zhang, and X. Sun, "Study on the Effects of EGR and Spark Timing on the Combustion, Performance, and Emissions of a Stoichiometric Natural Gas Engine," *ACS Omega*, vol. 5, no. 41, pp. 26763–26775, Oct. 2020.
- [130] L. Zhao, Y. Zhang, Y. Pei, A. Zhang, and M. M. Ameen, "CFD-Guided Evaluation of Spark-Assisted Gasoline Compression Ignition for Cold Idle Operation," *Sustainability 2021, Vol. 13, Page 13096*, vol. 13, no. 23, p. 13096, Nov. 2021.
- [131] C. Pera, V. Knop, and J. Reveillon, "Influence of flow and ignition fluctuations on cycle-to-cycle variations in early flame kernel growth," *Proceedings of the Combustion Institute*, vol. 35, no. 3, pp. 2897–2905, 2015.
- [132] B. R. Petersen and J. Ghandhi, "High Resolution Scalar Dissipation and Turbulence Length Scale Measurements in an Internal Combustion Engine," *SAE International Journal of Engines*, vol. 3, no. 1, pp. 65–83, Apr. 2010.
- [133] H. A. Alrazen and K. A. Ahmad, "HCNG fueled spark-ignition (SI) engine with its effects on performance and emissions," *Renewable and Sustainable Energy Reviews*, vol. 82, no. September 2017, pp. 324–342, 2018.

- [134] L. Bonneau, V. Robin, and T. Xavier, “A computational framework combining a basic turbulent combustion model, self-similar chemistry behavior, and a wall thermal law adapted for large-eddy simulations of a cyclically operating constant volume combustion chamber,” *Combustion and Flame*, vol. 244, p. 112212, Oct. 2022.
- [135] R. Y. Dahham, H. Wei, and J. Pan, “Improving Thermal Efficiency of Internal Combustion Engines: Recent Progress and Remaining Challenges,” *Energies 2022, Vol. 15, Page 6222*, vol. 15, no. 17, p. 6222, Aug. 2022.
- [136] K. Min *et al.*, “Autoignition of varied cetane number fuels at low temperatures,” *Proceedings of the Combustion Institute*, vol. 37, no. 4, pp. 5003–5011, Jan. 2019.
- [137] G. K. Lilik and A. L. Boehman, “Effects of fuel composition on critical equivalence ratio for autoignition,” *Energy and Fuels*, vol. 27, no. 3, pp. 1601–1612, 2013.
- [138] S. Tavakoli, M. V. Jensen, E. Pedersen, and J. Schramm, “Unburned hydrocarbon formation in a natural gas engine under sea wave load conditions,” *Journal of Marine Science and Technology (Japan)*, vol. 26, no. 1, pp. 128–140, Mar. 2021.
- [139] E. Malfi, V. De Bellis, F. Bozza, A. Cafari, G. Caputo, and J. Hyvönen, “A phenomenological model for the description of unburned hydrocarbons emission in ultra-lean engines,” <https://doi.org/10.1177/14680874211005063>, vol. 23, no. 6, pp. 995–1011, Mar. 2021.
- [140] Y. Zhang *et al.*, “Premixed combustion and emission characteristics of methane diluted with ammonia under F-class gas turbine relevant operating condition,” *Frontiers in Energy Research*, vol. 11, p. 1120108, Jan. 2023.
- [141] J. Fu, B. Deng, X. Liu, J. Shu, Y. Xu, and J. Liu, “The experimental study on transient emissions and engine behaviors of a sporting motorcycle under World Motorcycle Test Cycle,” *Energy*, vol. 211, p. 118670, Nov. 2020.
- [142] Y. Li *et al.*, “Combustion, performance and emissions characteristics of a spark-ignition engine fueled with isopropanol-n-butanol-ethanol and gasoline blends,” *Fuel*, vol. 184, pp. 864–872, Nov. 2016.
- [143] W. Guo, M. Xiao, Z. Zhang, Y. Wang, L. Shi, and K. Deng, “Effects of multiple injections on the combustion and hydrocarbon emission characteristics of the start cylinder in direct-start process,” *Fuel*, vol. 320, p. 123851, Jul. 2022.
- [144] H. A. Alrazen, A. R. Abu Talib, and K. A. Ahmad, “A two-component CFD studies of the effects of H₂, CNG, and diesel blend on combustion characteristics and emissions of a diesel engine,” *International Journal of Hydrogen Energy*, vol. 41, no. 24, pp.

- 10483–10495, Jun. 2016.
- [145] S. H. Park and C. S. Lee, “Combustion performance and emission reduction characteristics of automotive DME engine system,” *Progress in Energy and Combustion Science*, vol. 39, no. 1, pp. 147–168, Feb. 2013.
- [146] Y. Wang, Y. Chen, X. Liang, P. Tan, and S. Deng, “Impacts of lubricating oil and its formulations on diesel engine particle characteristics,” *Combustion and Flame*, vol. 225, pp. 48–56, Mar. 2021.
- [147] P. Kumar, S. Kumar, S. Shah, and S. Kumar, “Study of performance parameters and emissions of four stroke CI engine using solketal-biodiesel blends,” *SN Applied Sciences*, vol. 3, no. 1, pp. 1–8, Jan. 2021.
- [148] C. Gong, L. Yi, Z. Zhang, J. Sun, and F. Liu, “Assessment of ultra-lean burn characteristics for a stratified-charge direct-injection spark-ignition methanol engine under different high compression ratios,” *Applied Energy*, vol. 261, no. November 2019, p. 114478, 2020.
- [149] C. M. Gibson, A. C. Polk, N. T. Shoemaker, K. K. Srinivasan, and S. R. Krishnan, “Comparison of propane and methane performance and emissions in a turbocharged direct injection dual fuel engine,” *Journal of Engineering for Gas Turbines and Power*, vol. 133, no. 9, pp. 1–9, 2011.
- [150] H. A. Alrazen, A. R. Abu Talib, R. Adnan, and K. A. Ahmad, “A review of the effect of hydrogen addition on the performance and emissions of the compression – Ignition engine,” *Renewable and Sustainable Energy Reviews*, vol. 54, pp. 785–796, Feb. 2016.
- [151] F. V. Tinaut, A. Melgar, B. Giménez, and M. Reyes, “Prediction of performance and emissions of an engine fuelled with natural gas/hydrogen blends,” *International Journal of Hydrogen Energy*, vol. 36, no. 1, pp. 947–956, Jan. 2011.
- [152] T. Genova, M. Otero, A. Morales, B. Stiehl, S. Martin, and K. Ahmed, “Preheating and premixing effects on NO_x emissions in a high-pressure axially staged combustor,” *Combustion and Flame*, vol. 235, p. 111710, Jan. 2022.
- [153] H. Yuan, T. Tsukuda, Y. Yang, G. Shibata, Y. Kobashi, and H. Ogawa, “Effects of Chemical Compositions and Cetane Number of Fischer–Tropsch Fuels on Diesel Engine Performance,” *Energies 2022, Vol. 15, Page 4047*, vol. 15, no. 11, p. 4047, May 2022.
- [154] A. G. Erman, P. Hellier, and N. Ladommatos, “The impact of ignition delay and further fuel properties on combustion and emissions in a compression ignition engine,”

- Fuel*, vol. 262, Feb. 2020.
- [155] H. Biffiger and P. Soltic, “Effects of split port/direct injection of methane and hydrogen in a spark ignition engine,” *International Journal of Hydrogen Energy*, vol. 40, no. 4, pp. 1994–2003, Jan. 2015.
- [156] X. Duan, M. C. Lai, M. Jansons, G. Guo, and J. Liu, “A review of controlling strategies of the ignition timing and combustion phase in homogeneous charge compression ignition (HCCI) engine,” *Fuel*, vol. 285, Feb. 2021.
- [157] T. Wittka, B. Holderbaum, P. Dittmann, and S. Pischinger, “Experimental Investigation of Combined LNT + SCR Diesel Exhaust Aftertreatment,” *Emission Control Science and Technology*, vol. 1, no. 2, pp. 167–182, May 2015.
- [158] J. Serrano, F. J. Jiménez-Espadafor, A. Lora, L. Modesto-López, A. Gañán-Calvo, and J. López-Serrano, “Experimental analysis of NO_x reduction through water addition and comparison with exhaust gas recycling,” *Energy*, vol. 168, pp. 737–752, Feb. 2019.
- [159] S. Rajkumar, A. Das, and J. Thangaraja, “Integration of artificial neural network, multi-objective genetic algorithm and phenomenological combustion modelling for effective operation of biodiesel blends in an automotive engine,” *Energy*, vol. 239, p. 121889, Jan. 2022.
- [160] Shivakumar, P. Srinivasa Pai, and B. R. Shrinivasa Rao, “Artificial Neural Network based prediction of performance and emission characteristics of a variable compression ratio CI engine using WCO as a biodiesel at different injection timings,” *Applied Energy*, vol. 88, no. 7, pp. 2344–2354, Jul. 2011.
- [161] P. Tian, X. Liu, K. Luo, H. Li, and Y. Wang, “Deep learning from three-dimensional multiphysics simulation in operational optimization and control of polymer electrolyte membrane fuel cell for maximum power,” *Applied Energy*, vol. 288, p. 116632, Apr. 2021.
- [162] R. M. Hristev, “The ANN book,” in *GNU Public Licence*, 1998, pp. 41–45.
- [163] O. A. Montesinos López, A. Montesinos López, and J. Crossa, “Fundamentals of Artificial Neural Networks and Deep Learning,” *Multivariate Statistical Machine Learning Methods for Genomic Prediction*, pp. 379–425, 2022.
- [164] S. Roy, R. Banerjee, and P. K. Bose, “Performance and exhaust emissions prediction of a CRDI assisted single cylinder diesel engine coupled with EGR using artificial neural network,” *Applied Energy*, vol. 119, pp. 330–340, Apr. 2014.

- [165] R. Yang *et al.*, “An Artificial Neural Network Model to Predict Efficiency and Emissions of a Gasoline Engine,” *Processes*, vol. 10, no. 2, pp. 1–20, 2022.
- [166] Z. Tian, W. Gan, X. Zou, Y. Zhang, and W. Gao, “Performance prediction of a cryogenic organic Rankine cycle based on back propagation neural network optimized by genetic algorithm,” *Energy*, vol. 254, p. 124027, 2022.
- [167] J. Seo and S. Park, “Optimizing model parameters of artificial neural networks to predict vehicle emissions,” *Atmospheric Environment*, vol. 294, p. 119508, Feb. 2023.
- [168] A. Shirneshan, S. A. Bagherzadeh, G. Najafi, R. Mamat, and M. Mazlan, “Optimization and investigation the effects of using biodiesel-ethanol blends on the performance and emission characteristics of a diesel engine by genetic algorithm,” *Fuel*, vol. 289, p. 119753, Apr. 2021.
- [169] G. D’Angelo and F. Palmieri, “GGA: A modified genetic algorithm with gradient-based local search for solving constrained optimization problems,” *Information Sciences*, vol. 547, pp. 136–162, Feb. 2021.
- [170] J. Ochelska-Mierzejewska, A. Poniszewska-Marańda, and W. Marańda, “Selected Genetic Algorithms for Vehicle Routing Problem Solving,” *Electronics 2021, Vol. 10, Page 3147*, vol. 10, no. 24, p. 3147, Dec. 2021.
- [171] S. Katoch, S. S. Chauhan, and V. Kumar, *A review on genetic algorithm: past, present, and future*, vol. 80. Multimedia Tools and Applications, 2021.
- [172] H. Jiang, Z. Xi, A. A. Rahman, and X. Zhang, “Prediction of output power with artificial neural network using extended datasets for Stirling engines,” *Applied Energy*, vol. 271, p. 115123, Aug. 2020.

APPENDICES

A. List of Publications

1. **Cahyani Windarto**, Ocktaeck Lim, “Spark discharge energy effect on in-cylinder characteristics performance of rapid compression and expansion machine with spark ignition direct injection strategy”, *Fuel, Elsevier*, Volume 337, 2023. <https://doi.org/10.1016/J.FUEL.2022.127165>
2. **Cahyani Windarto**, Ardika Setiawan, Nguyen Ho Xuan Duy, Ocktaeck Lim, “Investigation of propane direct injection performance in a rapid compression and expansion machine: Pathways to diesel marine engine efficiency parity with spark discharge duration strategies”, *International Journal of Hydrogen Energy, Elsevier*, Volume 48, pp 33960-33980, 2023. <https://doi.org/10.1016/j.ijhydene.2023.05.131>
3. **Cahyani Windarto**, Ocktaeck Lim, “A comprehensive study of the effects of spark discharge duration on low-carbon combustion of high-pressure direct-injection propane: Factors affecting combustion, in-cylinder performance, and emissions”, *International Journal of Hydrogen Energy, Elsevier*, 2023. <https://doi.org/10.1016/J.IJHYDENE.2023.09.090>
4. **Cahyani Windarto**, Ocktaeck Lim, “The operating parameter optimization of spark duration effect on the performance and emission characteristics of direct-injection propane by genetic algorithm”, *Energy, Elsevier*, revision (Submitted date Sep 30, 2023).
5. **Cahyani Windarto**, Ocktaeck Lim, “A neural network approach on forecasting spark duration effect on in-cylinder performance of a large bore compression ignition engine fueled with propane direct injection”, *Fuel Processing Technology, Elsevier*, under review (Submitted date Sep 3, 2023).

B. List of Conferences

International Conferences

1. **Cahyani Windarto** and Octaek Lim, 13th International Conference of Applied Energy (ICAE) 2021, Bangkok, Thailand, 2021.
2. **Cahyani Windarto** and Octaek Lim, 14th International Conference of Applied Energy (ICAE) 2022, Bochum, Germany, 2022.
3. **Cahyani Windarto** and Octaek Lim, 6th International Conference of Mechanical Engineering Science and Technology (MEST) 2022, Surakarta, Indonesia.
4. **Cahyani Windarto** and Octaek Lim, 15th International Conference of Applied Energy (ICAE) 2023, Doha, Qatar, 2023.

Domestic Conferences

1. **Cahyani Windarto** and Ocktaeck Lim, KSAE, Annual Spring Conference, Shinhwa World, Jeju, 2020.
2. **Cahyani Windarto** and Ocktaeck Lim, KSAE, Annual Autumn Conference, Bexco, Busan, 2022.
3. **Cahyani Windarto** and Ocktaeck Lim, KSAE, Annual Spring Conference, Shinhwa World, Jeju, 2022.
4. **Cahyani Windarto** and Ocktaeck Lim, KSAE, KSAE Spring 2023 Conference Chapter Busan, Changwon and Ulsan, Ulsan, Korea, 2023.